EFFECT OF SINGLE WALLED CARBON NANOTUBES (SWNTs) ON THE ELECTROMECHANICAL PROPERTIES OF POLYIMIDE NANOCOMPOSITES

A Thesis

by

SUJAY DESHMUKH

Submitted to the Office of Graduate Studies of
Texas A&M University
in partial fulfillment of the requirements for the degree of

MASTER OF SCIENCE

December 2006

Major Subject: Aerospace Engineering

EFFECT OF SINGLE WALLED CARBON NANOTUBES (SWNTs) ON THE ELECTROMECHANICAL PROPERTIES OF POLYIMIDE NANOCOMPOSITES

A Thesis

by

SUJAY DESHMUKH

Submitted to the Office of Graduate Studies of
Texas A&M University
in partial fulfillment of the requirements for the degree of

MASTER OF SCIENCE

Approved by:

Chair of Committee, Zoubeida Ounaies
Committee Members, Jim Boyd
Jaime Grunlan
Head of Department, Helen Reed

December 2006

Major Subject: Aerospace Engineering

ABSTRACT

Effect of Single Walled Carbon Nanotubes (SWNTs) on the Electromechanical Properties of Polyimide Nanocomposites. (December 2006)

Sujay Deshmukh, B.E., University of Pune, INDIA

Chair of Advisory Committee: Dr. Zoubeida Ounaies

Nanocomposites show promise in various fields, ranging from aerospace vehicles to microelectronics. Specifically, electro-active nanocomposites would enable a whole new set of applications, where the nanocomposite material would exhibit strength, toughness, and electromechanical coupling. The broad goal of this thesis was to investigate potential electromechanical behavior in single walled carbon nanotube (SWNT)-polyimide (PI) composites. The specific objective was to measure and characterize the actuation response of SWNT–PI nanocomposites. Two different polyimides, non-polar CP2, and a weakly piezoelectric polymer (β-CN) APB-ODPA are used in the study. Electrical and dielectric characterization of the nanocomposites were carried out to better understand the effect of SWNTs on the different physical properties of the composites, and to identify the electroactive mechanism in the resulting composites.

(β-CN) APB-ODPA composites show a higher increase in both conductivity and dielectric constant with SWNT content as compared to the CP2 composites. The effect of SWNTs on remnant polarization (P_R) is quantified using the dielectric relaxation tests and Thermally Stimulated Current (TSC) experiments. Both experiments show an increase in the remnant polarization with SWNT content and a higher value for the (β-CN)APB-ODPA nanocomposites over CP2 nanocomposites.

Actuation tests employing a cantilever bending experiment were carried out on the nanocomposite samples while varying the SWNT content and electric field. The strains are seen to be proportional to the square of the electric field, indicating an electrostrictive response. Strain rate and the coefficient of electrostriction (M_{1333}) values are seen to increase with SWNT content and are higher for (β-CN) APB-ODPA nanocomposites than the CP2 nanocomposites. Electrostrictive strains can also be expressed as the square of polarization; hence the findings of the dielectric relaxation studies and TSC measurements can be correlated to the measured electrostrictive effect.

The cause for the enhancement in dielectric, dielectric relaxation and actuation response of the nanocomposites with the increase in the SWNT content and polarity of the matrix was explored. Among different possible causes special emphasis was given to the importance of the interface between the SWNTs and the matrix and the resulting increase in polarization as the main factor driving the enhancement.

ACKNOWLEDGMENTS

This work wouldn't have been possible without the contributions of a few special people. Research often benefits significantly from guidance, discussions and debates courtesy ones colleagues and teachers. I, too, have received valuable insights from some fine minds. I wish to thank my research advisor, Dr. Zoubeida Ounaies, for the technical guidance, faith and support she has provided, and my colleagues Sumanth and Atheer for helping me out whenever I needed it. Also, I would like to specially thank Dr. Ricardo Perez for being prepared to discuss and help out in any way he could.

This work was possible due to the financial support of the Texas A&M Aerospace Engineering Department and NASA Grant NCC1-528810. My work is essentially the extension of the efforts by the researchers at NASA Langley Research Center who deserve a special mention.

Also, any acknowledgements would be incomplete without acknowledging the love and support of my family and friends.

TABLE OF CONTENTS

Page

Page

LIST OF TABLES

LIST OF FIGURES

FIGURE Page

FIGURE Page

FIGURE Page

FIGURE Page

FIGURE Page

1. INTRODUCTION

1.1 Electro-Active Polymers

Actuation mechanisms find applications in space systems ranging from robotic arms needed for sampling systems to mechanisms needed for solar panel deployment[1]. Most of these systems have been a collection of mechanical, hydraulic or pneumatic components. Current research though, is being driven by a desire to incorporate the actuation response into the material system itself. These materials called *active materials* include traditional piezoelectric ceramics and comparatively new and novel materials like electro active polymers (EAPs). EAPs have come to the forefront as a popular family of active materials because of the numerous advantages they offer. EAPs are lightweight, flexible, ductile, possess high strength to weight ratio, good processability, large actuation stroke, superior sensing response and low acoustic and mechanical impedance. These materials thus hold a distinct advantage over active materials such as lead zirconium titanate (PZT) and shape memory alloys (SMAs) and can be useful in future space structure applications. Thus they are being envisioned as inexpensive, lightweight actuators which consume low power and actuate at low voltages. Types of EAPs include piezoelectric, electrostrictive and electrostatic polymers, liquid crystalline polymers, ionic gels, ionic polymer metal composites and conductive polymers. These materials show actuation and sensing response due to driving mechanisms that are either electronic or ionic in nature. More details will be provided later in the section

---

This thesis follows the style of *Macromolecules*

Along with space structures, EAPs materials also find applications in biomedical and electronics industry. Conducting polymers are one type of EAPs which have already been incorporated into commercial applications. They have been used in biomedical applications like blood vessel connectors[2], while in the electronics industry conducting polymers have found use in the manufacture of field effect transistors[3].

EAPs have also been heralded as "artificial muscles" due to apparent similarities with biological muscles in terms of achievable stress and force. Table 1.1[4] shows the comparison between the natural muscle and different EAPs. Currently the concept of artificial muscles is proving a strong motivation for investigating and developing these materials.

When classified broadly, these active materials are categorized based on the mechanism driving their electroactive nature into either electronic or ionic EAPs. In electronic EAPs the immediate cause for the strains is the electric field and typically they hold the actuation strains under a DC electric field. This actuation is usually due to movement of electrons or dipoles present in the system or the coulombic forces acting in the material. Electronic EAPs could be useful in robotic applications. They include piezoelectric, electrostrictive, electrostatic, pyroelectric, ferroelectric and liquid-crystal polymers (note that ferroelectric and pyroelectric polymers are subset of piezoelectric polymers). In ionic EAPs, the strains result from diffusion of ions and necessitate the use of an electrolyte with free ions for the electroactive response to occur under an applied field. These EAPs include gels, ionomeric polymer metal composites and conducting polymers.

Table 1.1 Comparison between natural muscle and EAPs[4]

Property	Mammalian skeletal muscle (max)	Electrostatic silicone elastomer	Ferroelectric polymers	Conducting polymers	Ionic polymer metal composites
Strain (%)	>40	120	3.5-7	2-12	0.5-3.3
Stress (MPa)	0.35	0.3-3.2	20-45	5-34	3-15
Work Density (kJ/ m^3)	40	10-750	320-1000	100	5.5
Strain Rate (%/s)	>50	34000	≥ 2000	1-12	3.3
Specific Power (W/kg)	284	500		150	2.56
Efficiency (%)	40	25-80		18	2.9

1.1.1 Electronic EAPs

These polymers include materials in which mechanisms are predominantly piezoelectric, electrostrictive, electrostatic or liquid crystal polymers. They are electric field driven polymers where strains are caused by the response of dipoles, atoms or molecular groups in the material to the applied field. Their response to the applied field is fast but requires high magnitudes of driving fields.

1.1.1.1 Piezoelectricity

Piezoelectricity was discovered in 1880 by the Curie brothers [5] in crystals like quartz, topaz and rochelle salt. This phenomenon manifests in materials which are non centro-symmetric in nature (i.e they lack a center of symmetry). Piezoelectric materials show a linear coupling between their mechanical and electrical properties. Pressure results in a generation of an electric charge on the faces of the material [6, 7]. Conversely, when an electric field is applied the crystals show a change in dimension [6]. The cause behind this phenomenon is a separation between the centers of positive and negative charges in the unit cell of the crystal, called a dipole. Then under an applied pressure or an electric field what results is a charge on the surface (direct effect) or a strain in the crystal (converse effect). Figure 1.1 explains this in detail where in the first case compressive and tensile forces are applied and in the second electric field is applied first in the same direction as the dipole then in a reverse direction.

The constitutive equations describing the linear coupling between the mechanical and electrical components are [7]:

$$S_{ij}=s_{ijmn}T_{mn}+d_{ijn}E_n \tag{1.1a}$$

$$D_i=d_{imn}T_{mn}+\varepsilon_{in}E_n \tag{1.1b}$$

where, S_{ij}, T_{mn}, E_n, and D_i are the strain tensor, stress tensor, electric field vector, and the electric displacement vector respectively. The terms s_{ijmn}, d_{nij}, and ε_{in} are the elastic stiffness tensor, piezoelectric strain tensor, and the permittivity tensor respectively.

Piezoelectric crystals like quartz find applications in ultrasonic interferometers [8]. Piezoelectric ceramics find applications as piezoelectric vibrators and transducers [9] thus

finding use in applications like sonar [10]. These materials are used in commercial applications like gas ignition devices and snow-skis.

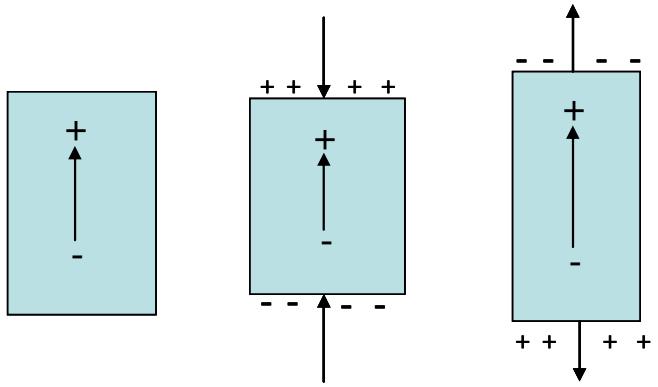

(a)

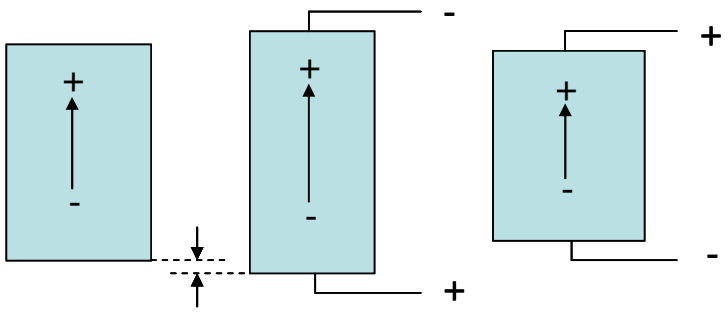

(b)

Figure 1.1 a) Direct piezoelectric effect where charge buildup is due to an external applied force, and b) converse piezoelectric effect where change in dimension is experienced upon applying electric field.

Piezoelectricity is observed not only in non-centrosymmetric ceramics but also in polymers. Broadhurst and Davis[11] state the requirements for a piezoelectric polymer as: a) presence of permanent molecular dipoles, b) ability to orient these dipoles, c) ability to sustain this orientation and d) ability to show large strains under stress. In semicrystalline polymers the piezoelectric response results from a polar crystalline phase by orienting the crystallites[12]; while in amorphous polymers the piezoelectric type behavior is due to orienting and "freezing in" of the molecular dipoles [12].

Polyvinylidene fluoride (PVDF) is a commercially available semicrystalline polymer. Kawai et al [13] have shown a strong piezoelectric response in PVDF and its copolymers trifluoroethylene (TrFE) and tetrafluoroethylene (TFE). Most of the amorphous polymers investigated for piezoelectric behavior have been nitrile substituted polymers like in polyacrylonitrile (PAN)[14, 15]. Weak piezoelectric behavior has also been observed in polymers like polyvinyl chloride(PVC) [16] and polyvinyl acetate(PVAc)[17-20].

1.1.1.2 Electrostriction

Electrostriction is a polarization related phenomenon exhibited by all dielectric materials. When an electric field is applied to a dielectric material polarization develops in it. This is usually accompanied by a deformation of the material where the strains are proportional to the square of polarization. Polarization experienced by any dielectric material under an applied field is either atomic, electronic, interfacial or dipolar in nature. The details of each will be discussed in a subsequent section. The types of polarization causing the electrostrictive effect are electronic, ionic [21] and dipolar

polarization. Electronic polarization is due to the displacement of the electron cloud surrounding the positively charged nucleus with respect to it, ionic polarization results from separation of the positive or negative ions in a compound and dipolar polarization is due to re-orientation of dipoles under an applied field. Figure 1.2(a) demonstrates that irrespective of the polarity of the applied field the electronic polarization would lead to an expansion. Figure 1.2(b)[22] represents the electrostrictive effect due to ionic polarization. Under an applied field the lattice is distorted due to relative movement of the ions. Reversing the direction of the field shows a similar effect. Also a net strain exists in the material. Figure 1.2c demonstrates the electrostrictive effect due to reorientation of random dipoles in a dielectric, due to an applied field. Thus electrostriction is a quadratic non linear electromechanical coupling between the polarization experienced by the dielectric and the strains developed in response to the electric field.

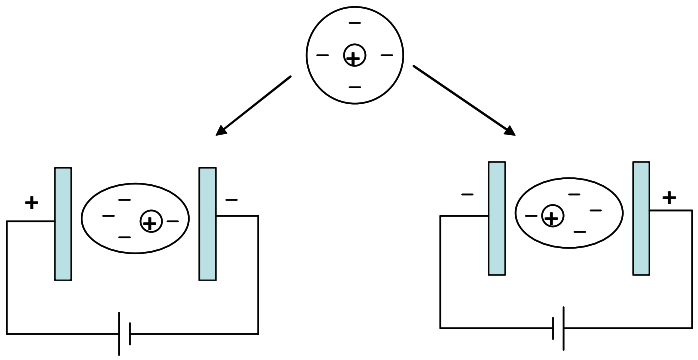

(a)

Figure 1.2 (a) Electrostriction due to electronic polarization (b) Electrostriction due to atomic polarization (c) Electrostrictive strains in a dielectric with randomly oriented dipoles

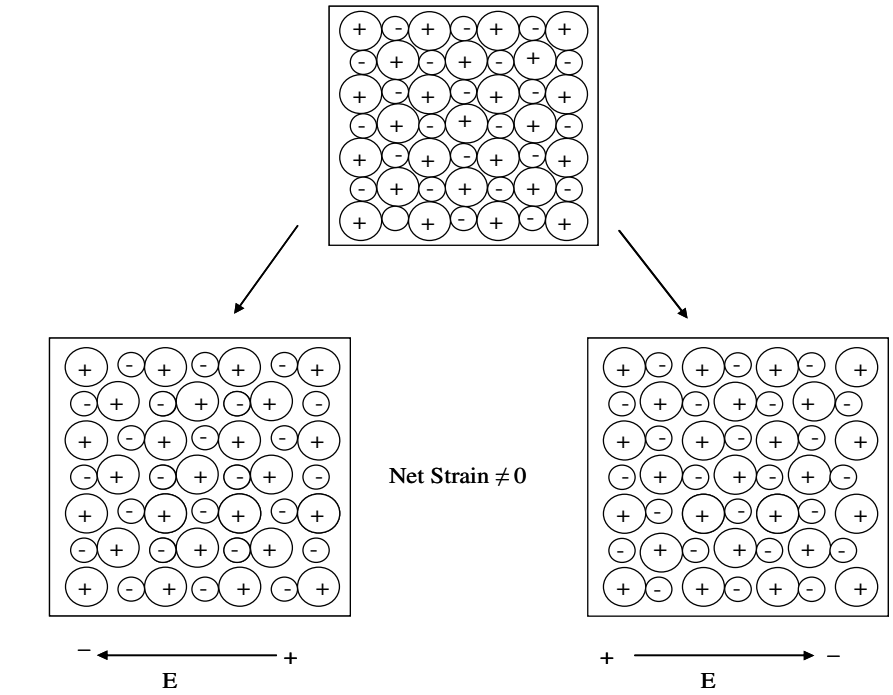

(b)

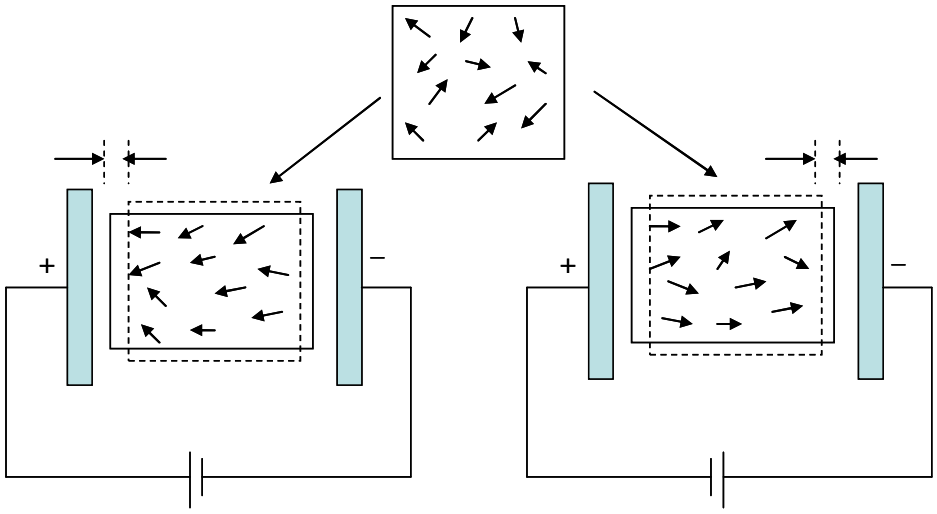

(c)

Figure 1.2 Continued

In electrostriction, the strain S_{ij} is related to the polarization as [21];

$$S_{ij} = g_{kij} P_k + Q_{klij} P_k P_l + W_{klopij} P_k P_l P_o P_p \quad (1.2)$$

The first term on the right hand side is the contribution due to piezoelectricity which relates first order polarization to second order strain through the third order piezoelectric constant g, the second is due to quadratic electrostriction which relates quadratic polarization to the strain through the fourth order electrostrictive coefficient and the last term summarizes contribution due to higher order electrostriction. Now assuming that the material has a center of symmetry (this allows us to drop the piezoelectric term) and neglecting the higher order terms the equation reduces to[21],

$$S_{ij} = Q_{klij} P_k P_l \quad (1.3)$$

P_k and P_l are the polarization vectors and Q_{ijkl} is the coefficient of electrostriction. Most dielectric materials are linear dielectrics where the applied field and the resulting polarization are linearly related. Polarization can then be expressed in terms of the electric field as[23],

$$P_i = \varepsilon_0 (\varepsilon_{ij} - 1) E_j \quad (1.4)$$

Where ε_0 and ε_{ij} are the permittivities of space and the dielectric material respectively. Hence the electrostrictive strain can then be written in terms of the electric field vectors E_r and E_s as[23],

$$S_{ij} = M_{rsij} E_r E_s \quad (1.5)$$

Where M_{ijrs} is the electrostriction coefficient related to the electric field. The two coefficients are related to each other through,

$$M_{ijrs} = \varepsilon_0^2 (\varepsilon_{kr} - 1)(\varepsilon_{ls} - 1) Q_{ijkl} \quad (1.6)$$

In most materials this electroactive response is very weak with very low strains of the order of 10^{-7} for 1 MVm^{-1} but some perovskite type oxides show electrostrictive strains of the order of 10^{-3} [24]. Electrostrictive coefficients (Q) range from 10^{-3} m^4/C^2 in relaxor ferroelectrics to 10^3 m^4/C^2 in some polymers [23]. Lead manganese niobate (PMN), with a perovskite structure was first introduced as a electrostrictive material [21, 25]. The absence of a hysteric nature in these actuator materials has lead to their proposed use as stacked actuators [26], interferometric dilatometers[27], deformable mirrors[28] etc. But there are also drawbacks associated with the electrostrictive response of the materials. Non-uniform fields develop in the material as a result of impurities, inhomogeneties or internal electrodes (as in the case of a multilayer actuator) in the material. This results in cracks due to a mismatch of stresses generated which may ultimately lead to the actuator breakdown[24].

A silicone-rubber based electrostrictive film has been used to make an acoustic actuator[29] which uses the displacement of the film normal to its surface to displace air as its operating principle. Su et. al. [30, 31] have observed high strains in grafted elastomers (~4%). Graft elastomer consists of a flexible polymer backbone and a grafted polar crystalline group. The crystalline phase is the active phase that responds to the applied field resulting in strains. Large electrostrictive strains have been shown in high-energy electron-irradiated polyvinylidene fluoride trifluroethylene P(VDF-TrFE) due to a large change in the lattice strain when the material goes from ferroelectric to paraelectric phase[32]. By using high energy electron radiation ferroelectric phase at room temperature

can be converted to paraelectric phase. This phase transformation is associated with large changes in the lattice dimensions resulting in strains. High strains of about 5% under an applied field of 150MV/m have been demonstrated for these materials. Li[33] has also demonstrated high electrostrictive response (~2%) at an electric field of 13 MV/m in P(VDF-TrFE) composite with copper-phthalocyanine (CuPc) as the secondary phase due to an enhanced polarization in the composite that results from the exchange coupling between the constituents. Watanabe et. al[34] have demonstrated an electrostrictive response in films made of polyurethane. In this study bending electrostriction was observed in these polymers and the direction of the bend depended on the presence of phenylimino or nitrophenyl groups. Figure 1.3 shows the experimental setup for the bending experiment used. An asymmetric space charge distribution in the sample under an applied field is thought to be the cause of the bending. The bending thus depends on the injection and transport of charge through the material. The charge transport and distribution and hence the direction of bend depends on the phenylimino or nitrophenyl groups present. The charge carrier is an electron or electron hole depending on the chemical structure. In case of the phenylimino group which is easily electrochemically oxidized (Figure 1.4a) an electron hole is expected to be the carrier and the cathode tends to expand causing the bend towards the anode. For the nitrophenyl group the tendency to undergo electrochemical reduction (Figure 1.4b) means an electron would be transported. The space charge distribution causes the anode to expand leading to a bend towards the cathode.

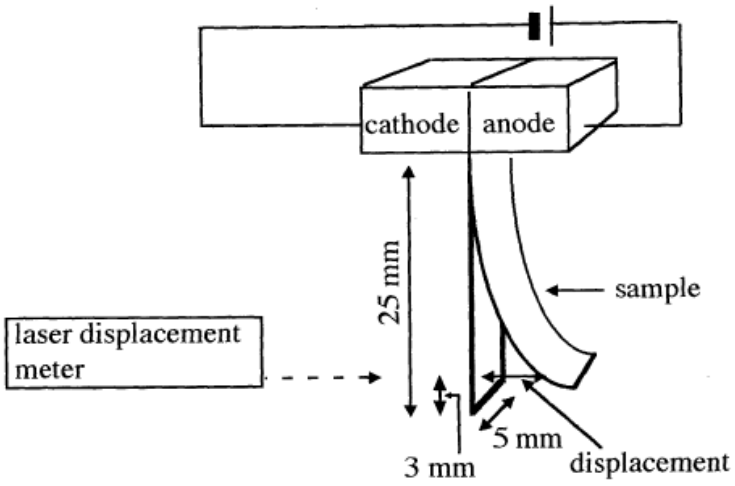

Figure 1.3 Bending experiment using polyurethane by Watanabe et. al [35]

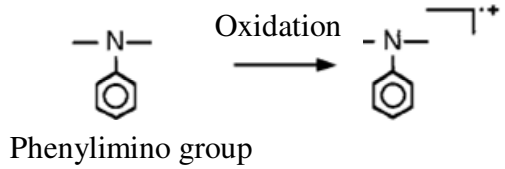

(a)

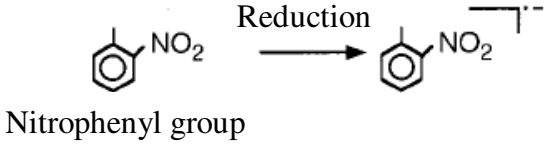

(b)

Figure 1.4 (a) Oxidation of the phenylimino group and (b) Reduction of the nitrophenyl group [34]

Further this group has also managed to control the direction of bend by doping the polymer with salts[36]. Doping with sodium acetate leads to a bend towards the cathode while doping with zinc bromide leads the polymer to bend towards the anode. The bend depends on the strength of the cation and anion of the salts. The presence of cations and anions affects the charge injected and ultimately the bend. Presence of cation causes the expansion of the cathode leading to a bend towards the anode. Anion causes the expansion of the anode and hence the sample bends towards the cathode. Table 1.2 documents some other polymeric and ceramic electrostrictive materials with the achieved strains and applied electric fields [37-39].

Table 1.2 Some polymeric and ceramic electrostrictors and the corresponding electrostrictive strains[37-39]

Electrostrictive material	Achieved strains (%)	Electric field (MV/m)
Polyurethane (Deerfield)[37]	11	160
Silicone (Dow Corning)[37]	32	144
Barium Titanate ($BaTiO_3$)[38]	~0.83	1
Lead Manganese Niobate (PMN)[39]	~0.1	1

1.1.1.3 Electrostatic Actuation

Electrostatic actuation is caused in dielectric materials by coulombic forces acting on a soft material sandwiched between two electrodes. Figure 1.5 shows the actuating principle in these actuators. When an electric field is applied across the soft material (usually an elastomer) with compliant electrodes, the polymer tends to shrink in thickness and expand in the plane. The charges on the two electrodes attract each other and cause a pressure to act on the polymeric material [4, 40]. Depending on the flexibility (elastic modulus) of the material, large mechanical strains are achieved under an applied field. The pressure acting on the film P due to the applied field E is [4]

$$P = \varepsilon_0 \varepsilon_r E^2 \tag{1.7}$$

Where ε_r and ε_0 are the relative permittivity of the polymer and permittivity of free space respectively. Acrylic and silicone elastomers have been shown to demonstrated such an actuation response[4, 40-44]. Depending on the boundary conditions strains greater than 100% have been measured in these materials due to electrostatic actuation.

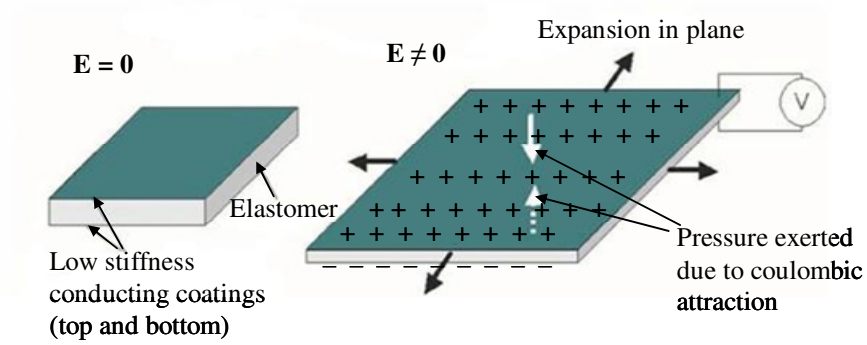

Figure 1.5 Actuation principle of electrostatic actuators (adapted from Kornbluh et. al.[40])

1.1.1.4 Liquid Crystal Polymers

Liquid crystalline (LC) polymers actuate due to re-orientation of the crystalline phase present in the polymer. Under an applied field the reorientation of the liquid crystals takes place [45, 46] as seen in Figure 1.6. These liquid crystals are attached to the polymer backbone (in Figure 1.6 it is polysiloxane backbone) but are flexible enough to experience a reorientation under an applied field. The LC molecules (known as mesogens) possess a polarization which facilitates their reorientation under an applied field. The mesogens are connected to the polymer backbone through flexible alkyl spacers. The mesogens also have crosslinkable end groups attached to them which yield the elastomer. The reorientations are what causes stresses and ultimately strains in these polymeric materials. Strains of the order of 4% have been obtained under an applied field of 1.5 MV/m at 133 Hz[46].

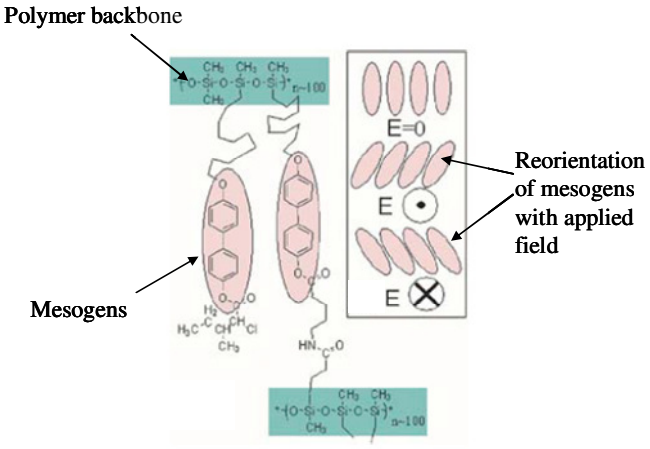

Figure 1.6 Reorientation of mesogens leading to strain. E=0 shows no strains while for E into and out of the plain the mesogens reorient in opposite direction to give strain (adapted from Lehmann et. al. [46])

1.1.2 Ionic EAPs

Ionic EAPs actuate as a result of ion diffusion. These EAPs actuate at low voltages. The mechanisms for this phenomenon will be discussed shortly for each of the ionic EAPs. The disadvantages they face include: presence of an electrolyte for the actuation to take place, a typically slow response and a low electromechanical efficiency. They usually provide large actuation strokes and their response can be engineered by changing the chemistry of the system. Some examples of ionic polymers will be described below although briefly since the mechanism of interest in this study is electronic.

1.1.2.1 Ionic Polymer Gels

Ionic polymer gels are three-dimensional networks of cross-linked macromolecular polyelectrolytes that swell or contract in aqueous solutions on addition of alkali or acids[47]. The electrochemistry of gels is the driving force in this actuation. Under an applied field hydrogen is released at cathode and oxygen at anode. Thus region near cathode becomes more basic while that near the anode is acidic. This asymmetry between the two sides causes the bending of the sample. The bending response is not a material property but depends on the dynamics of the electrolytic reactions, geometry of the system, composition of the electrolyte, electrodes and the history of the gel. Figure 1.7 shows such an experiment which causes the polyacrylic acid gel rod in a sodium hydroxide solution to bend towards the cathode under an applied electric field. The first experimental evidence of electrically activated gels was provided by Hamlen et. al.[48] in samples made from a copolymer of polyvinyl alcohol (PVA) and polyacrylic acid

(PAA). The activation of these materials depended on the total ionic concentration inside the polymer. The samples were immersed in an external solution and had a conductor incorporated in it. The fiber of the material was made either positive or negative. On being made positive (5V) hydrogen evolved and the solution became alkaline and the fiber extended in length. When the fiber was made negative oxygen evolved making the solution acidic and leading to a contraction of the fiber.

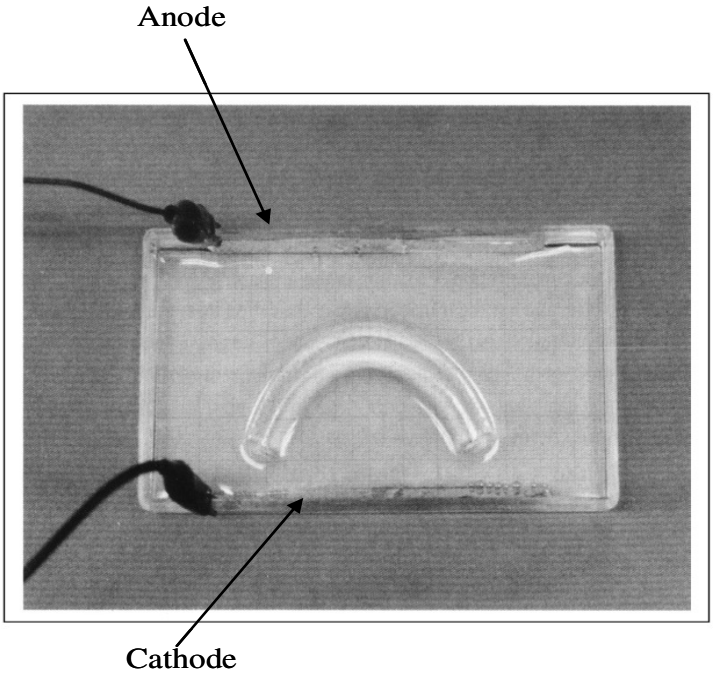

Figure 1.7 Ionic polymer gel actuation (polyacrylic acid gel rod in NaOH) [49]

1.1.2.2 Ionomeric Polymer Metal Composites (IPMCs)

IPMCs are polyelectrolyte polymer solutions with anions covalently fixed to the polymer chain and the matrix is then doped with counter-ions to neutralize it. Under an applied field the positive ions move towards the cathode which is followed by the water to hydrate these ions. This movement is what causes the bending in the sample [50]. There are several commercially available ionomer membranes such as Nafion (DuPont) and Flemion (Asahi glass), with the difference being the presence of sulfonate (Nafion) or carboxylate (Flemion) groups in the matrix [50]. Different counter-ions have been used such as H^+, Li^+, Na^+, K^+, Rb^+ and Cs+ [51]. Figure 1.8 demonstrates the actuation of a Nafion-based IPMC under an applied electric field [52]. IPMCs have been discussed for application as biomimetic actuators and sensors [53] and also investigated for an application dealing with quantification of pressure at the base of the human spine [54].

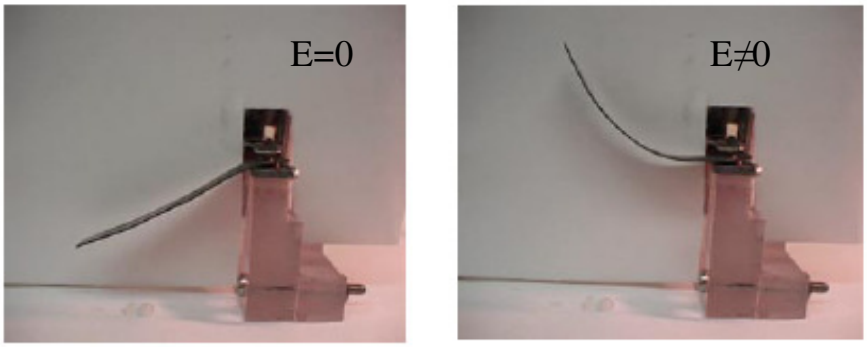

Figure 1.8 Ionic polymer-metal composites response to electric field [52]

1.1.2.3 Conductive Polymers

Conductive polymers are organic materials with conjugate molecular chains doped with ions in the polymer solvent. They are also known as conjugate polymers. Reduction and oxidation reactions in the polymer under an applied field lead to addition or removal of charge from the polymer chain and movement of ions to counter this imbalance of charge [4]. Thus the movement of these ions is accompanied by movement of the solvent leading to contraction or expansion of the material. Figure 1.9 shows the case of polypyrrole which contracts on reduction and expands if oxidized [55]. On oxidation, anions (A^-) enter to balance the charge as electrons are removed leading to the expansion. Thus the insertion of ions is the critical factor in the actuation of these materials. Besides the previously mentioned applications of blood vessel connectors [2] and field effect transistors [3], these materials also are useful in supercapacitors [56] , batteries [57], and sensors [58] among others.

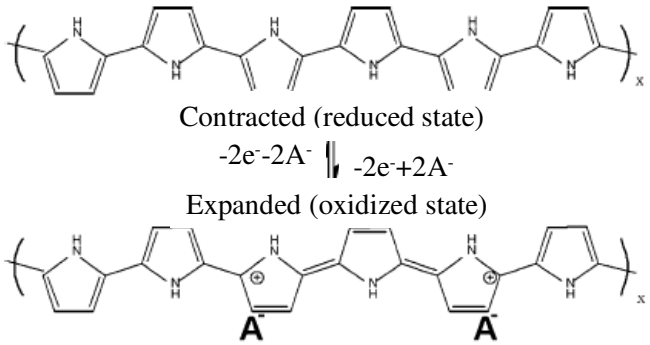

Figure 1.9 Reduction-oxidation reactions of polypyrrole [55]

1.2 Carbon Nanotubes (CNTs)

1.2.1 Background and Applications

Oberlin et al[59] managed to make hollow carbon fibers in 1976 by pyrolysing a mixture of benzene and hydrogen. The diameters of these fibers ranged from 2 to 50 nm. This could have been the first discovery of carbon nanotubes (CNTs). These carbon allotropes were then discovered in 1991 by Iijima [60] using the arc discharge evaporation method. These allotropes of carbon are slender fullerenes with a high aspect ratio. The walls of these "tubes" are made up of hexagonal lattice of carbon with the ends capped by hemispheres. Nanotubes are classified into single walled carbon nanotubes (SWNTs) and multi walled carbon nanotubes (MWNTs). SWNTs can be described as a single layer of graphene rolled into a seamless tube and capped at both ends by hemispheres. Similarly MWNTs can be seen as made up of multiple layers of graphene sheets (multiple walls). Figure 1.10 (a, b) shows schematics of an SWNT and an MWNT while (c) shows a specific case of MWNT where there are just two layers of graphene which make up the wall of the nanotube, called a double walled nanotube (DWNT).

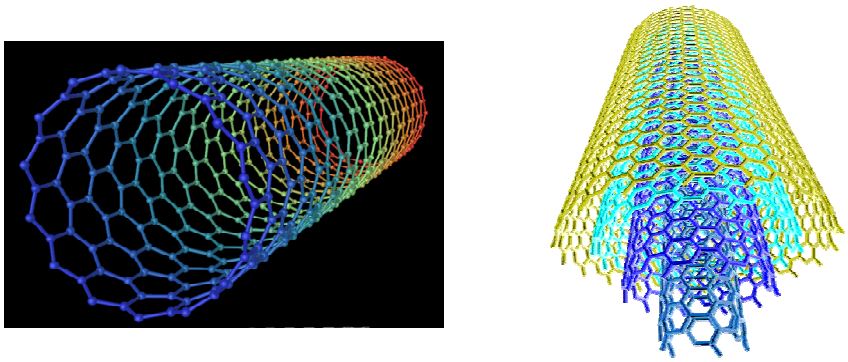

(a) (b)

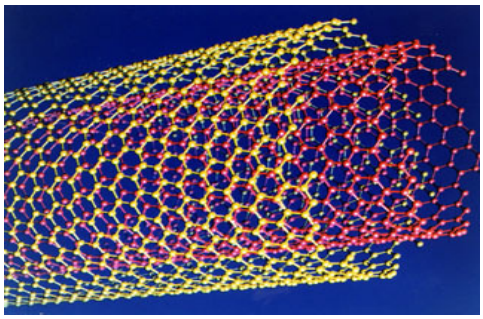

(c)

Figure 1.10 (a) Single walled carbon nanotube (SWNT)[61], (b) Multi walled carbon nanotube (MWNT)[62] and (c) Double walled carbon nanotube (DWNT) [63]

The diameters of SWNTs have been reported in the range of 1-5 nm while the lengths range from 1 – 30 μm[64]. SWNTs as long as 4cm have also been reported[65]. DWNTs show a range of 2-6 nm in diameters and 2-50 μm in length. MWNT in comparison show diameters ranging from 13-50 nm and lengths to the order of 10-500 μm[64, 66].

SWNTs have created a lot of enthusiasm in the research community because of a wide repertoire of properties which are absent in most engineering materials. These

materials have been reported to possess tensile modulus as high as 1 TPa and strength of the order of 200 GPa [67-69], which is 100 times that of steel but at a fraction of its weight. They also possess excellent electrical [70] and thermal properties [71] and have been investigated as quantum wires. The electric and thermal properties depend on the tube chirality, diameter and length.

The way the graphene layer is wrapped to form a tube is represented by a pair of indices called the chiral vector $C_h = na_1+ma_2$. n and m denote units in two directions in the honeycomb crystal lattice of graphene. The choice of n and m decides the nature of the nanotubes: they are zigzag or armchair when m=0 and n=m respectively, and chiral otherwise. Figure 1.11 shows the chiral vector (C_h) and chiral angle θ in a nanotube. The diameter of a nanotube is given by, $d_t = \frac{a}{\pi}\sqrt{n^2+m^2+nm}$ where a is the lattice constant of 2.49 Å [72]. Nanotubes have a unique electronic structure ranging from metallic (n-m=3p, p is an integer) to semiconducting (n-m≠3p) with large band gap.

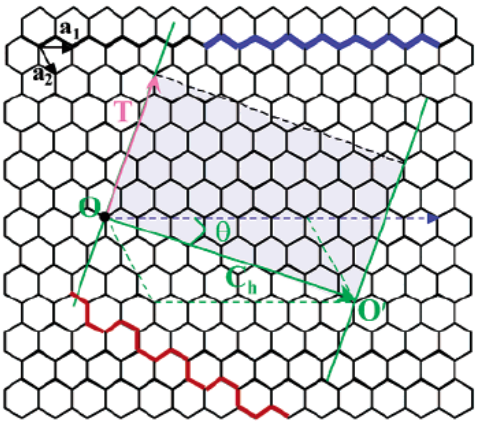

Figure 1.11 Representation of chirality in a nanotube[73]

A number of researchers have focused on analyzing the nature of bonds in SWNTs and how they differ from bonds in graphene [74, 75]. Carbon has six electrons which occupy $1s^2$, $2s^2$, and $2p^2$ atomic orbitals. In graphite the four outer electrons of carbon form three sp^2 hybridized σ bonds and one π bond [76]. Each carbon atom is bonded to three others in the same plane by strong covalent bond (σ) and by a weak van der Waals force with the fourth (π). Thus graphite usually occurs as a layered material. By bending the graphene sheet as in the case of a SWNT, an asymmetry is introduced in the π orbital overlap, bringing into close proximity the segments of the orbital in the cavity and spaces out the outer ones [74]. The coulombic repulsion increases within the cavity leading to a rehybridization of the π orbital from sp^2 of graphite to something intermediate between sp^2 and sp^3 (sp^3 has four σ bonds). Thus a radial polarization at each atomic site is thought to exist due to tilting of the σ bond by an angle as the curvature of the graphene sheet increases. Again, this is the result of the charge redistribution in the π orbital. Figure 1.12 represents this scenario schematically. Figure 1.12(a) shows the σ bond and the π orbital in the case of graphene, while Figure 1.12(b) represents the changes that take place due to curvature of the graphene layer such as in the case of SWNT. Due to symmetry of the nanotube however no net polarization exists in it. This can be seen in Figure 1.13. Due to curvature and redistribution of charge a local dipole will exist but it will be cancelled out by another dipole in the opposite direction resulting in zero net dipole moment. Experimental techniques like ultraviolet photoemission spectroscopy, x-ray photoemission spectroscopy (XPS) and Fourier transform infrared spectroscopy (FTIR) have been used to study the electronic structure of nanotubes[75, 77]. The XPS core

energy loss spectra are stronger for carbon nanotube than for graphite which is related to the curved nature of the graphene sheets. The enhancement in loss spectra is associated with the loss in symmetry of the π electron density.

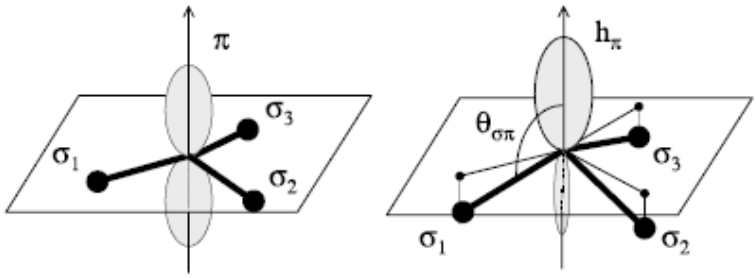

(a) (b)

Figure 1.12 (a) π-orbitals of the graphene sheet are symmetric and perpendicular to the σ bonds. (b) In SWNT each σ bond is tilted down which breaks the symmetry of the π orbital charge distribution.[74]

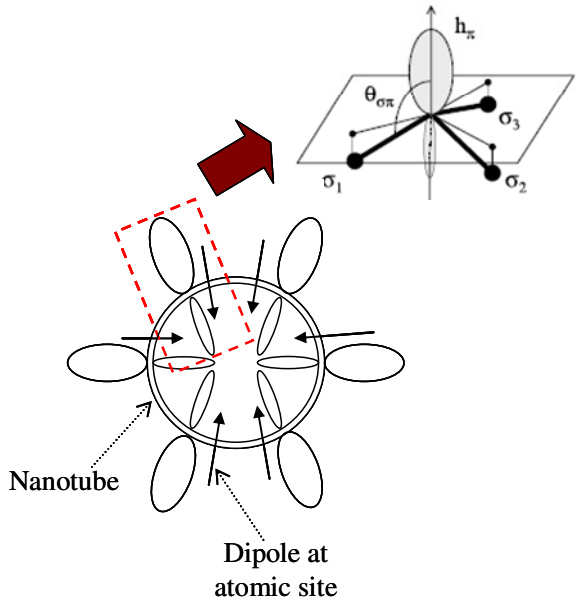

Figure 1.13 Existence of local dipole moments at each atomic site. Net radial dipole moment on the nanotube is zero as the moments cancel each other out due to symmetry.

Also during the σ-π rehybridization the π band is shifted to a lower energy level. If the shift is big enough and the π band crosses the Fermi energy, the tube becomes metallic and a good electrical conductor.

SWNTs have been proposed for numerous applications due to their unique combination of properties. Bonard et al. [78] have investigated the field emission properties of these materials. Numerous applications of carbon nanotubes have been proposed taking advantage of this property including a flat panel display [79] and in a cathode ray lighting element, where the nanotube materials act as field emitters [80]. Nanotubes have also been proposed for application in energy [81] and hydrogen storage [82]. Nanotubes are also interesting as chemical sensors [81] as they are very sensitive to substances that affect the amount of injected charge [83]. Due to the advantage of their nano-dimensions they are envisioned as the next generation nano-probes, sensor and actuators. The next section deals with the efforts made towards understanding the electromechanical properties of these novel materials.

1.2.2 Electromechanical Properties of CNTs

Apart from the impressive CNT suite of properties discussed, this unique structural form of carbon also exhibits an electromechanical coupling as has been demonstrated by different researchers. Kim et al.[84] have demonstrated the application of MWNTs as nanotweezers. Figure 1.14 shows the tweezers prepared by depositing nanotubes on to the metal electrodes.

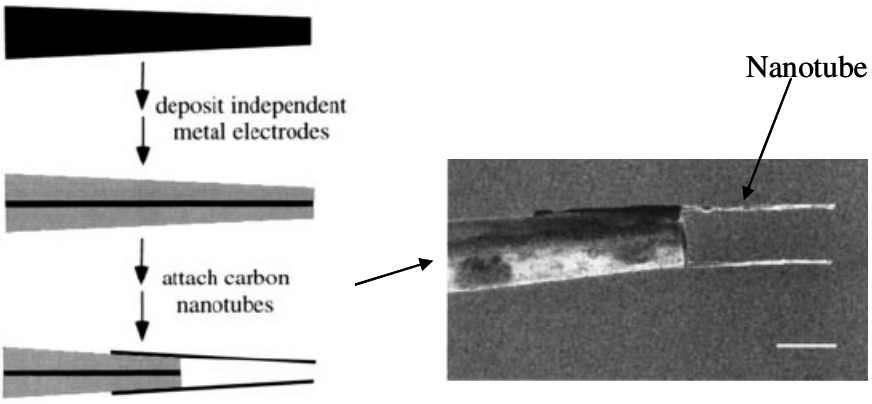

Figure 1.14 Nanotweezers using nanotubes (adapted from[84]) {scale bar is 200nm}

On applying a bias electric field to the nanotubes the tweezers close and they open when a field of same polarity is applied to both the electrodes. The reason cited by the researchers is the balance of elastic energy loss by the electrostatic energy gain. Thus electrostatic forces were responsible for this electromechanical coupling.

Baughman et al have shown dimensional changes in SWNTs and SWNT sheets called Bucky Paper. They achieved this by isolating an SWNT on a silicon chip (Figure 1.15) and applying a square wave potential between the SWNT and the substrate. An electron or electron hole is thus injected into the SWNT depending on polarity using an atomic force microscopy (AFM) tip. Consequently, they observed a change in the length of the tube and attributed it to the weakening of the carbon-carbon bonds due to injection of the electron, which populates states with anti-bonding character. Adding an electron

hole (removing electron) has a similar effect and depopulates the bonding states though it is less effective compared to adding electron.

Bucky paper is a mat of tangled SWNT ropes[85] with a large number of SWNTs. Figure 1.16 shows an SEM of such a SWNT mat or a Bucky paper. In the Bucky paper actuation experiment [86], the paper was immersed into an electrolyte and was used as an electrode. Changing the applied voltage injects charge into this paper, which is then compensated by electrolyte ions at the surface forming a double layer (Figure 1.17). An electron or electron hole is injected into the nanotube depending on the potential applied. Figure 1.17 shows the double layer formation in nanotubes when an electron is injected in one nanotube and electron hole in the other leading to formation of double layer on each but of opposite polarity. Electron or electron hole injection into the nanotubes causes dimensional changes leading to a macroscopic strain shown as a bending displacement of a bimorph in a cantilever arrangement (Figure 1.18). The figure shows two strips of SWNTs operated in NaCl solution. These strips are stuck to a double sided scotch tape and the potential is applied. The ions shown on the strips in the figure represents the ions on the nanotube surface forming the double layer. The configuration shows a bending response on applying an electric field caused due to the change in nanotube dimensions which in turn is a result of the electron or electron hole injection. Changing the potential applied causes the actuator to bend in the opposite direction as the electron and electron hole injection is reversed. The actuation results from quantum chemical and double layer electrostatic effects. These bucky paper actuators hold the advantage of superior mechanical and electrical properties of nanotubes along with their

ability to actuate. The strains observed were around 0.2% with applied voltage of 0.2-0.5V with maximum predicted strains of 1% at a voltage of 1V.

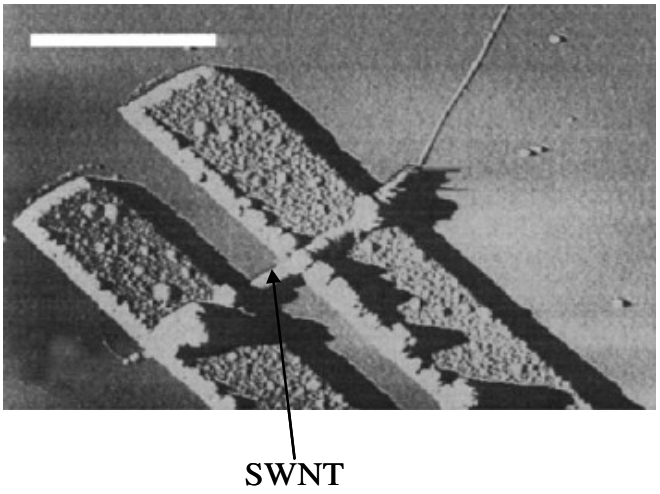

Figure 1.15 AFM image of the SWNT actuation experiment setup (adapted from [87]) {scale bar is 1μm}

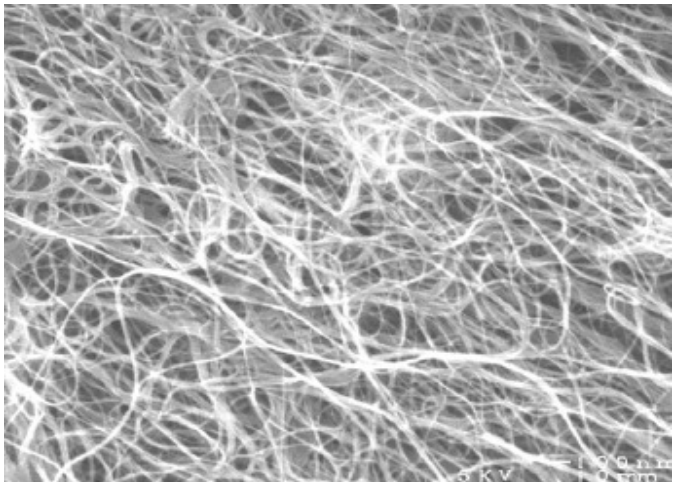

Figure 1.16 SEM image of a Bucky paper[85]

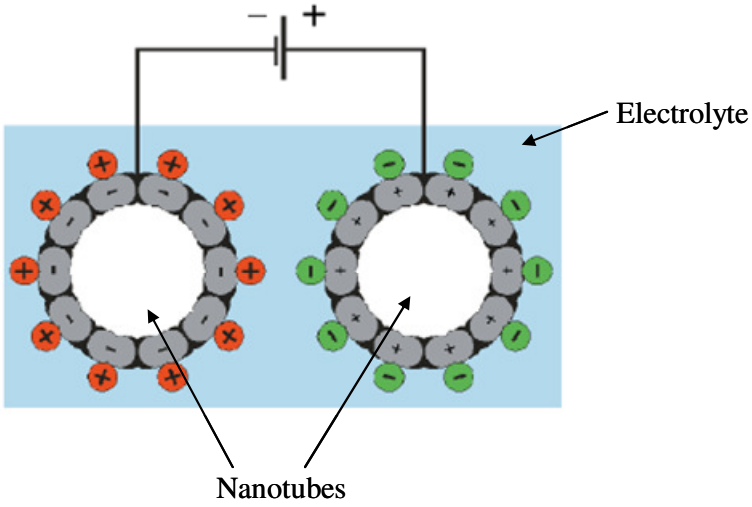

Figure 1.17 Formation of a double layer in a nanotube immersed in electrolyte. Applying a voltage to two nanotube electrodes injects charges of opposite signs which are then balanced by the ions in the surrounding electrolyte denoted by the positive and negative spheres[86]

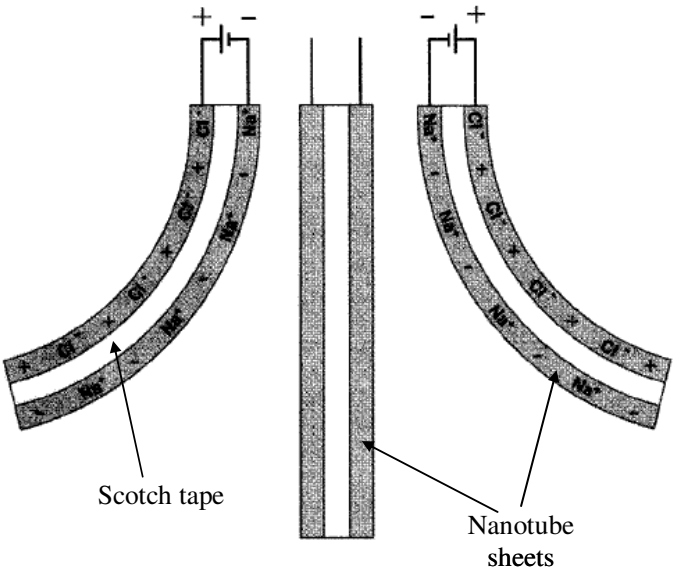

Figure 1.18 Bending of the Bucky paper under an applied field. Na+ and Cl- are the ions in the electrolyte while the + and – signs denote the charges injected into the nanotube sheets[86]

Further study by Barisci et al.[88] has sought to increase the rate of actuation in these nanotube sheets which is related to the ion transport rates in the electrolyte that is used. The study uses resistance compensation by applying a higher field to account for the resistance drop through the electrolyte and achieves a $0.1\%s^{-1}$ increase in the strain rate. Nanotube materials as actuators are thus being explored as new and novel actuator materials.

1.3 Carbon Nanotube – Polymer Composites

The research on carbon nanotube – polymer composites has developed and gained in importance in the last decade or so. The endeavor is to incorporate the exceptional mechanical, electrical and thermal properties of CNTs into polymers by taking advantage of their high interfacial area, potentially resulting in high strength, tough, multifunctional composites which can perform more than one function by the virtue of enhancement of different properties such as mechanical strength, thermal and electrical conductivity. The interfacial region in the nanocomposites plays the important role of connecting the nanotubes and the polymer matrix. Since the nanotubes have a high aspect ratio (length/diameter ~ 1000), they possess a large surface area to volume ratio and this large surface area translates into a larger interfacial region in nanotube based nanocomposites compared to other conventional fillers like carbon fibers.

The biggest hurdle researchers have faced till date is achieving efficient dispersion of CNTs in polymer. CNTs have a tendency to form agglomerates due to van der Waals attraction leading to a difficulty in separating the nanotubes and dispersing them evenly

in the polymer matrix. Different processing methods have been used to address this issue. Though they may be fundamentally different in philosophy, all of the processing methods try to address issues like de-agglomeration of nanotube bundles, dispersion of nanotubes and interfacial bonding between the nanotube and the matrix without destroying the integrity and aspect ratio of the nanotubes [89, 90]. Preprocessing is carried out as the first stage to achieve the said objectives. This includes eliminating the catalyst residue from the nanotubes through annealing and acid treatments [91, 92], de-agglomeration by ultrasonication [93] or electrostatic plasma treatment [90, 94], and in some cases, chemically functionalizing the nanotubes for an enhanced interaction between the nanotubes and the polymer [95, 96].

The next step involves processing the nanocomposites using techniques like melt mixing, solution casting and in-situ polymerization. Melt mixing is carried out in the case of nanotube-thermoplastic polymer nanocomposites. Melt mixing includes processing techniques such as extrusion, injection and blow molding, and internal mixing[90]. As the concentration of nanotubes increases, more energy is required for the melt mixing to efficiently disperse nanotubes due to the increase in melt viscosity with nanotube content. Polymer composites with up to 25vol% MWNTs have been reported using high energy melt mixing techniques[97]. These processes are fast, simple, and are not solution-based. In solution processing, both thermoplastics and thermosets have been used to make nanocomposites. In this method polymer is dissolved in a solution, nanotubes are then added and dispersed in the solution and then the solution is evaporated to give a well-dispersed nanocomposite. Such nanocomposites based on

epoxy[98] and polystyrene[99] polymer matrices, amongst others, have been reported using this technique. Another widely used method is i*n-situ* polymerization which is a specific technique using solution processing. In i*n-situ* polymerization, the polymerization of the organic constituents takes place in the presence of nanotubes. The general practice involves sonicating the nanotubes in a solution themselves before adding to the constituents. [93]. This process fares well compared to the others in terms of achieving good dispersion and better interaction between the polymer and the nanotubes.

The role of the interface in nanocomposites is being recognized as critical to achieving an efficient dispersion and enhancement in properties. Vaia and Wagner [100] state six characteristics distinguishing polymer nanocomposites from traditional composites resulting from the nanoscopic dimensions and high aspect ratio of the inclusions;

- A very low percolation threshold (~0.1-2 vol%)
- Inclusion-inclusion correlation at low vol%
- Large density of inclusions per inclusion volume (10^6-10^8 inclusions/μm^3)
- Extensive interfacial area per volume of particles (10^3-10^4 m^2/ml)
- Short distances between inclusions (10-50 nm at 1-8 vol%)
- Comparable size scales between the inclusions, distance between the inclusions and relaxation volume of particle chains.

The interfacial region is ascribed properties different from the inclusion and the polymer matrix. This region is usually thought to extend into the matrix through approximately $4R_g$ distance where R_g is the radius of gyration[100]. In polymers, many

important static and dynamic properties are dependent on this term. In nanocomposites in general, due to large number of inclusions, the size of interfacial region is comparable to that of the distance between the inclusions. Thus the relative volume fraction and importance of the interfacial region becomes more significant in nanocomposites. Good dispersion and strong interaction between the inclusions and matrix go hand in hand. Good dispersion results in more inclusion interfacial area available and better properties. Hence researchers have concentrated their efforts on strengthening the polymer – nanotube interaction to exploit the properties of CNTs.

In CNT – polymer composites the CNTs used are either as produced, where they have not been subjected to any alterations, or functionalized where the nanotubes and the polymer share an interaction due to chemically adding functionality to the nanotubes. As produced nanotubes can also share a non-covalent interaction with the polymer matrix either by treating the nanotubes with surfactants, by polymer wrapping or due to the nature of the polymer matrix itself. Here there is an added functionality but the chemical modification of the nanotubes is avoided.

In the CNT polymer composites using as-produced, unmodified CNTs, Shaffer and Windel[101] were amongst the first to carry out an investigation into the mechanical properties of nanotube-polymer composites. They did so on MWNT- poly vinyl alcohol(PVA) composites made by the solution processing method. The stiffness of the material was considerably low at room temperature. The axial modulus of the nanotubes used to achieve a good fit for the observed experimental in plane stiffness was around 150 MPa which was well below values predicted for MWNTs (~50 GPa). These low

values were attributed to the poor load transfer between the matrix and the nanotubes. The nanotubes used in the study were unfunctionalized. Both, purity of the nanotubes and issues with the interfacial bonding were the reasons behind the low values. This means that when the interfacial adhesion is weak the load transfer between the matrix and the nanotube does not occur efficiently and the polymer ends up taking most of the stress. Qian et al.[99] had better results with MWNTs and polystyrene with around 40% increase in the elastic modulus at 1wt% MWNT loading. They achieved this by using better quality nanotubes and using sonication to predisperse the nanotubes in a solution before using the solution processing method, thus improving dispersion leading to better reinforcement of the polymer. MWNT pull out tests using an AFM tip measure the interfacial shear stress required to pull out the nanotube[102] have shown values around 47 MPa which is high compared to that of less than 10MPa observed in conventional fibers embedded in polymer. Other literature on this subject also reveals that including pristine nanotubes in polymer for enhancing mechanical properties is advantageous but the gains observed do not justify the use of high cost materials like nanotubes. The solution for this issue seems to be in increasing the strength and nature of the interaction between the nanotubes and the polymer matrix they are embedded in.

The walls of the carbon nanotubes are usually unreactive to most polymer matrices. Anchoring or bonding the nanotubes either covalently or non-covalently with the polymer matrix would help in achieving a better dispersion due to the improved interaction between the nanotubes and the polymer matrix. This can be done in two ways, using covalent or non-covalent functionalization. Covalent functionalization

involves chemically modifying the nanotubes to add a functional group to the nanotube wall so they interact more effectively with the polymer matrix called covalent functionalization. Second technique involves promoting interaction while avoiding chemical modification of the nanotubes and has no added functional group to the nanotube and is termed as non-covalent functionalization. Figure 1.19 shows the different covalent and non-covalent functionalizations used in carbon nanotubes.

The governing principle behind chemically functionalizing the nanotubes is to add a molecular group that is covalently bonded to the wall of the nanotube (Figure 1.19a); another similar method is adding a reactive group at the defect points in the nanotube which are caused during purification (Figure 1.19b). These added groups then react chemically with the polymer chains leading to a better bonding between the nanotube and the polymer matrix. Covalent functionalization promises an effective interaction with the polymer matrix due to the freedom of attaching suitable groups to the nanotubes which can mechanically lock with the matrix chains or react with them.

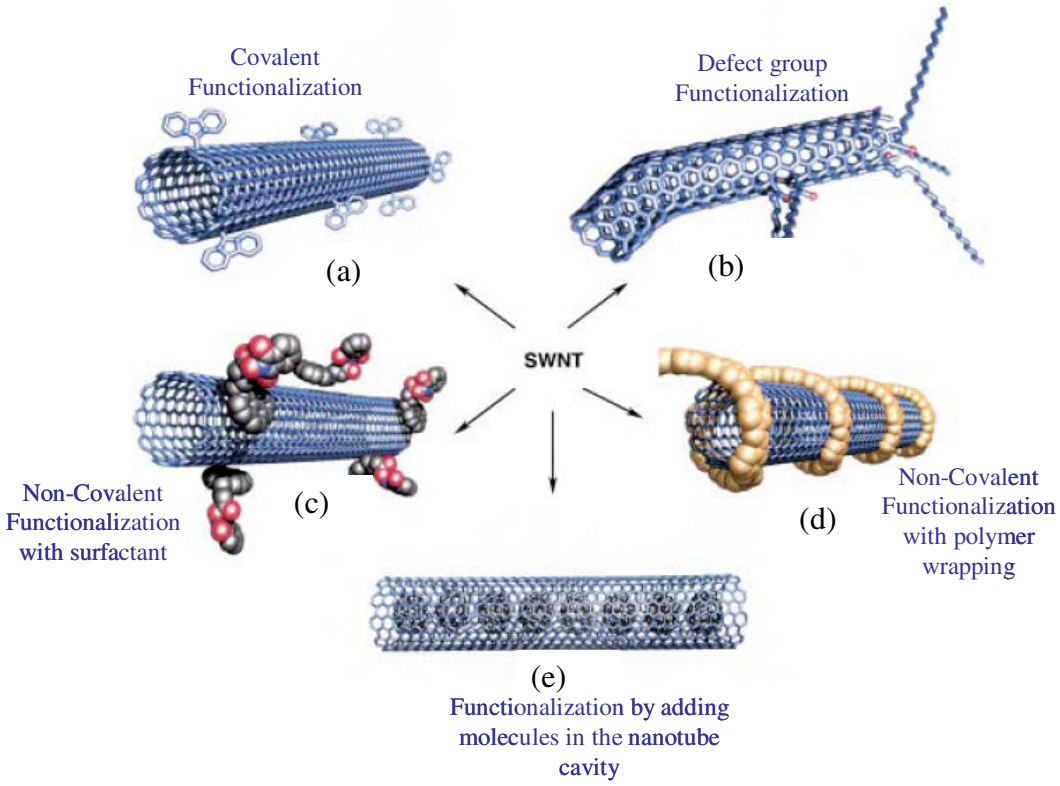

Figure 1.19 (a) Covalent functionalization, (b) defect group functionalization, (c) non-covalent functionalization using surfactant,(d) non-covalent functionalization with polymer wrapping, (e) endohedral functionalization (adapted from [96])

Ramanathan et al. [103] discuss amino functionalization of nanotubes by adding amine or amide group onto the SWNT wall. The amide functionalized nanotubes were then used to make poly(methyl methacrylate) (PMMA) – SWNT nanocomposites[104] as shown in Figure 1.20. The amide group then reacts with PMMA forming a stronger bond between the nanotubes and polymer leading to better dispersion and improved mechanical properties. Figure 1.21a shows the SEM image of the fracture of 1% pristine SWNT-PMMA composite while 1.21b shows that of 1% amide functionalized SWNT-

PMMA composite. SEM images show a better dispersion of functionalized nanotubes compared to the pristine. This study also sees an increase of around 86% in the storage modulus for the functionalized SWNT-PMMA composite compared to a 48% increase for the pristine case, both compared to pure PMMA.

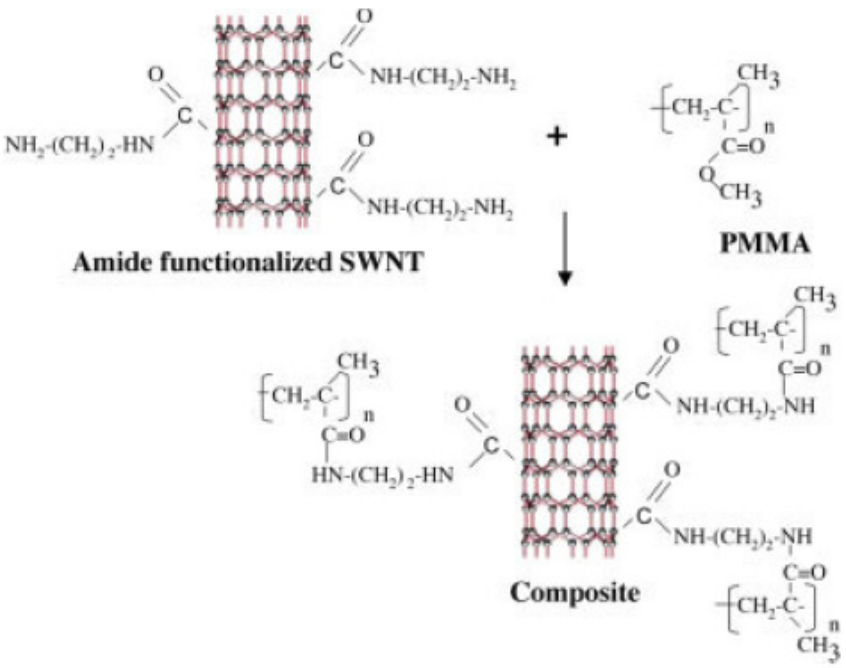

Figure 1.20 Amide covalent functionalization of SWNTs used to improve dispersion of SWNT-PMMA composite[104]

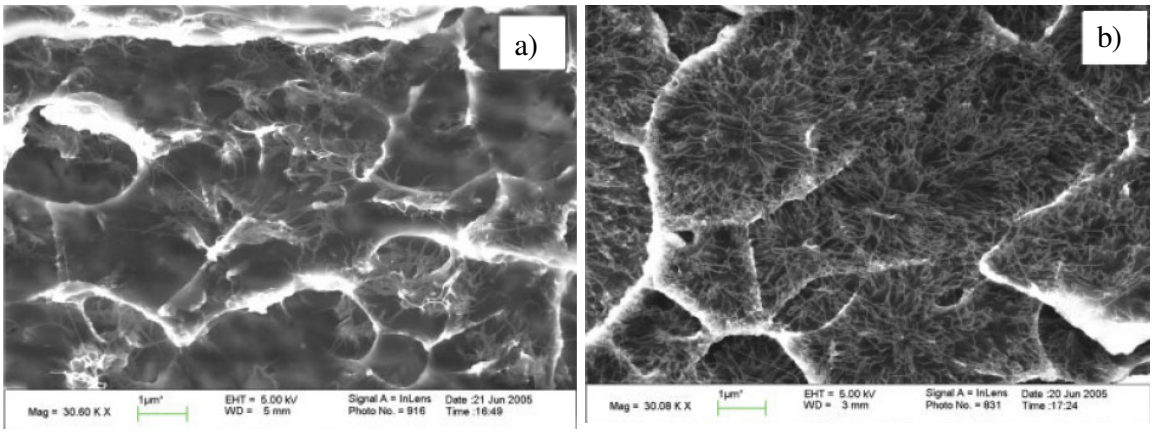

(a) (b)

Figure 1.21 SEM images of fracture surfaces of (a) 1% unfunctionalized SWNT +PMMA and (b) 1% amide functionalized SWNT+PMMA[104]

Miyagawa et al[105] have studied the properties of fluorinated SWNT-Epoxy nanocomposites. A DMA was used to determine the mechanical properties of these composites. An increase of 33% was seen in the storage modulus at 0.3wt% SWNT content at room temperature. The fluorine atoms in the functionalized nanotubes are said to disrupt the van der Walls forces between the nanotubes leading to a better dispersion and hence mechanical properties. Figure 1.22 shows one experiment which demonstrates the increase in the interfacial shear strength between a MWNT and an epoxy matrix. The MWNTs used in the study are amine functionalized. The strength is demonstrated as the outermost layer of the nanotube, which is still bonded to the epoxy matrix, remains embedded in the matrix even after the MWNT is pulled out[106]

The effect of functionalization although is not all positive on the mechanical properties of nanotubes themselves and nanotube polymer composites. Garg and

Sinott[107] have shown using molecular dynamics simulations that the mechanical strength of the nanotubes actually decrease by around 15% due to chemical functionalization.

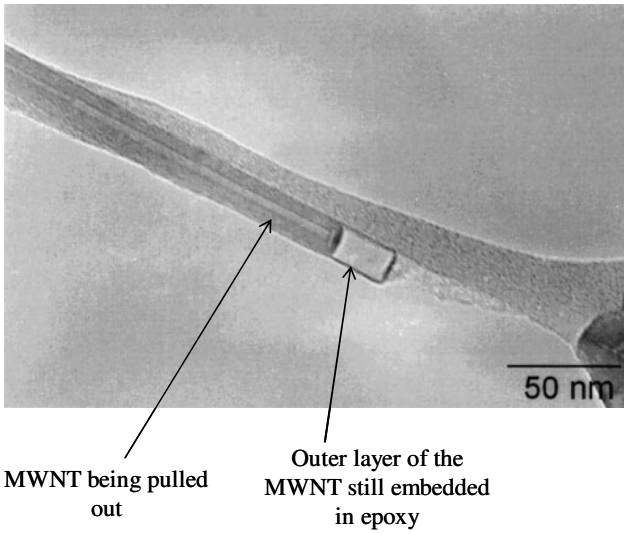

Figure 1.22 Interaction between functionalized MWNT and epoxy(adapted from[106])

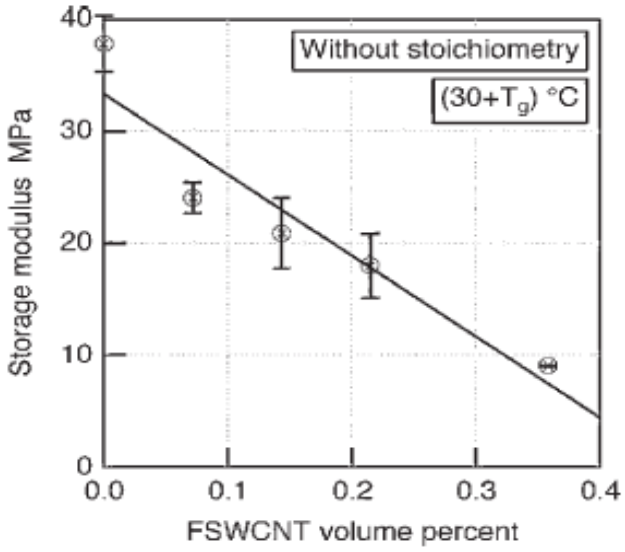

Figure 1.23 Decrease in storage modulus of Epoxy nanocomposite as a function of fluorinated SWNT content above Tg of Epoxy[105]

Though Miyagawa et al[105] see an increase in storage modulus at room temperature they see a decrease in the modulus value as a function of the fluorinated SWNT content above its T_g as seen in Figure 1.23

Other studies with functionalized nanotube polymer composites show no appreciable enhancement in properties. Santos et al[108] have studied the properties of COOH functionalized MWNTs dispersed in PMMA by *in-situ* polymerization. An increase in tensile strength was seen for 1.5 wt% functionalized MWNT-PMMA samples compared to 1 wt% pristine and 1 wt% functionalized nanotube-PMMA composites. But the tensile strength of the composites with 1 wt% pristine and 1wt% functionalized nanotubes was similar. Thus studies on functionalized nanotube - polymer composites do not provide unequivocal evidence of the advantages on mechanical properties of using functionalized nanotubes instead of pristine nanotubes in CNT- polymer nanocomposites.

The biggest drawback in functionalizing CNTs is the dramatic changes in their electrical? properties [109]. The functionalization alters the Fermi level and thus the electron energy levels of the nanotubes. This occurs due to introduction of an impurity state near the Fermi level. The addition of a covalent bond on the nanotube leads to the formation of σ bonds at the expense of the π bond. This affects the conduction band and hence the electrical conductivity of the nanotubes. Thus multifunctional applications which rely on the electrical conductivity of the nanotubes to add a useful functionality will suffer.

Non-covalent functionalization is another means to increase the interaction between the nanotubes and the polymer while preserving the desirable electrical properties of the nanotubes. This can be achieved by using surfactants (Figure 1.19c), non-covalent functionalization by wrapping the nanotube with a polymer which occurs due to a need to avoid unfavorable interactions between the apolar nanotube walls and the solvent used (Figure 1.19d), and endohedral functionalization where a guest molecules are added in the inner cavity to modify the reactivity of the nanotube (Figure 1.19e)[96]. Non-covalent functionalization of nanotubes to aid dispersion is gaining popularity amongst researchers because, in theory, it promises to achieve the desired dispersion and mechanical properties while keeping the electronic properties of the nanotubes unchanged. There have been various studies related to taking advantage of the non-covalent functionalization of nanotubes towards their dispersion in acids, water and polymers.

Ramesh et al.[110] have observed efficient dispersion of SWNTs in superacids due to the protonation of the material, leading to a fractional positive charge over the tube, hence leading to repulsion between them thus avoiding agglomeration. This is schematically represented by Figure 1.24.

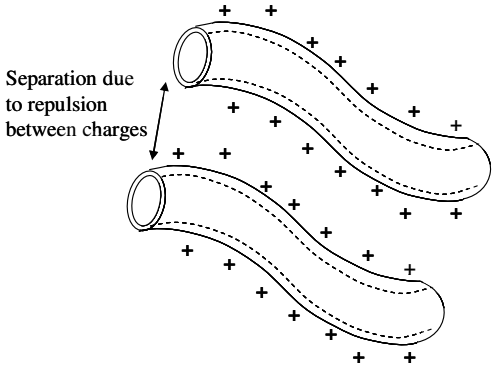

Figure 1.24 Separation between nanotubes due to repulsion caused by protonation

The stability depends on the strength of the base ion in the system. An isotropic system is seen at very low concentration of SWNTs. As the concentration increases to about 0.25% long strands are seen as the neighboring strands experience repulsion due to protonation shown by a Transmission electron microscopy (TEM) image shown in Figure 1.25. At high concentrations of SWNTs nematic mesophase type nature is observed. Figure 1.26 shows a scanning electron microscope (SEM) image of aligned nanotube bundles deposited due to deprotonation by use of water at a high SWNT concentration of 4 %. Thus a nematic mesophase can be inferred from the image.

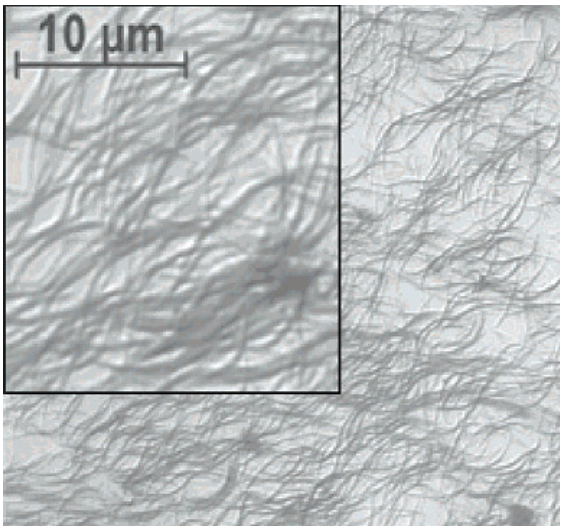

Figure 1.25 TEM image of 0.25% SWNT concentration in 100% sulfuric acid[110]

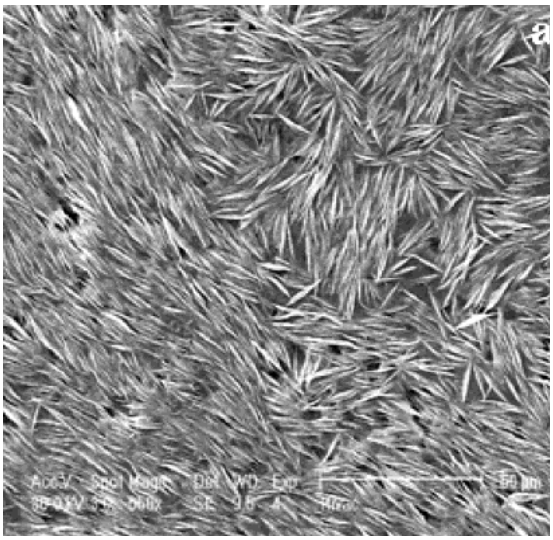

Figure 1.26 SEM image of precipitated aligned SWNT species from 4% SWNT in oleum (20%SO3)[110]

O'Connel et al. [111] have managed to solubilize SWNTs in water by non-covalently associating them with linear polymers like polyvinyl pyrrolidone (PVP) and polystyrene

sulfonate (PSS). This is a result of a thermodynamic drive to eliminate the hydrophobic interface between the tubes and the aqueous medium. The wrapped polymer also manages to disrupt the nanotube - nanotube interaction which usually leads to agglomerates. Figure 1.27 shows different possibilities of PVP wrapping onto the SWNT.

Thus this is another account of a non-covalent interaction leading to a better dispersion of nanotubes. Figure 1.28 shows a tapping mode AFM image of the PVP-SWNT supramolecular aggregates adsorbed onto the amine-functionalized substrates; it indicates that most aggregates are a single SWNT associated with a monolayer of polymer indicating a separation between nanotubes and a good dispersion.

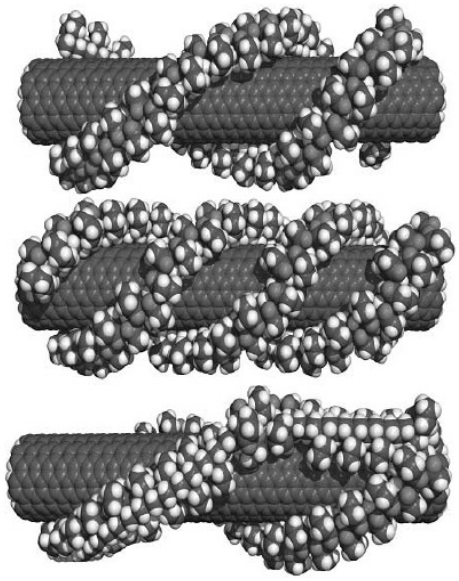

Figure 1.27 Possible wrapping arrangements of PVP on SWNT[111]

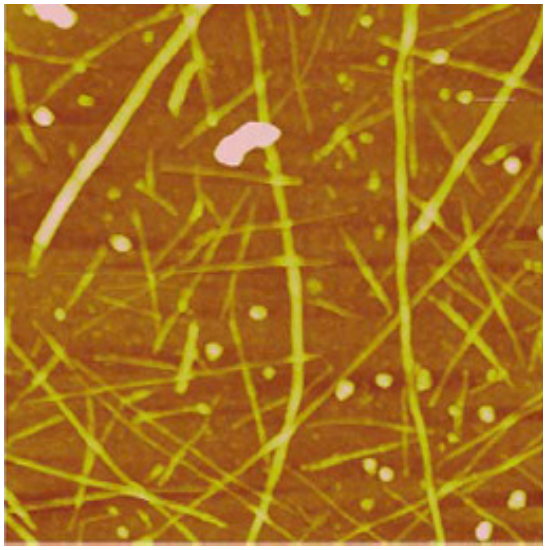

Figure 1.28 Tapping mode image of PVP-SWNTs on a functionalized substrate [111]

A unique study was carried out by Chen et al. [112] to aid dispersion and mechanical property improvement of polymer-SWNT nanocomposites. They have used non-covalent functionalization for efficient dispersion. Rigid and conjugate macromolecules, poly(p-phenylene ethynylene)s (PPEs) are used to non-covalently functionalize and solubilize the SWNTs and attain good dispersion in the polymer (Parmax) matrices. The non-covalent interaction was attributed to a π- π interaction between the carbon nanotube walls and the backbone of PPE. This group was able to engineer the properties of the nanocomposites. Figure 1.29 illustrates different PPEs used in this study to non covalently functionalize the nanotubes. PPE1 provides a weak van der Waals attraction

and modest mechanical locking between the aliphatic side chain and Parmax. PPE2 due to its branched aliphatic chain leads to a stronger interlocking compared to PPE1. PPE3 provides the strongest interaction with van der Waals forces, mechanical interlocking and in addition a π- π interaction between ferrocenyl groups and Parmax. The Parmax 2% PPE1-SWNT composite showed an increase of 8% in the tensile strength to break and an improvement of 36% in the Young's modulus compared to pristine Parmax and a ten orders of magnitude increase in the electrical conductivity. Parmax 2% PPE2-SWNT composite showed an enhancement of 47% in tensile strength and 51% in Young's modulus with respect to the pristine Parmax. Correspondingly the third composite Parmax 2% PPE3-SWNT shows an enhancement of 72% in the tensile strength and twelve orders of magnitude increase in the electrical conductivity. The study was thus successful in tailoring the interface between the nanotube and polymer matrix by noncovalent means. Improvement in mechanical properties was achieved without sacrificing the excellent electrical properties of nanotubes due to their unique electronic structure.

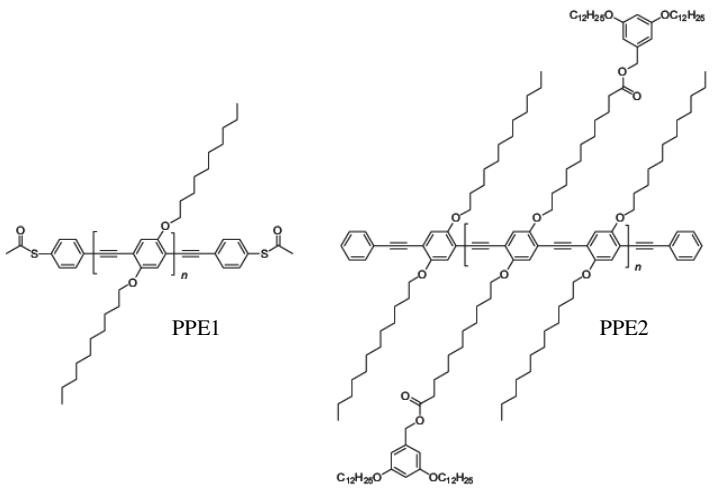

(a) (b)

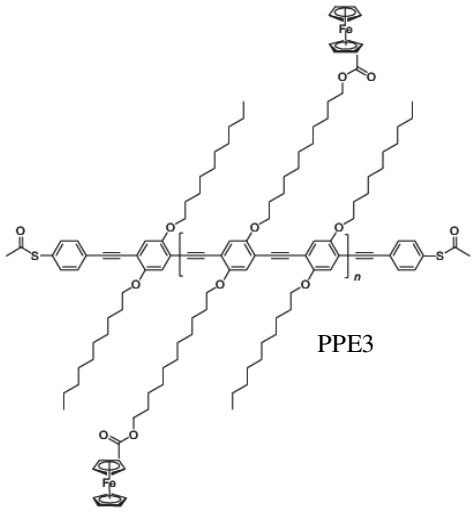

(c)

Figure 1.29 Chemical structures of PPEs used to non-covalently functionalize parmax (a) PPE1 with aliphatic side chains, (b) PPE2 with branched aliphatic side chains and (c) PPE3 ferrocenyl-group-terminated aliphatic side chain[112]

Another study by Wise et al. [113] has demonstrated that an interaction is possible between the SWNT and the polyimide matrix. The interaction is identified between the electronegative nitrile group (CN) and the SWNTs in a polar polyimide-SWNT nanocomposites. This is thought to result from an electron donor-acceptor relationship between the SWNT and the polymer respectively. Raman spectroscopy showed an upshift in the 1592 cm^{-1} G band frequency of the SWNTs of around $4cm^{-1}$ when dispersed into the polyimide matrix. Also Fourier transform infrared spectroscopy (FTIR) was performed to investigate the change in the CN stretching mode. A downshift of $2cm^{-1}$ was seen. Both these results indicate a charge transfer between the nitrile group and the SWNT. Wise et al. believe that the SWNT acts as the electron donor. Further the electronegativity of the monomer was computed to be -5.11 eV while the experimentally derived values of SWNTs are at -4.8 to -5.0 eV. Thus the chemical potential equalization drives the partial charge transfer from the SWNT to the monomer confirming the hypothesis. The polar nature of the polymer matrix and the consequent interaction between the nanotube and the dipole in the polyimide result in a non-covalent functionalization and a good dispersion.

Along with the improvement in mechanical properties in CNT- polymer composites, other properties like electrical and thermal conductivity and optical properties also see an improvement. Due to the high aspect ratio of CNTs, the concentration required to achieve conductivity in the CNT-polymer composites is usually very low. A threshold of as low as 0.05-0.06 vol% SWNTs has been reported in polyimide nanocomposites[93, 113, 114]. Due to their low percolation thresholds, these composites have been suggested for

electrostatic discharge applications in aerospace structures since they combine optical transparency and electrical conductivity [114]. Applications have also been suggested by a group at DuPont for use of MWNT-polyaniline composites as printable conductors for organic electronics devices[115]. Carbon nanotubes have been added to conducting polymers to enhance their mechanical strength and conductivity, and reduce thermal degradation[116, 117]. MWNT-epoxy composites have shown an enhancement in thermal conductivity of about 110-120%[98] due to the presence of the MWNTs. Both SWNTs and MWNTs have known to possess non-linear optical properties and thus the nanotube composites may also find applications as optical devices [118]. Their unique optical properties occur due to the nanoscale dimensions and electronic band structure of the nanotubes.

Thus carbon nanotube-polymer composites have been investigated in detail, part of which has been discussed here, for different applications, trying to take advantage of enhancement in properties that result from incorporating carbon nanotubes into a polymer matrix. The investigations predominantly have been into mechanical, electrical and thermal properties of these carbon nanotube based nanocomposites.

1.4 Problem Statement

The preceding sections have reviewed the development and applications of EAPs and carbon nanotube-polymer nanocomposites. Nanocomposites show promise of application in various fields, ranging from aerospace vehicles to microelectronics. EAPs are exciting new active materials which will also find applications in different spheres of

our lives. If nanocomposites are made electro-active, this offers a union of both these fields and a new set of applications. One would be able to make strong, tough, active structures wherein the active nature is the property of the material itself.

Polyimides for example find application in aerospace vehicles as support structures due to their light weight, flexible nature and their ability to with stand harsh space environments. But these polymeric materials do not show any active response, and cannot be incorporated into systems which require an actuation or a sensing function like sampling systems or solar panel deployment mechanisms in aerospace vehicles. The main challenge in such a scenario is to create an active nature in such materials and also take advantage of the inherent properties they offer. Efforts have been made to change the nature of the polymer itself by engineering dipoles onto the main chain to make them active [119-121]. But even these polyimides do not show a measurable actuation response. The other route is to create an active nature in these polymers by adding inclusions. Earlier studies have shown an increase in the piezoelectric constants of piezoelectric polyimides with increase in SWNT content. This provides a strong motivation to investigate the effect of SWNTs not only in sensor applications but also on the actuation ability of polymers.

The broad goal of this research was to investigate whether polymer nanocomposites based on carbon nanotubes can have an active nature along with enhanced mechanical and electrical properties. The study focuses on developing a nanocomposite capable of actuating by dispersing the nanotubes into a non-polar polymer. An electromechanical coupling is thus created in these nanocomposites due to the interaction between the

nanotubes and the polymer matrix. This is a key development as carbon nanotube-based nanocomposites have till date not demonstrated an electromechanical (actuation) response.

SWNTs are dispersed in two different polymers. The first is a non-polar polyimide CP2 with diamine 1,3-bis(3-aminophenoxy) benzene (APB) and dianhydride 2,2-bis (3,4-anhydrodicarboxyphenyl) hexafluoropropane (6FDA) and the second is a polar polyimide (β-CN)APB-ODPA with a nitrile substituted diamine, 2,6-bis(3-aminophenoxy) benzonitrile (β-CN) APB, and dianhydride, 4,4-oxydiphthalic anhydride (ODPA). Uniformly dispersed nanocomposites are prepared by a novel technique involving *in-situ* polymerization under sonication. These nanocomposites with varying SWNT content are then tested for actuation with an in house setup using both DC and AC fields. The actuation response to these fields is studied at different field strengths, SWNT loading and polyimide matrices. The electromechanical response is assessed qualitatively and quantitatively. The mechanism behind the actuation is determined as electrostriction and the physical phenomenon driving this mechanism is studied using dielectric relaxation studies.

The objectives of this study are: (1) to study the creation of an actuation response in a non-polar polyimide by adding carbon nanotubes; (2) to quantify the actuation response and its dependence on field, carbon nanotube content and polarity of the polymer matrix; (3) to compare the physical properties of polar polyimide nanocomposites with that of the non-polar nanocomposites; and (4) to investigate the mechanism driving the actuation response and the effect of different physical factors on it.

1.5 Organization of Sections

This study on the design and enhancement of an actuation response in polyimides is divided into five Sections. Section 1 deals with the background on Electro-active polymers, single walled carbon nanotubes (SWNTs) and SWNT-polymer composites. The importance of the interface and the efforts to enhance the same are also discussed. The problem statement of the study is then introduced.

Section 2 is the experimental section which describes processing of polyimide-SWNT nanocomposites, microscopy studies, and characterization of electrical, dielectric, mechanical and electromechanical properties of the composite films. The experimental setups and methodology used for the measurement of electrical, dielectric, mechanical and the electromechanical properties of the composite films are discussed. Dielectric relaxation spectroscopy techniques consisting of thermally stimulated current (TSC) measurements and impedance analysis are described. These techniques are used to measure the dipolar relaxation in the nanocomposites.

Section 3 discusses the results obtained for the electrical, dielectric, mechanical, actuation characterization, dielectric relaxation spectroscopy and microscopy results for both the non-polar and polar polyimide-SWNT composites. These properties are compared for both cases and as a function of SWNT content. The possible sources of enhanced remnant polarization and actuation are also discussed.

Section 4 gives the conclusions of the study and recommends future follow up work.

2. EXPERIMENTAL

2.1 Processing and Scanning Electron Microscopy (SEM) of SWNT-Polymer Composites

The SWNTs used in this study are laser-ablated SWNTs acquired from Rice University, and those made by a high pressure carbon monoxide (HIPCo) process. In the laser-ablated process a mixture of carbon and transition metals are evaporated by a laser impinging on a graphite-metal composite target [122, 123]. The target is kept in a controlled environment at temperatures around 1200^0C and in the presence of an inert gas. The nanotube vapor condenses on the cooler part of the reactor. HIPCo uses carbon monoxide as the carbon source. This is a gas-phase catalytic process which involves passing carbon monoxide along with an organometallic catalyst ($Fe(CO)_5$) in a heated furnace [124]. $Fe(CO)_5$ decomposes to give iron clusters which act as nuclei around which SWNTs are deposited.

An aromatic colorless polyimide (PI), CP2 (APB-6FDA) [93] whose chemical structure is shown in Figure 2.1, and a polar polyimide (PI), (β-CN)APB-ODPA [113] whose chemical structure is shown in Figure 2.2 are used as the matrix materials. The SWNT-PI composites are prepared by in situ polymerization under sonication. The diamine and dianhydride used to prepare CP2 are; 1,3-bis(3-aminophenoxy) benzene (APB) and 2,2-bis (3,4-anhydrodicarboxyphenyl) hexafluoropropane (6FDA) respectively, and those used for the (β-CN)APB-ODPA are; 2,6-bis(3-aminophenoxy) benzonitrile (β-CN)APB (diamine), and 4,4-oxydiphthalic anhydride (ODPA--dianhydride).

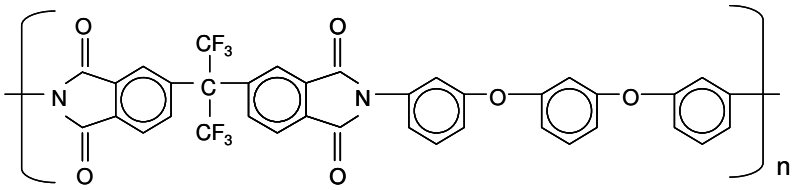

Figure 2.1 Chemical structure of CP2

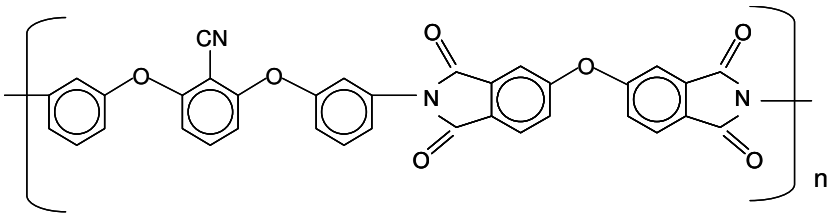

Figure 2.2 Chemical structure of (β-CN) APB-ODPA

Both PIs were developed by researchers at NASA Langley Research Center. CP2 was developed by St.Clair et al[125] and (β-CN) APB-ODPA by Simpson et al[126].

The SWNT-CP2 composites were prepared at NASA Langley by Park et al.[93] using the following process. SWNTs are dispersed in anhydrous dimethyl formamide (DMF). After stirring, APB is added to the solution then the 6FDA. The whole process is carried out with stirring, in a nitrogen purged flask immersed in a 40kHz ultrasonic bath. This is done until the solution viscosity increases and stabilizes. Sonication is terminated after 3 hours and the stirring is continued for several hours to form a SWNT-poly(amic acid)

solution. Acetic anhydride and pyridine are added to chemically imidize the SWNT-poly(amic acid) solution. The SWNT-CP2 solution is then cast onto a glass plate and dried in a dry air flowing chamber. The dried tack free film is then thermally cured in an air circulating oven at 110, 170, 210, and 250°C for 1 hour each to obtain solvent-free SWNT-CP2 film. A series of nanocomposite films are prepared with the SWNT concentrations varying from 0 to 2 vol% [93]. The SWNT-β-CN APB ODPA composites were prepared by a similar method with SWNTs concentrations varying from 0 to 5 vol% [113].

Scanning Electron Microscope is an electron microscope that produces high resolution images of the sample surface. In an SEM an electron beam is produced either by accelerating electrons from a cathode to an anode or by using field emission technique. The beam passes through scanning coils in the objective lens which then deflects the beam over the sample surface using the raster method. The scattered electrons are detected to form the high resolution image of the surface. SEM images are taken to study dispersion and SWNT-Polyimide interaction using a Zeiss 1530 high resolution, variable pressure FE (Field Emission) SEM. The SWNT – PI composites are fractured after immersing and freezing in liquid nitrogen. The conductive coating used is Pt-Pd.

2.2 Electrical and Dielectric Characterization of SWNT-Polyimide Films

Electrical and dielectric characterization of nanocomposite films provides us with a qualitative tool to analyze the dispersion of SWNTs in the polyimide. The dielectric and

conductive response of a polymer is a result of its capacitive nature (ability to store charge) and its conductive nature (ability to pass charge). Figure 2.3 is a schematic representation of the equivalent circuit model of a polymer under test shown by a resistor and a capacitor in parallel. In polymer, the capacitive nature decreases as its conducting nature increases in response to added inclusions or impurities and hence it is represented by the equivalent circuit model with the resistor and capacitor in parallel.

The phase angle (θ) is the lag between the input voltage, V_{in} and output current, I_{out}. In capacitors this angle is 90° while resistors have a value of 0°. Hence for the capacitor and resistor in parallel this value is somewhere between 0° and 90°. The I_{out} for the polymeric material can then be separated into capacitive and conductive components as,

$$I_{capacitive} = I_{out}\sin(\theta) \quad (2.1a)$$

$$I_{conductive} = I_{out}\cos(\theta) \quad (2.1b)$$

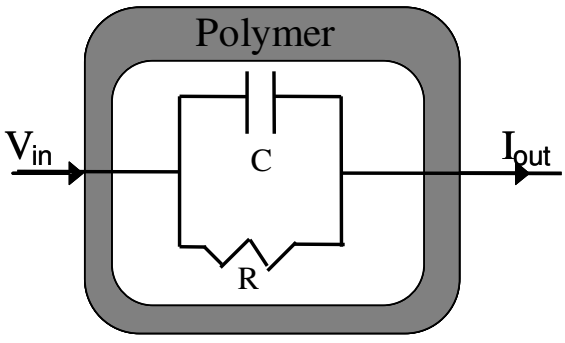

Figure 2.3 Equivalent circuit model for dielectric polymer

The capacitance (C_p) of the material is then given by;

$$C_P = \frac{Q}{V} = \frac{I_{out}}{V_{in}\omega}\mathrm{Sin}(\theta) \tag{2.2}$$

Where, Q is the charge on the capacitor under a voltage V, angular frequency $\omega = 2\pi f$, where f is the test frequency and θ is the phase angle. Resistance (R_p) of the material is then given by;

$$R_P = \frac{V}{I} = \frac{V_{in}\omega}{I_{out}\mathrm{Cos}(\theta)} \tag{2.3}$$

Conductance (G_p) of the material is the inverse of resistance;

$$G_p = \frac{1}{R_p} \tag{2.4}$$

Figure 2.4 shows the schematic of the experimental setup used in the lab to measure the capacitance and conductance in the nanocomposite films. The faces of the samples are electroded using a silver paint and silver deposited by vapor evaporation to form conducting surfaces. The input signal V_{in} is applied by the QuadTech precision LCR meter (Figure 2.5), which also measures the output current I_{out}. The samples are connected to the LCR meter through the teflon sample holder.

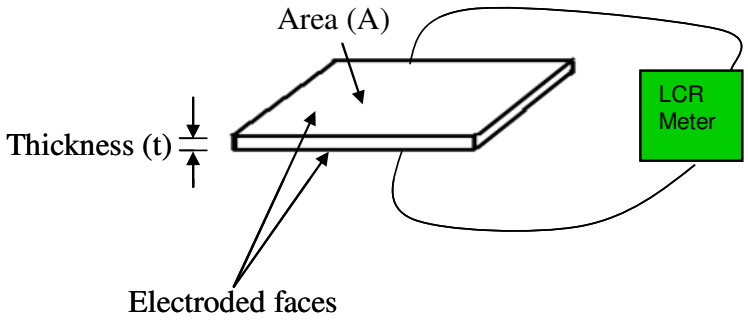

Figure 2.4 Measurement of electric and dielectric properties of SWNT-polyimide nanocomposites

Figure 2.5 LCR meter

The dielectric and conductive properties of the material are described by complex permittivity (ε^*) and complex conductivity (σ^*). These values have a real and a complex part given by

$$\varepsilon^* = \varepsilon' + i\varepsilon'' \quad (2.5a)$$

$$\sigma^* = \sigma' + i\sigma'' \quad (2.5b)$$

ε' and ε'' are the dielectric constant and loss, while σ' and σ'' are the conductivity and loss respectively. The dielectric constant (ε) of the material then depends on the capacitance , the thickness of the sample t and the electroded area A;

$$\varepsilon' = \frac{(C \cdot t)}{(\varepsilon_0 \cdot A)} \tag{2.6}$$

where ε_0=8.85x10^{-12} F/m is the permittivity of free space.

The dielectric loss is given by;

$$\varepsilon'' = D_f \cdot \varepsilon' \tag{2.7}$$

D_f is the dissipation factor. This value is also called loss tangent (tanδ) and is equal to tan(90° - θ).

Also the real part of conductivity (σ') is described by;

$$\sigma' = \frac{G_P \cdot t}{A} \tag{2.8}$$

2.2.1 Electric Characterization of Percolation Behavior in SWNT-PI Nanocomposites

AC electrical conductivity is measured over a range of frequencies (20Hz – 1MHz) and SWNT content using the QuadTech precision LCR meter. Electrical measurements are essential to study the percolation transition, where the material starts behaving as a conductor instead of a dielectric. It can be inferred that the lower this transition the better the dispersion of the SWNTs in the matrix. The low percolation transition means a low concentration of nanotubes is forming a conducting path. Aspect ratio, which is the ratio

of length to diameter of the nanoinclusions, plays a pivotal role in the concentration of inclusions needed to form a percolated structure, the higher the aspect ratio the lower the percolation threshold.

To understand what percolation means, flow of water through a porous medium is a helpful example. When the water is able to pass through the porous material, the percolated structure is said to have formed. Also the minimum concentration of pores at which the water manages to pass through is called the percolation concentration. In simplest terms when a percolated structure is said to have formed it means one or a cluster of pores is connected to another such cluster throughout the material. Electrical percolation is similar to the case discussed where instead of the "flow" of water through the porous media we consider the "flow" of electrons (conduction) through the material.

Electrical percolation has been analyzed using different techniques. Random resistor networks method[127], excluded volume method and numerical simulations[114] amongst others have been proposed. Random networks model involves random arrangement of the conducting and non-conducting phases. A 3-D mesh of resistors is created and then either by removing some connectors or nodes randomness is assigned to the structure. A minimum critical volume fraction is then computed which is necessary to form a percolated structure. The calculations are done analytically or computationally to solve for percolation in such a structure[127]. The excluded volume of an object is defined as the volume into which the center of another similar object cannot penetrate. For the case of cylindrical inclusions it has been predicted that the percolation threshold is inversely

proportional to this excluded volume. Simulations have been carried out by starting with an empty cell and adding inclusions till a percolated structure was formed[114].

Experimentally, dielectric spectroscopy has been employed to detect the percolation structure formed in polymer matrices by conducting fillers such as carbon black[128] and MWNTs [129]. MWNTs, unlike SWNTs for which the conductivity depends on the chirality of the tube, are always conductive. The percolation threshold is the concentration of the inclusions at which a conductive path is formed through the composite. The electrons can now pass through the material, in this case the polymeric composite, when a voltage difference is applied across it. The conductivity and dielectric constant values measured at different frequencies and nanotube concentrations give us an insight into this, which will be discussed in depth in the results section.

Furthermore the dependence of the DC conductivity on the inclusion content near the percolation threshold is given by the power law equations [127, 129];

$$\sigma' \propto \left(v_c - v\right)^{-s} \quad \text{for } v < v_c \tag{2.9a}$$

$$\sigma' \propto \left(v - v_c\right)^{m} \quad \text{for } v > v_c \tag{2.9b}$$

Where, v_c is the percolation threshold concentration and v is the concentration of the inclusion phase. Static permittivity also depends on the inclusion concentration given by,

$$\varepsilon_s \propto \left|v - v_c\right|^{-s} \quad \text{for } v < v_c,\ v > v_c \tag{2.10}$$

2.2.2 Dielectric Characterization and Dielectric Relaxation Spectroscopy

AC dielectric measurements are also carried out for the nanocomposites over the same range of frequencies (20Hz – 1MHz) using the QuadTech precision LCR meter.

Dielectric constant values are calculated using equation 2.6 from the capacitance measured by the meter. Closely related to these measurements is the dielectric relaxation study of the nanocomposites.

Dielectric relaxation measurements are carried out to investigate the polarization inherent to the structure of the polymer and/or the enhanced polarization due to presence of nanotubes. Dielectric relaxation occurs due to different polarizations present in the material system. Also each dielectric relaxation has a characteristic relaxation time and frequency. Figure 2.6 shows the different polarizations and their corresponding relaxation frequencies. These different polarizations are briefly summarized below[21];

a) Electronic polarization ($P_{electronic}$): This occurs due to the displacement of the electron density around the nucleus with respect to it due to applied electric field. Figure 2.6 (a) shows the change in shape from circular to ellipsoidal of the atom in response to the electric field.

b) Ionic polarization (P_{ionic}): is caused due to a separation of positive and negative ions by an applied field. Figure 2.6 (b) shows the separation between the ions under an applied field.

c) Dipolar polarization ($P_{dipolar}$): This is due to contributions of permanent and induced dipoles created due to the applied field. The orientation of dipoles under an applied field is demonstrated in Figure 2.6 (c)

d) Interfacial and space charge polarization ($P_{interfacial}$): Interfacial polarization is caused in a heterogeneous material due to ease in motion of charges through one phase compared to others. This leads to accumulation of charges at the

component interface in a multi-component system. This process is demonstrated in Figure 2.6 (d).

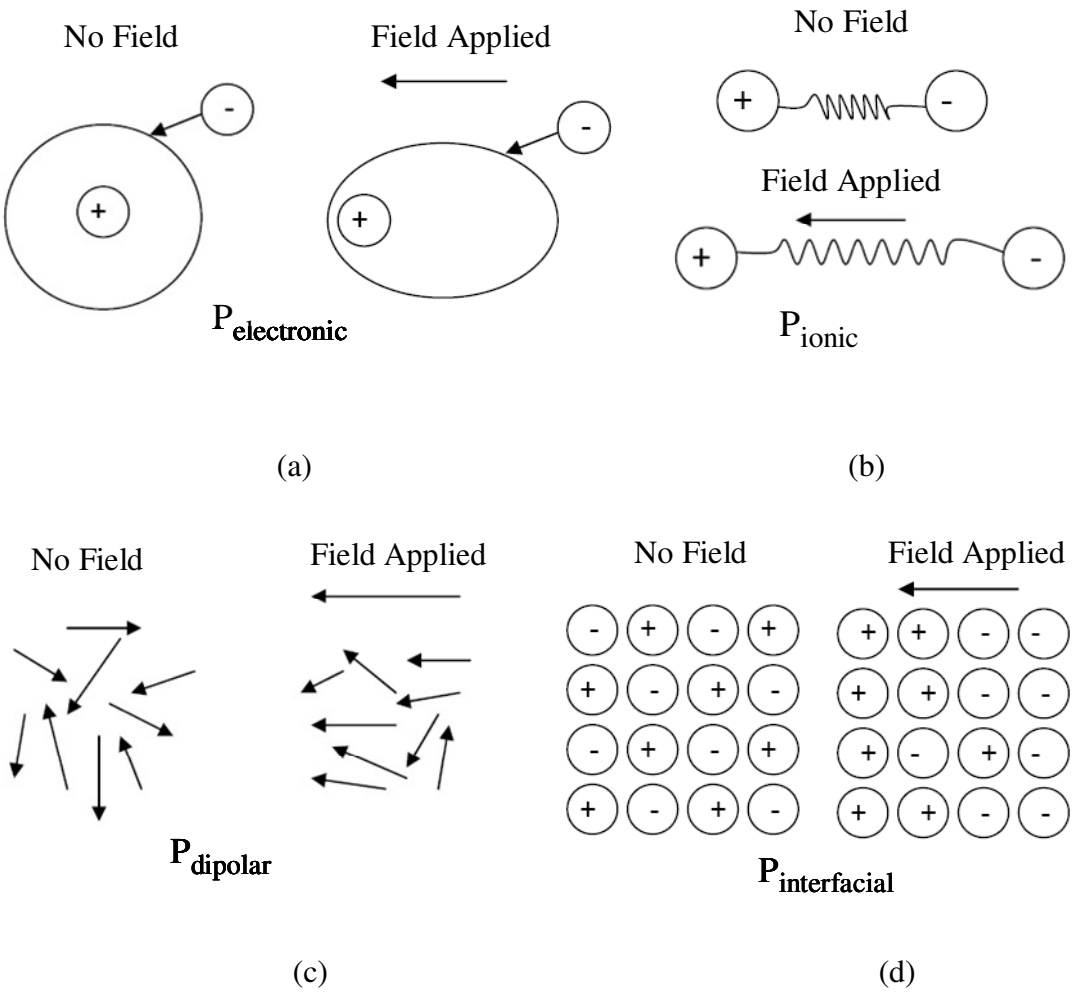

Figure 2.6 (a) Electronic polarization, (b) ionic polarization, (c) dipolar polarization, (d) interfacial polarization and (e) relaxation frequencies of different polarizations (adapted from [130, 131])

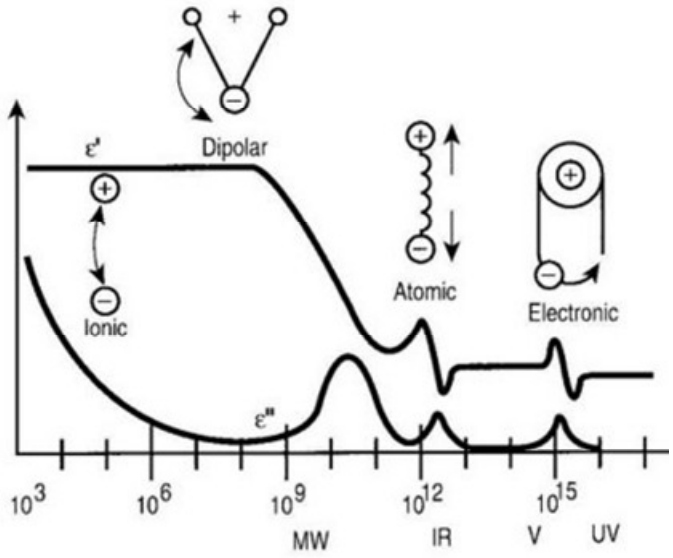

(e)

Figure 2.6 Continued

Dielectric constant as a function of temperature and thermally stimulated current (TSC) measurements are two methods used to detect and study the dielectric relaxation of the SWNT -polyimide composites.

2.2.2.1 Dielectric Relaxation

The dielectric relaxation results from movement of permanent and induced dipoles called dipolar relaxation and that of the electric charges called ionic relaxation in response to the applied electric field. The first dielectric relaxation spectroscopy technique involves measuring the dielectric constant as a function of temperature at different frequencies using a Sun Systems environmental chamber in combination with the QuadTech precision LCR meter to study the dielectric relaxation in the

nanocomposites. Characteristic relaxation time (τ) is defined as the time required for the dipoles or ions to return to their original configuration. The frequency at which this occurs is called the relaxation frequency. Relaxation in polymers is also temperature dependent. As temperature increases the polymer chains, and the dipoles if they are present, tend to relax .

The nanocomposite sample is held in a teflon holder with leads connected to the LCR meter. This setup is kept inside the environmental chamber. The temperature is varied within the chamber and the capacitance and loss factor are measured and then used to compute the real and imaginary parts of the dielectric permittivity. The relaxation of the dipoles in a system is measured by a quantity $\Delta\varepsilon$ called the dielectric relaxation strength, which is the difference between the static (ε_s) and high frequency (ε_∞) limit on dielectric constant,

$$\Delta\varepsilon = \varepsilon_s - \varepsilon_\infty \tag{2.11}$$

Using the Clausius Mossotti equation,

$$\frac{N_0 \cdot \alpha}{3 \cdot \varepsilon_0} = \frac{\varepsilon' - 1}{\varepsilon' + 2} \tag{2.12}$$

where N_0 is the number molecules per unit volume, α is the polarizability, ε_0 is the permittivity of space and ε' is the dielectric constant of the material, the Onsanger formula is then derived as[132, 133] ;

$$\Delta\varepsilon = \frac{N\mu^2}{3kT\varepsilon_0}\left(\frac{n^2+2}{3}\right)^2\left(\frac{3\varepsilon_s}{2\varepsilon_s + n^2}\right) \tag{2.13}$$

N is the number of dipoles per unit volume, k is the Boltzmann constant, T is temperature in K , n is the refractive index and $n^2 \approx \varepsilon_\infty$.

This value also quantifies the remnant polarization. Polarization (P) is defined as;

$$P = (\varepsilon - 1)\varepsilon_0 E \tag{2.14}$$

Remnant polarization P_R is defined by,

$$P_R = P_s - P_\infty \tag{2.15}$$

P_s is the polarization at low frequency and P_∞ is that at high frequency and are given by;

$$P_s = (\varepsilon_s - 1)\varepsilon_0 E \tag{2.16a}$$
$$P_\infty = (\varepsilon_\infty - 1)\varepsilon_0 E \tag{2.16b}$$

where, E is the applied electric field. The remnant polarization takes the linear form,

$$P_R = (\varepsilon_s - \varepsilon_\infty)\, \varepsilon_0 E$$
$$= \Delta\varepsilon\, \varepsilon_0 E \tag{2.17}$$

This polarization is due to contributions by dipoles present in the system. The $\Delta\varepsilon$ value can also be measured by using temperature instead of frequency. The behavior of dipoles under high temperature is analogous to that at low frequency, while the value of dielectric constant at low temperature is analogous to that at high frequency (Figure 2.7). At low frequency the dipoles present in the system which have a relatively high relaxation time can be oriented as the fluctuations in the electric field are low but at high frequency these dipoles lag behind the high frequency field. Similarly, in high temperature criteria the thermal energy provided to the system relaxes the polymer chains and allows the dipoles to be oriented easily similar to the low frequency case. And at low temperature the dipoles are difficult to move due to close packing of the

polymer chains and this condition is analogous to the high frequency case described earlier.

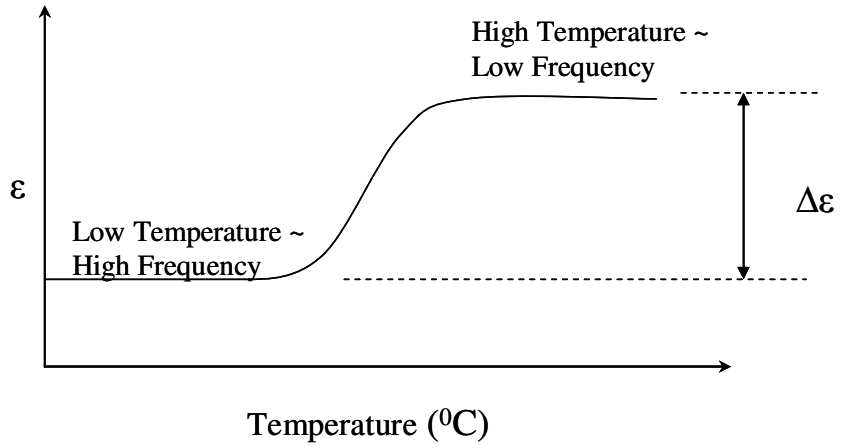

Figure 2.7 Dielectric constant as a function of temperature

2.2.2.2 Thermally Stimulated Current Measurements (TSC)

The thermally stimulated current method was proposed by Bucci et al [134]. Dielectric relaxation in polymers has been investigated to a large extent using the TSC. Certain correlations between the macroscopic properties of the polymer and the molecular structure have become possible because of this technique. It has become a powerful tool for characterizing the dielectric relaxation phenomenon in polymers. The low-equivalent frequency (10^{-3} to 10^{-4}Hz) results in a good resolution of the complex spectra resulting from the depolarization current measurement. This makes TSC very attractive technique for detection of dipoles present in the system. TSC is thus sensitive to different dielectric relaxations in the system due to this good resolution. TSC has been used in different

studies to study the dielectric relaxation phenomenon in polymers. Teyssedre et al[135] have discussed the study for Poly(ethylene terephthlate) (PET). Studies on other amorphous polymers like Poly (vinyl chloride) (PVC) and Poly (methyl methacrylate) (PMMA) have also been conducted[136]. Lacabanne et al[137] have discussed the effect of temperature on the dielectric relaxation time. The study also explored the results in the light of free volume and statistical thermodynamic theories.

Figure 2.8 shows the Setaram TherMold TSC/RMA sample cell[138]. An electroded sample is sandwiched between stainless steel disks, to which electrical contacts are made to allow poling of the sample and current measurement. This whole setup is placed in a controlled temperature chamber. The samples are usually vacuum dried and helium is pumped into the chamber to avoid arcing. The chamber is maintained at atmospheric pressure.

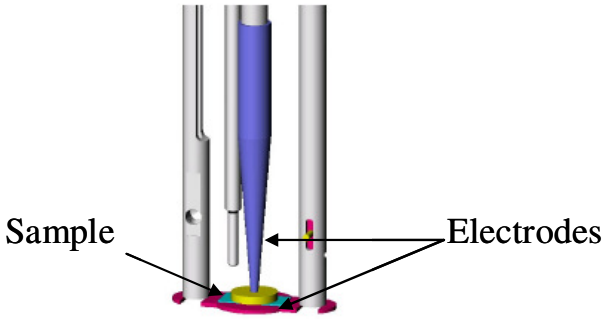

Figure 2.8 The TSC sample cell (adapted from[138])

The general method used involves polarizing the sample at a static field, E_p, at the polarization temperature, T_p, (Figure 2.9) in order to make sure the polarization reaches equilibrium. In the polymer or polymer nanocomposite case, the sample is poled by DC electric field around the glass transition temperature, T_g. The poling time is 20 minutes and is kept the same for all samples. The sample is then cooled rapidly to room temperature using liquid nitrogen (with the electric field still on) and then re-heated slowly at a constant heating rate (1°C/min) to 300°C. Upon heating the chains slowly start to relax which in turn leads to the dipolar relaxation. A current (also known as the depolarization current) is recorded due to the return of the dipoles to equilibrium state. This current shows peaks as seen by an idealized case in Figure 2.10. These peaks in the measured current physically denote the dipolar reorientation due to the relaxation and are used to calculate the dielectric relaxation strength $\Delta\varepsilon$ and remnant polarization P_R[139, 140];

$$\Delta\varepsilon = \frac{1}{\beta}\int_{T_1}^{T_2} I(T)\, dT \tag{2.18}$$

$$P_R = \Delta\varepsilon\, \varepsilon_0\, E = \int_{t_1}^{t_2} I(t)\, dt \tag{2.19}$$

where β is the heating rate and T_1, T_2, t_1, t_2, are the initial temperature, final temperature, initial time and final time for the peak (as illustrated in Figure 2.10).

Thus dielectric constant as a function of temperature and TSC measurements are used to evaluate the dielectric relaxation phenomenon and hence the behavior of dipoles in the nanocomposite films.

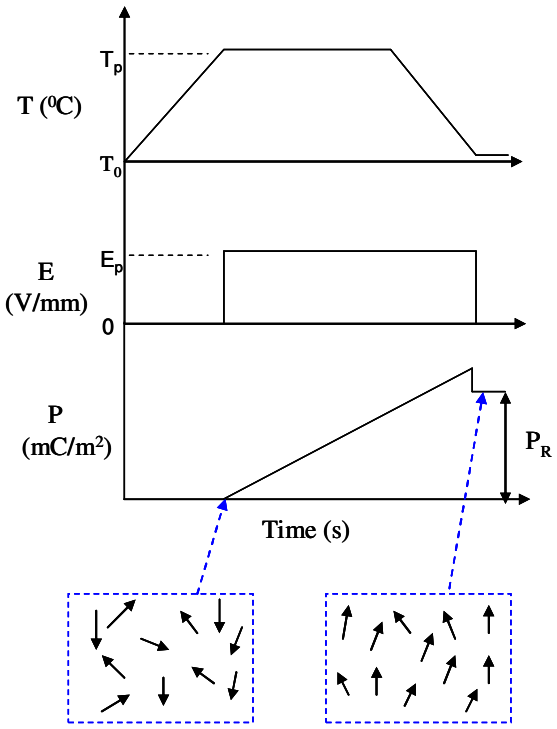

Figure 2.9 TSC poling cycle

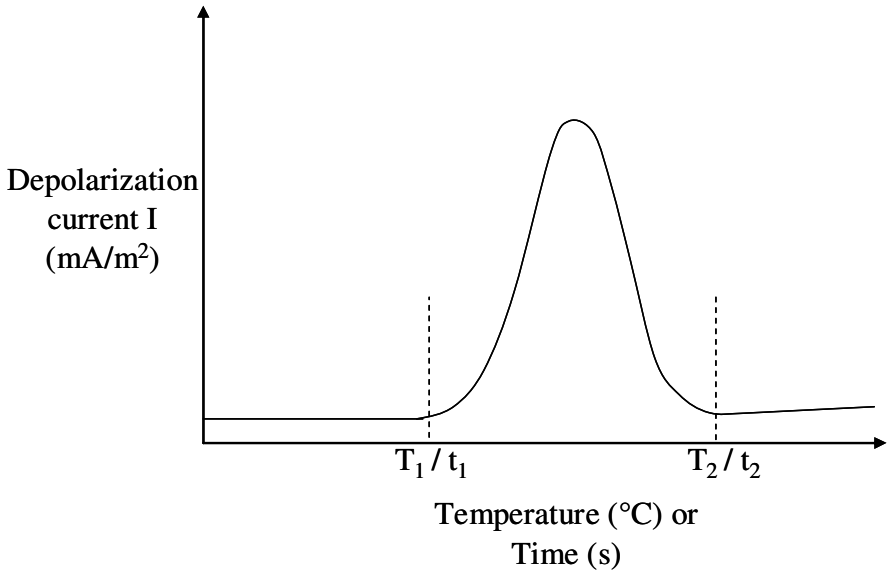

Figure 2.10 TSC heating cycle

2.3 Electromechanical (Actuation) Characterization

The nanocomposite films are coated with a thin silver layer by a vapor deposition process at NASA Langley Research Center. Thickness of the samples ranges from 30 to 60 μm. The thickness of the silver layer is kept at 100nm. The film samples are cut into strips of around 3cm x 0.5cm area, which are then used for the electromechanical tests. Figure 2.11 shows the experimental set-up used while Figure 2.12 represents the bending experiment schematically. The nanocomposite strips are sandwiched between glass plates with provisions for leads. This setup is then suspended vertically in an acrylic box chamber. The leads allow the application of electric field (DC or AC) to the strip. The bending of the sample is captured by a Fastcam high speed camera setup. An auxiliary light source is also used for better visibility. The captured videos are analyzed using Photron image analysis software**.** This software allows measurement of the sample displacement by analyzing the sample position in successive video frames.

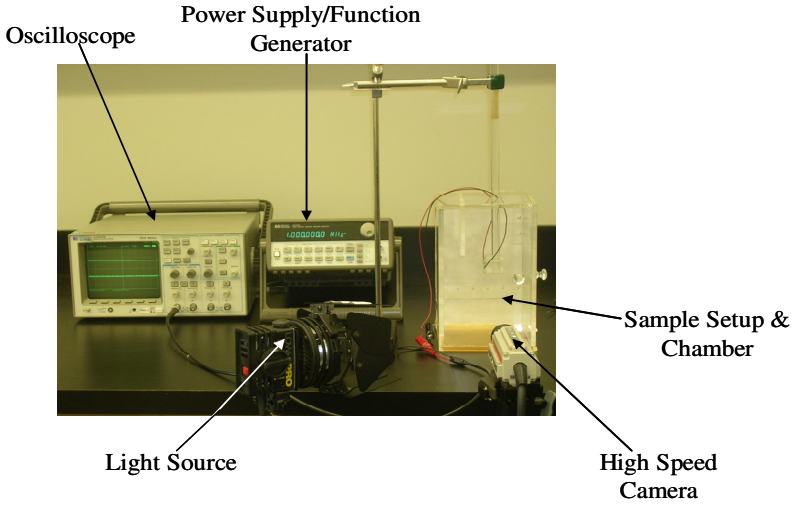

Figure 2.11 Actuation setup

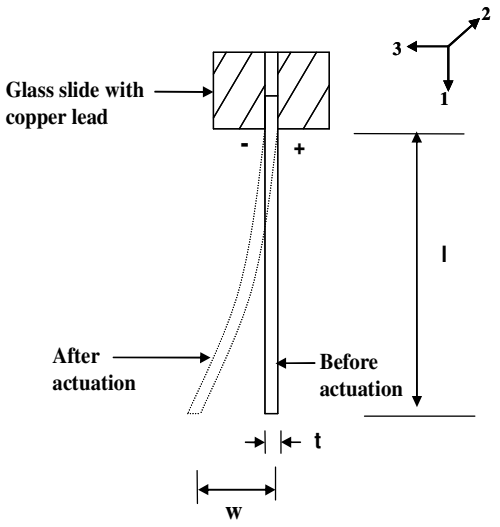

Figure 2.12 Bending actuation

The elongation strain is computed by modeling the bent strip as a cantilever beam under uniformly loaded condition, assuming a constant radius of curvature. We use the Euler Bernoulli beam theory for our calculations. This gives us a good starting point for the calculation of strains. Assuming a uniformly loaded beam (the electric field is uniform along the length of the actuation samples) with tip displacement w, thickness t and length L, the stress (T) acting on the outermost layer under a moment M is given by[141],

$$T = \frac{M}{I}\,\frac{t}{2} \tag{2.20}$$

I is the moment of inertia of the beam.

Furthermore,

$$M = \frac{FL^2}{2} \tag{2.21}$$

F is the load acting per unit length. The tip displacement can also be expressed as

$$w = \frac{F L^4}{8EI} \tag{2.22}$$

E is the elastic modulus of the beam. Assuming Hooke's law to be valid we then find the longitudinal strain in the outermost layer of the beam as,

$$S_{13} = \frac{2wt}{L^2} \tag{2.23}$$

The strain S_{13} is measured along the length (1-direction) due to an electric field applied through the thickness (3-direction). This expression is identical to that derived by [36] using trigonometric considerations instead of beam equations.

3. RESULTS AND DISCUSSION

SEM studies and electrical measurements, which will be discussed shortly, are carried out to investigate the quality of dispersion of the nanotubes in the polyimide matrices. Results of dielectric measurements, dielectric relaxation spectroscopy along with the actuation measurements will also be discussed in this section.

3.1 Processing and Scanning Electron Microscopy (SEM) of SWNT-Polymer Composites

The SWNT-PI composites are prepared by *in-situ* polymerization under sonication a process developed by researchers at NASA Langley Research Center[93, 113]. This technique uses sonication to more efficiently disperse the nanotubes. Polymerization takes place as the constituents are mixed with the pre-dispersed solution of SWNTs in the presence of sonication. The viscosity of the solution increased with the nanotube content. Mechanical stirring along with sonication was employed to get well dispersed films. The optical transparency of the films remained high till 1vol% SWNT content[93]. It is important to note that the SWNTs used are as-produced without any surfactants or chemical functionalizations.

The two key factors in judging the quality of the nanocomposites are the dispersion of the nanoinclusions in the polyimide matrix and their adhesion to it. Previous studies on these SWNT-PI composites [93, 113, 142] have shown a good dispersion using transmission electron microscopy (TEM) and optical microscopy. Figure 3.1 shows the optical microscopy images of 0.05vol% and 2vol% SWNT+(β-CN) APB-ODPA composite

samples. These images do not show large aggregates of the nanotubes indicating a good dispersion of nanotubes in the polyimide matrix.

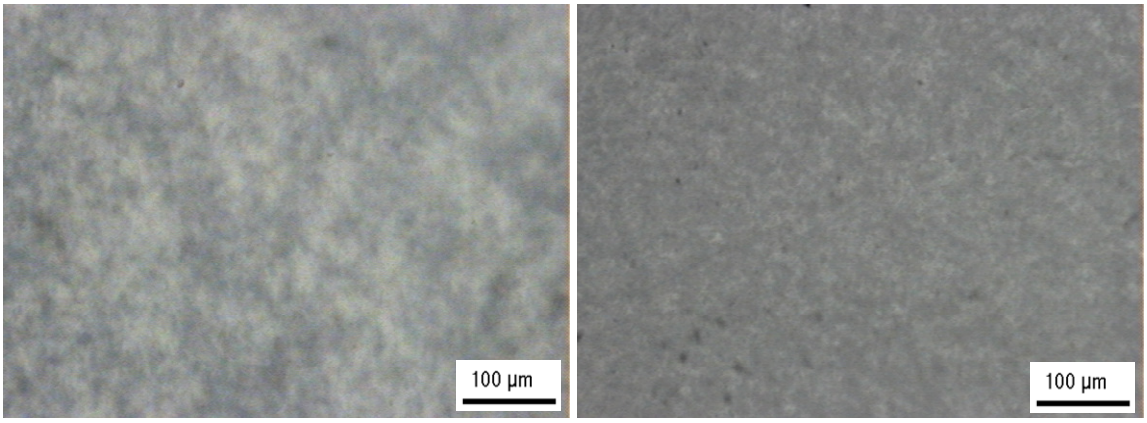

(a) (b)

Figure 3.1 Optical micrographs of (a) 0.05 vol% SWNT+(β-CN) APB-ODPA (b) 0.2 vol% SWNT+(β-CN) APB-ODPA[142].

In this study, SEM is carried out on the fracture surface of the nanocomposites to further investigate the quality of dispersion and the adhesion between the nanotubes and the polyimides. Figure 3.2 shows SEM images of 0.5% and 2% SWNT + CP2 nanocomposite fracture surfaces. Figure 3.2(a) shows nanotubes evenly dispersed in the sample showing good dispersion but they do not appear anchored in the polymer. Also the nanotubes seem straight and show little wavy or bent nature. Figure 3.2 (b) shows evidence of polymer wetting of the nanotube and hence polymer and nanotube adhesion. Thus though there is some evidence of adhesion between the nanotube and polymer it does not appear strong in nature.

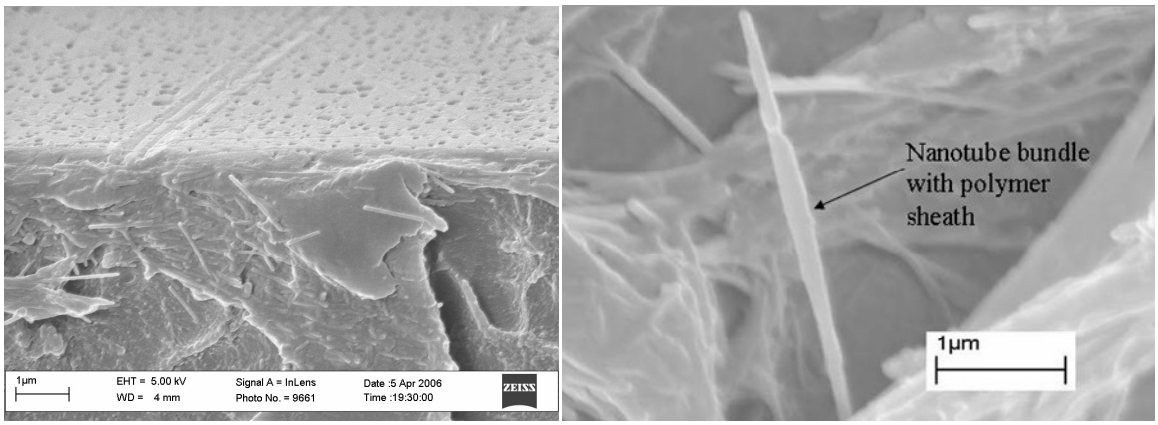

(a) (b)

Figure 3.2 (a) SEM of 0.5%SWNT+CP2 showing the SWNTs not anchored in the polymer (b) SEM images of 2%SWNT+CP2 showing Polymer wetting of the nanotube

Figure 3.3 shows SEM results for the 0.5%SWNT+ (β-CN) APB-ODPA samples. Figure 3.3 (a) shows a good dispersion of SWNTs in the polymer matrix. Thin bundles of nanotubes appear evenly distributed and anchored in the polymer matrix. Figure 3.3 (b) shows a bent nanotube or bundle of nanotube with polymer wrapped around it. Thus a better adhesion seems to be present in this case with nanotubes seemingly anchored in the polyimide matrix. This is an indication that the SWNT-polyimide interaction is stronger for the (β-CN) APB-ODPA polyimide than for CP2.

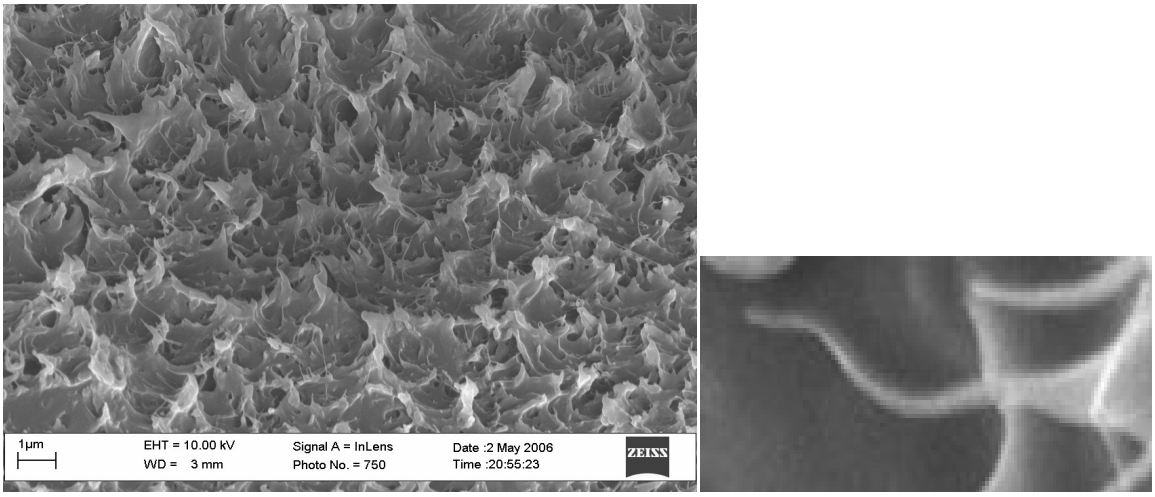

(a) (b)

Figure 3.3 SEM images of 0.5%SWNT+(β-CN) APB-ODPA, (a) image shows a good dispersion of nanotubes, (b) SWNTs seem anchored in the polymer matrix

3.2 Electrical and Dielectric Characterization of SWNT-Polyimide Films

3.2.1 Electrical Characterization

The conductivity data of SWNT+CP2 is plotted as a function of frequency in Figure 3.4 along with standard deviation for each frequency and SWNT content data point. Conductivity shows an increase with frequency up to 0.02 vol% above which it remained constant with frequency. The increase in conductivity with frequency below percolation is characteristic of dielectric materials and can be explained by the energy band theory. Electrons are identified by their energy states. Valence energy band comprises of the low energy states while the conduction band refers to high energy states. In a dielectric material, the energy difference between the valence and conduction band known as the energy band gap is large. Conduction occurs when the valence

electrons can move to the conduction band. In polymers, there are two main types of conduction phenomenon intra-molecular and inter-molecular. In the first case, overlapping of orbitals as in the case of carbon double bonded with another carbon leads to a decrease in the energy band gap and can lead to conduction. In case of inter-molecular conduction, electrons jump from one molecule to another. Here an orbital overlap does not exist and the molecules are generally held together by van der Waals type forces. As the frequency of the applied electric field increases one would expect an increase in conduction as the electrons are imparted with higher vibrational energy. Conduction can then occur either though a tunneling or a hopping mechanism. Tunneling occurs when the electrons move from one atom to another by tunneling through the energy barrier while in hopping mechanism the electron which has a sufficiently high energy can overcome the energy barrier[143].

Above percolation however there is already a conducting path formed through the composite and frequency does not have an effect on the conductivity of the composite. The data suggests a percolation transition at around 0.02-0.05 vol% of SWNT in the nanocomposite. It is also observed that at any given frequency, the conductivity increases with SWNT content.

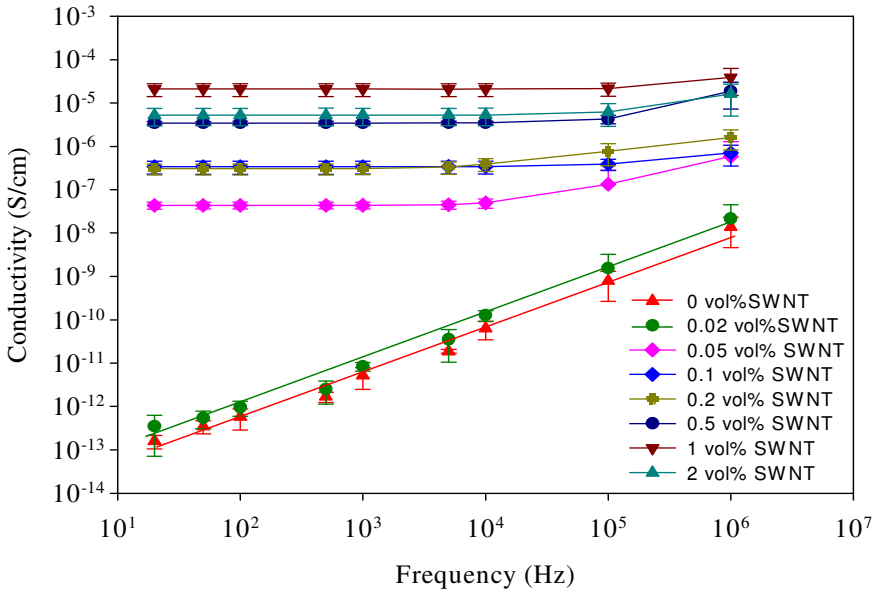

Figure 3.4 Conductivity of different SWNT – CP2 composite samples as a function of frequency.

To quantify the percolation threshold, electrical conductivity results are plotted as a function of SWNT concentration in Figure 3.5 for both SWNT+CP2 and SWNT+ (β-CN) APB-ODPA composites. These values are computed at 20Hz frequency with standard deviation and then extrapolated to the DC case. The quality of dispersion and the percolation threshold can be deduced from these results. Figure 3.5 allows a comparison between conductivities for the two composites. Both composites show an increase in the value with SWNT content. This increase is seen till around 1 vol% SWNT content above which a plateau is seen. It is also observed that (β-CN) APB-ODPA based composites show around 1-2 orders higher value than CP2 based composites at around 0.5-2vol% SWNT content. Nanotubes show conductivities of

around $10^3 – 10^4$ S/cm [144, 145]. Thus for SWNT content of around 1 vol% rule of mixtures would give a value of around 10^2 S/cm in these polyimide composites. But the values observed are to the order of $10^{-6} – 10^{-4}$ S/cm. The reason for this could be attributed to fact that the percolation that is described here occurs due to a quantum tunneling effect between nanotubes rather than a physical contact between them[114].

For the SWNT+CP2 composites the conductivity is linear with $v\text{-}v_c$ on a logarithmic scale (Figure 3.6) described by Equation 2.9 b:

$$\sigma' = K (v\text{-}v_c)^m \tag{3.1}$$

where σ is the conductivity of the nanocomposite, v is the volume fraction of the SWNT in the nanocomposite, v_c is the percolation volume fraction , K and m are fitted constants. A best fit to the data results when K=1.83 x 10^{-5} S/cm and m = 1.6, resulting in a v_c = 0.04vol%. Theoretically, the coefficient K represents the conductivity of the nanotube. This low percolation threshold is a result of good dispersion and the high aspect ratio of the SWNTs. The aspect ratio of the SWNT bundles corresponding to the percolation threshold predicted by Ounaies et al[114] was around 700 , corresponding to seven hexagonally close packed nanotubes in a bundle. Increasing (or decreasing) the number of nanotubes in the bundle led to a decrease (or increase) in the aspect ratio and increase (or decrease) in the percolation volume fraction. The experimental percolation threshold value lies in between the theoretically predicted value of 0.023vol% by using the excluded volume approach [114] and 0.07vol% by using the 7 hexagonally close packed SWNTs.

A similar study was done on the (β-CN) APB-ODPA based polyimide [130] the percolation threshold was determined at 0.06vol% SWNT content. These low percolation threshold values indicate a very good dispersion of the nanotubes in the non-polar (CP2) and polar ((β-CN) APB-ODPA) polyimide matrices. Also based on the excluded volume approach dispersion of small bundles of 7 is indicated.

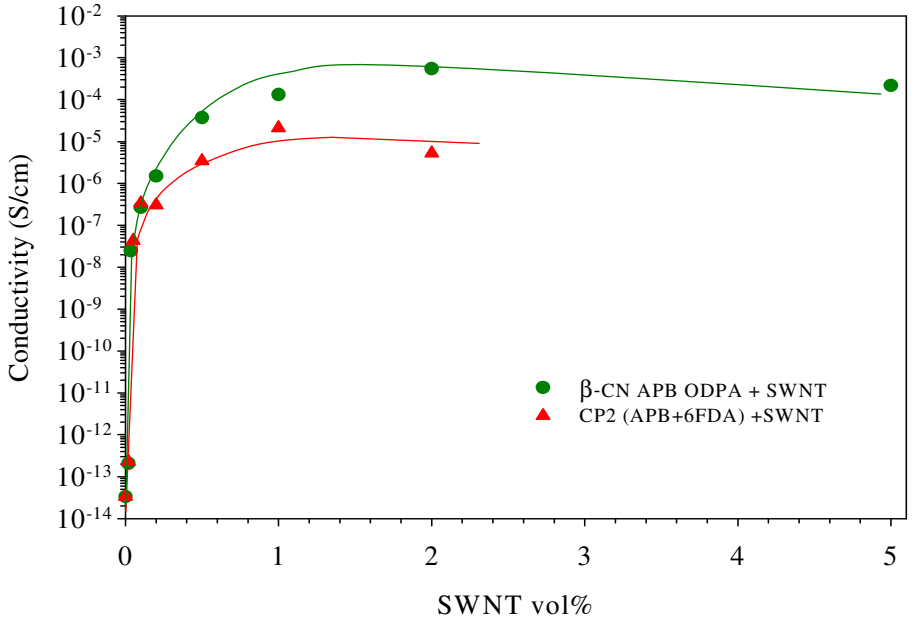

Figure 3.5 Comparison of conductivity values extrapolated to DC of different SWNT content samples for both the polyimide matrices

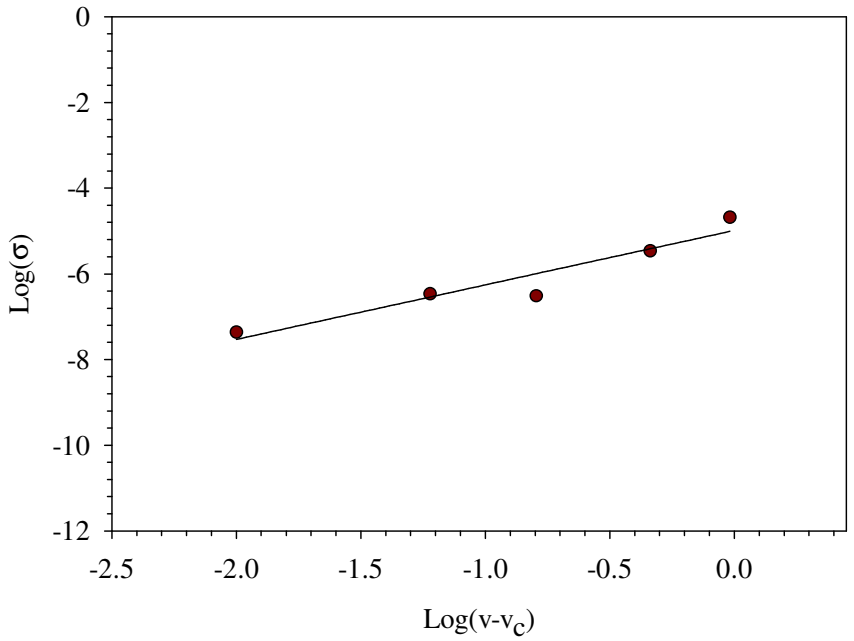

Figure 3.6 Log plot to determine the percolation threshold for CP2 nanocomposites

3.2.2 Dielectric Characterization and Dielectric Relaxation Spectroscopy

Figure 3.7 shows the dielectric constant (with standard deviation) as a function of frequency at different SWNT content for CP2 nanocomposites. Below and around percolation the value remains constant with frequency up to 1Mhz. Above percolation however a general decrease in the trend is observed. This is attributed to the increasing contribution of interfacial polarization due to increasing heterogeneity. Interfacial polarization in part explains the increase in the dielectric constant seen with the SWNT content. This polarization however is prevalent at low frequencies of applied field. Thus as the frequency increases the contribution by interfacial polarization to the dielectric constant decreases.

Figure 3.8 shows the comparison of dielectric constant at different SWNT vol% for both types of nanocomposites for the extrapolated DC case. The (β-CN) APB-ODPA values have been adapted from [130]. A high value is seen above the percolation threshold. The value increases until 0.5vol% SWNT content for the CP2 case above which the value plateaus off. For the (β-CN) APB-ODPA case however the increase in the dielectric constant is much larger than that observed for CP2. A difference of up to 3 orders is seen between the two types of composites for concentrations of 0.5vol% and above. This increase in the dielectric constant for both cases indicates an increase in the ability of the material to store electrical energy. (β-CN) APB-ODPA seems to fair better than CP2 in storing this energy. This additional storage seems to be the result of an increased dipolar polarization in the (β-CN) APB-ODPA polyimide compared to the CP2 case. The SWNTs used in both studies are different. The CP2 study uses laser ablated nanotubes[93] and the (β-CN) APB-ODPA uses HIPCo processed SWNTs [113]. Though this could be one of the factors in this big disparity in the dielectric constant values, it seems unlikely that the nanotubes from both batches which are reported to be around the same purity (~97%) would cause a huge difference in dielectric constant values between the two different types of composites. It is thus more likely that the reason for the large difference is polarity of the matrix and the relationship the nanotubes share with the matrix.

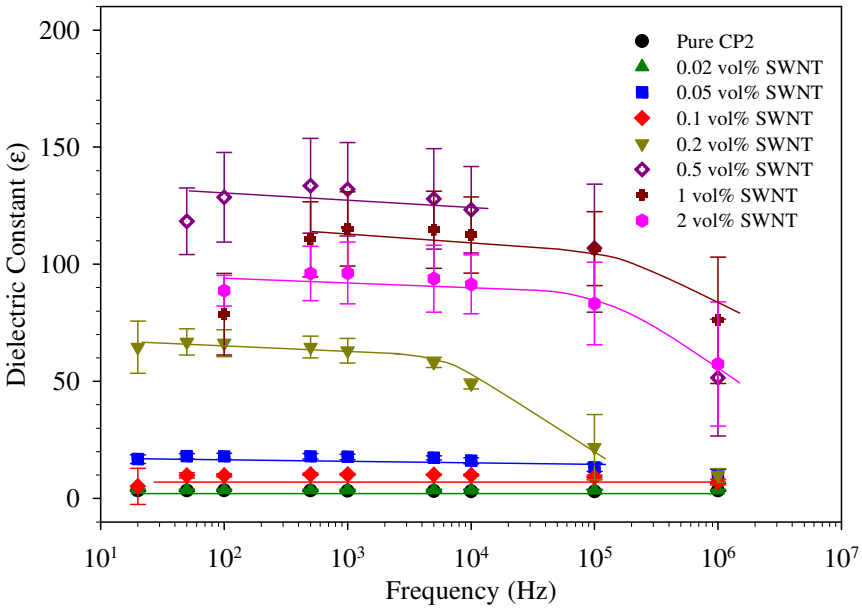

Figure 3.7 Dielectric constant of different SWNT – CP2 composite samples as a function of frequency

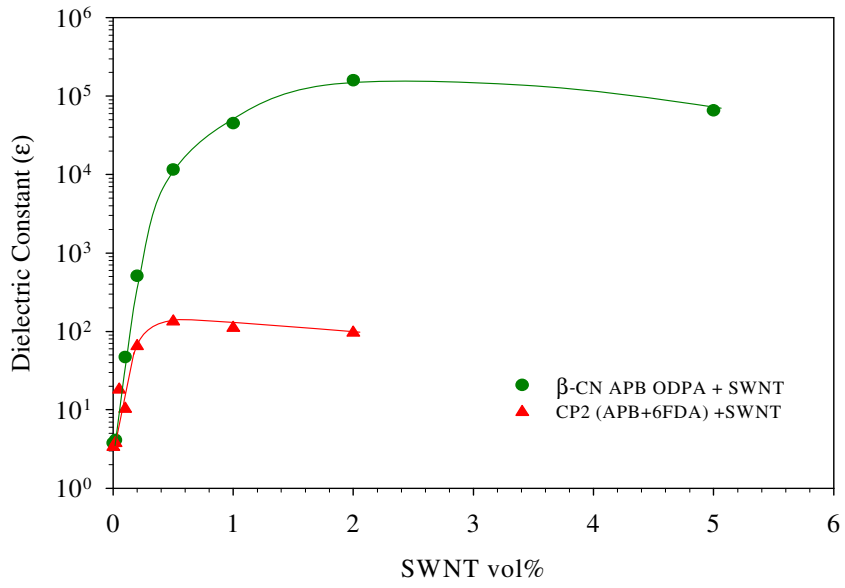

Figure 3.8 Comparison of dielectric constant as a function of SWNT loading for both matrices

3.2.2.1 Dielectric Relaxation

Figure 3.9 shows the increasing difference between the high and low temperature values of dielectric constant values ($\Delta\varepsilon$) for different SWNT loading at 21.5Hz for the SWNT-CP2 composites. The values of $\Delta\varepsilon$ measured for both CP2 and (β-CN) APB-ODPA are listed in Table 3.1. The values that are not reported are because samples with that particular concentration were not available (for CP2) and for (β-CN) APB-ODPA composite samples (adopted from [130]) the missing values are due to the inconclusive nature of the tests where a distinct plateau was not seen. This value quantifying the increase in the dipolar relaxation shows an increase with SWNT loading. Also it can be seen that this value is higher for (β-CN) APB-ODPA nanocomposites than for the CP2 nanocomposites. Equation 2.17;

$$P_R = \Delta\varepsilon\, \varepsilon_0 E \tag{3.2}$$

relates $\Delta\varepsilon$ to the remnant polarization P_R (due to dipolar orientation) experienced by a dielectric in response to an applied field. The higher this value higher is the mobility of the dipoles present in the system giving higher remnant polarization. Thus remnant polarization increases with the SWNT content in both composites and is higher for (β-CN) APB-ODPA nanocomposites than for CP2 nanocomposites.

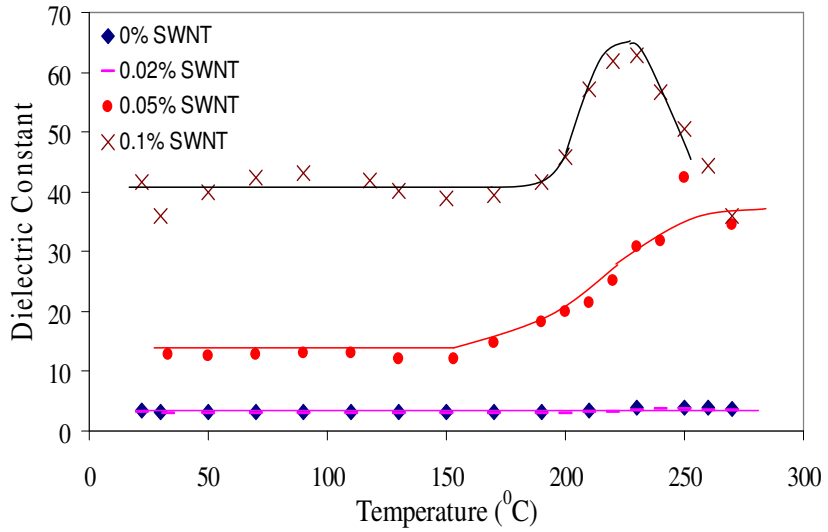

Figure 3.9 Dielectric constant as a function of temperature for SWNT-CP2 composites at 21.5 Hz

Table 3.1 Comparison of Δε as a function of SWNT loading for CP2 and (β-CN) APB-ODPA based nanocomposites

SWNT loading (Vol%)	$\Delta\varepsilon_{@21.5Hz}$ (CP2)	$\Delta\varepsilon_{@20Hz}$ ((β-CN) APB-ODPA)
0	0.69	4.41
0.02	0.72	9.69
0.035	-	10.59
0.05	21	-
0.075	-	48
0.1	24	-

3.2.2.2 Thermally Stimulated Current Measurements (TSC)

Figure 3.10 shows the polarization induced by TSC tests for three different samples, pure CP2, 0.05vol% SWNT-CP2 and 0.1vol% SWNT-CP2 at the same poling temperature. An increase is observed in the induced polarization with the SWNT content and applied voltage. Figure 3.11 shows the induced polarization as a function of the poling temperature for a 0.1%SWNT sample. A higher polarization is also seen for poling temperatures closer to the glass transition of the system, which is around 200°C. This indicates that the induced dipoles tend to relax around the same temperatures as the polymer chains.

Thus the TSC proves an effective tool to confirm the effect of SWNTs on the dipolar polarization and the effect that the polarity of the matrix. The increase in polarization seen with the SWNT content and due to the polar (β-CN) APB-ODPA matrix is attributed to dipolar polarization. The fact that higher polarization is seen around the glass transition temperature further strengthens the argument that the polarization is due to contribution by the dipoles. The increase in the nanotube content thus increases the dipolar polarization experienced by the sample at a particular electric field. This enhancement in polarization could also be a result of induced dipoles due to the presence of the nanotubes, hence explaining the increase with the nanotube content.

The higher polarization seen by 0.05 vol%SWNT+(β-CN) APB-ODPA compared to 0.1vol%SWNT+CP2 samples seen in Figure 3.12 also shows that the polarity of the polyimide matrix enhances the polarization. This could be due to additional dipoles

present in the polyimide itself and/or due to increase in the strength of the induced dipoles due to the polarity of the matrix.

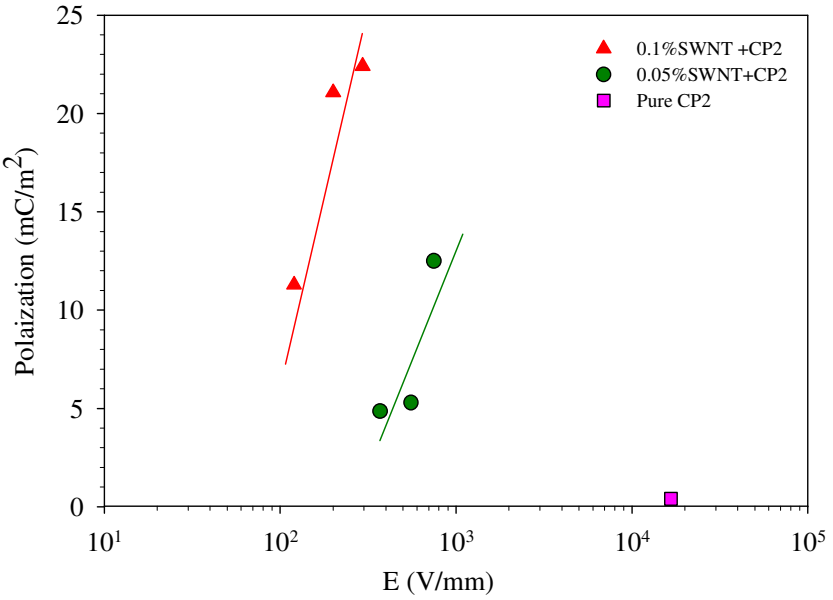

Figure 3.10 Induced polarization in CP2 nanocomposites by TSC

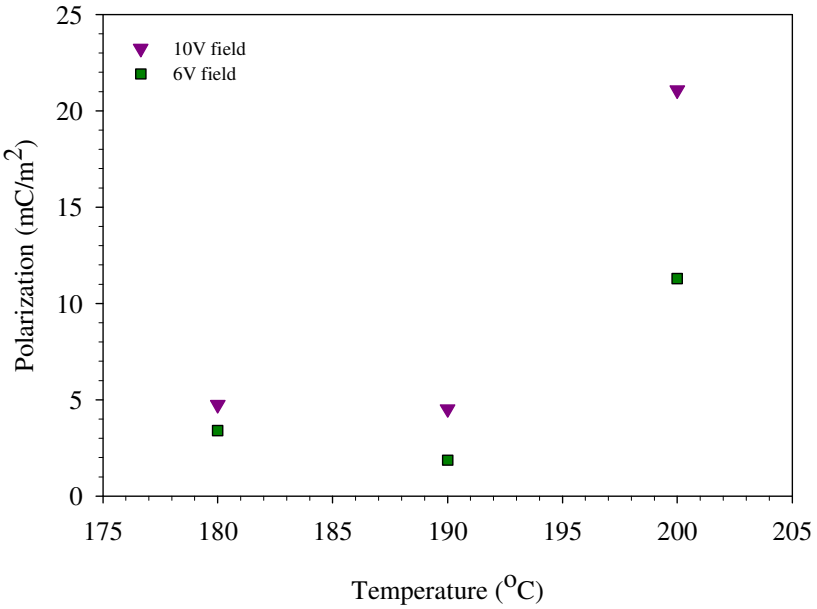

Figure 3.11 Induced polarization as a function of poling temperature (0.1% SWNT+CP2)

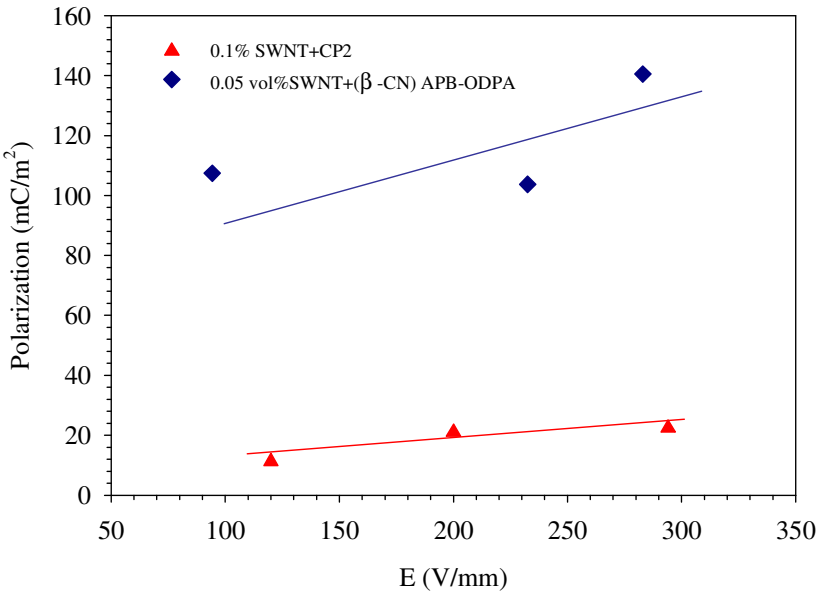

Figure 3.12 Comparison of induced polarization between 0.05vol% SWNT+(β-CN) APB-ODPA and 0.1vol% SWNT+ CP2 nanocomposites in TSC

The dielectric studies provide an insight into the remnant polarization experienced by a dielectric under an applied electric field. Dielectric constant as a function of SWNT vol% (Figure 3.8) shows an increase in value with the content. Dielectric spectroscopy (Table 3.1) also shows a SWNT content dependence of the relaxation in the composites. Finally the TSC studies (Figure 3.10) confirm an increase in the induced polarization under an applied field with the nanotube content. All these results indicate an enhancement of polarization experienced by SWNT-polyimide nanocomposites with the carbon nanotube content and polarity of the polyimide matrix itself. Higher the nanotube content higher is the polarization experienced by the nanocomposites. Also more polar the polyimide higher is the polarization.

3.3 Electromechanical (Actuation) Characterization

Thin sample strips of thickness around 30-50 microns are tested for actuation response with DC and AC electric fields. Nanocomposite samples below the percolation threshold (0.04vol% SWNT for SWNT+CP2 and 0.06vol% SWNT for SWNT+(β-CN) APB-ODPA nanocomposites) do not show any actuation response in response to electric field.

3.3.1 Strain vs E

Bending actuation strain measurements indicate a nonlinear response to the applied field for the CP2 and (β-CN) APB-ODPA nanocomposites. Figure 3.13 shows the strain data of the CP2 nanocomposite samples at 0.1, 1 and 2vol% SWNT loading for the cantilever bending experiment under a DC electric field. It is seen that the actuation

response gets stronger as the electric field and nanotube content increases. Figure 3.14 shows the same results for the (β-CN) APB-ODPA nanocomposites case with nanotube loading of 0.2vol%, 0.5, 1 and 2vol%. Here too the actuation strains are seen as a function of the nanotube content and electric field similar to the CP2 nanocomposites. In the actuation experiments another observation is that the direction of the bend is independent of the polarity of the electric field. Figure 3.14 demonstrates the independence of the strain data to the direction of applied field indicating a quadratic (electrostrictive) actuation response.

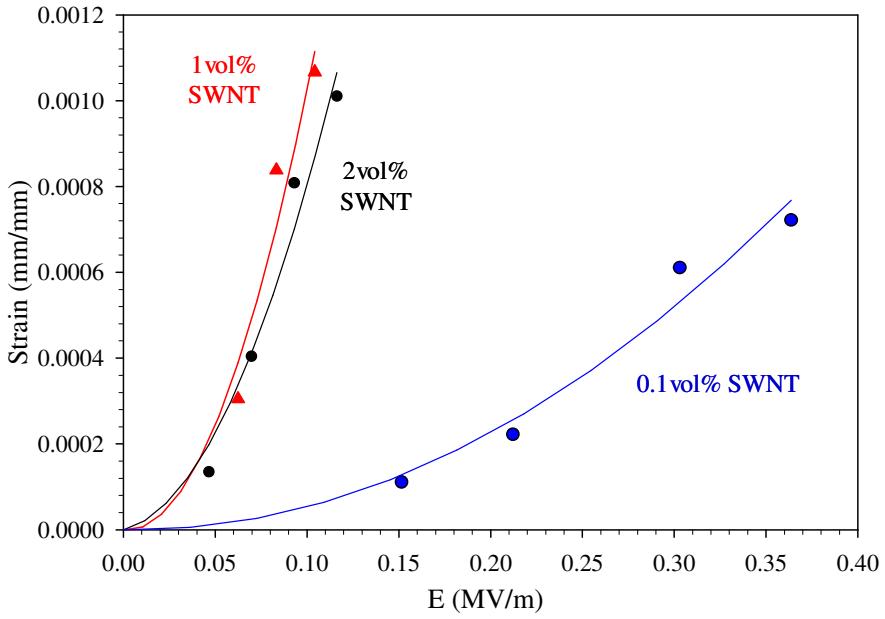

Figure 3.13 Strain vs electric field for SWNT + CP2 (DC)

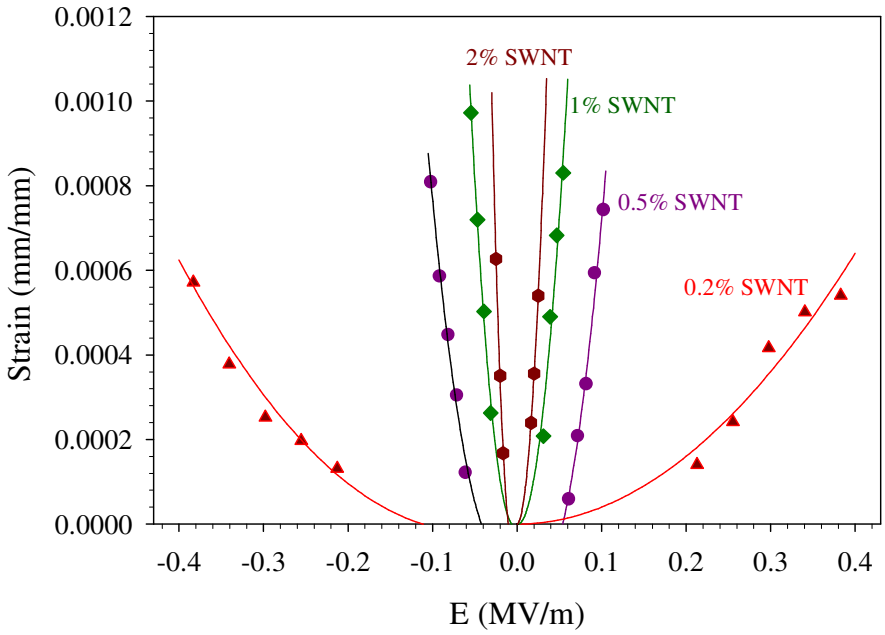

Figure 3.14 Strain vs electric field for SWNT + (β-CN) APB-ODPA (DC)

3.3.2 Strain vs Time

Strain rates are also measured for the DC electric field bending experiments. Figure 3.15 shows the trend of strain with time at different voltages for 0.5vol% SWNT loading in CP2 polyimide. The strain increases linearly after an initial lag of a few seconds, and then plateaus off in the last stage before the supply is stopped. An increase in the strain rate is thus seen with an increase in the applied voltage. Similar observations are made at different vol% SWNT loading. Strain rates are compared in Table 3.2 for different electric fields and SWNT vol %. The strain rate at 7V for 0.5vol% SWNT is greater than that for 0.1vol% SWNT at the same voltage; it is noted that the thickness of samples was

the same. Thus, the strain rate increases with increase in voltage and carbon nanotube loading.

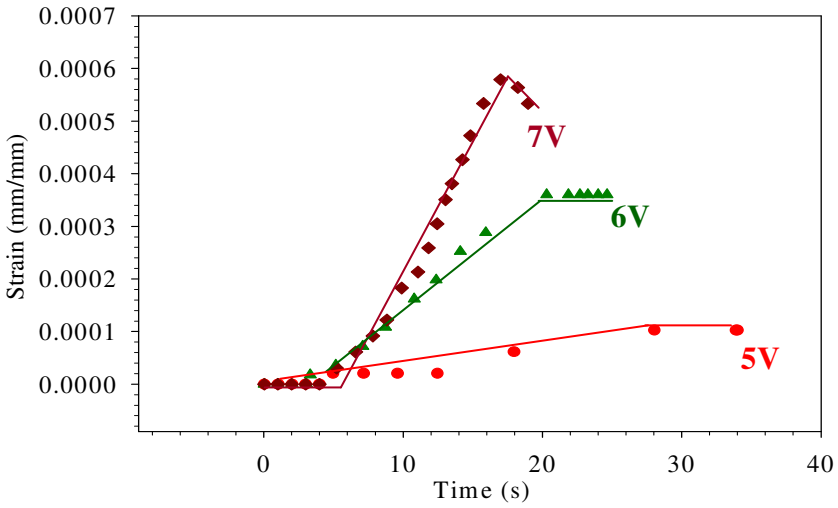

Figure 3.15 Strain vs time for 0.5 vol% SWNT + CP2 nanocomposite

Table 3.2 Strain rates for SWNT+CP2 nanocomposites (0.1vol% and 0.5vol%SWNT)

Voltage (V)	Strain Rate (s^{-1})	
	0.1vol% SWNT	0.5vol% SWNT
5	-	4×10^{-6}
6	-	2×10^{-5}
7	4×10^{-5}	5×10^{-5}

Figure 3.16 shows the strain as a function of time for 0.5 vol% SWNT content in (β-CN) APB-ODPA. Here too the strain rate increases with the applied voltage. Table 3.3 also gives the strain rate values of the strain vs time plots shown in Figure 3.16. To compare the strain rates of both polyimide-based nanocomposites, the strain rates are plotted as a function of applied field for the 0.5vol% SWNT case in Figure 3.17. The strain rates in both cases increase with applied field but the strain rate for (β-CN) APB-ODPA nanocomposite is higher than that of CP2 for the same electric field. The data thus shows a faster response of the (β-CN) APB-ODPA based nanocomposites compared to the CP2 based nanocomposites.

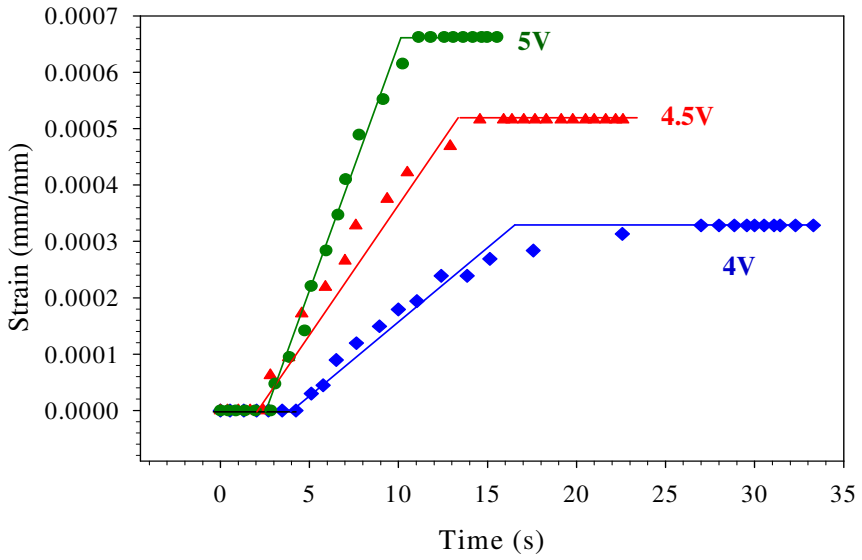

Figure 3.16 Strain vs time for 0.5vol% SWNT + (β-CN) APB-ODPA nanocomposite

Table 3.3 Strain rates for SWNT+ 0.5vol% (β-CN) APB-ODPA nanocomposites

Voltage (V)	Strain Rate (s^{-1})
	0.5vol% SWNT
4	3×10^{-5}
4.5	4×10^{-5}
5	8×10^{-5}

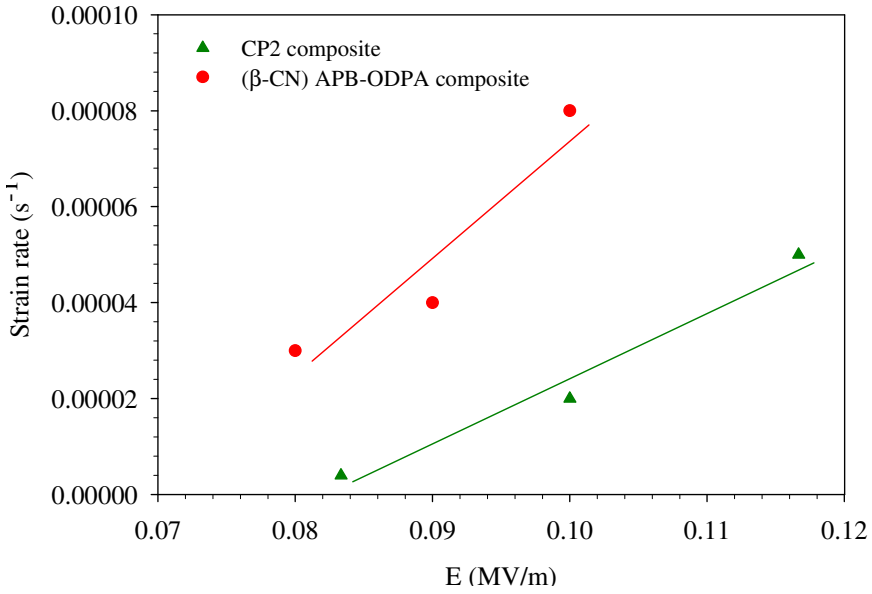

Figure 3.17 Strain rate comparisons for 0.5vol%SWNT + CP2 and 0.5vol%SWNT+ (β-CN) APB-ODPA nanocomposites

3.3.3 Strain vs E^2

The strain vs electric field data indicates a quadratic dependence of strain on the applied electric field. Figure 3.18 shows the variation of strain with the square of the applied field at different SWNT vol% loading for the SWNT+CP2 nanocomposites. A linear trend is observed in the data. Figure 3.19 shows the data for a AC square function applied field with a frequency of 0.5 Hz. This data also shows a linear relationship between the strains and the squared electric field. Also when the DC actuation data for SWNT+(β-CN) APB-ODPA composites is analyzed similarly (Figure 3.20), a linear trend and hence a quadratic relationship between the applied field and measured electromechanical strains is confirmed. All these results point towards an electrostrictive response in the SWNT-polyimide nanocomposites.

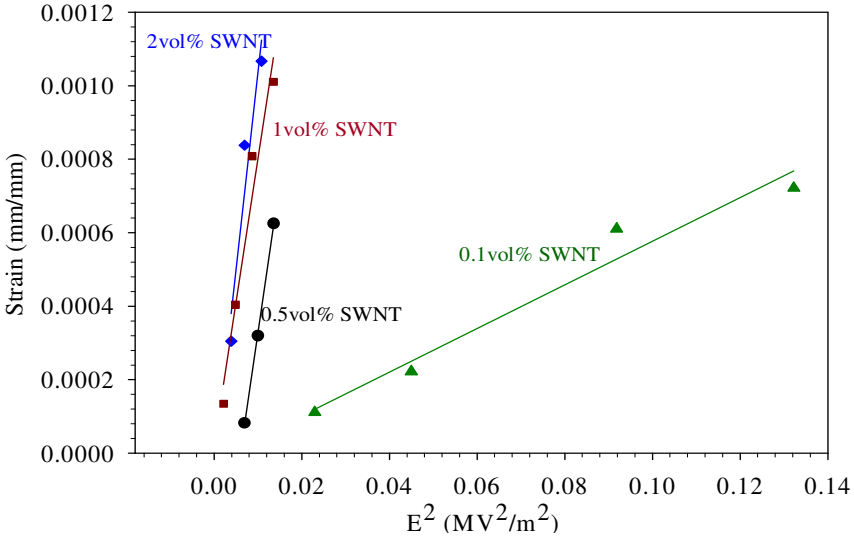

Figure 3.18 Strain vs squared electric field for SWNT + CP2 (DC)

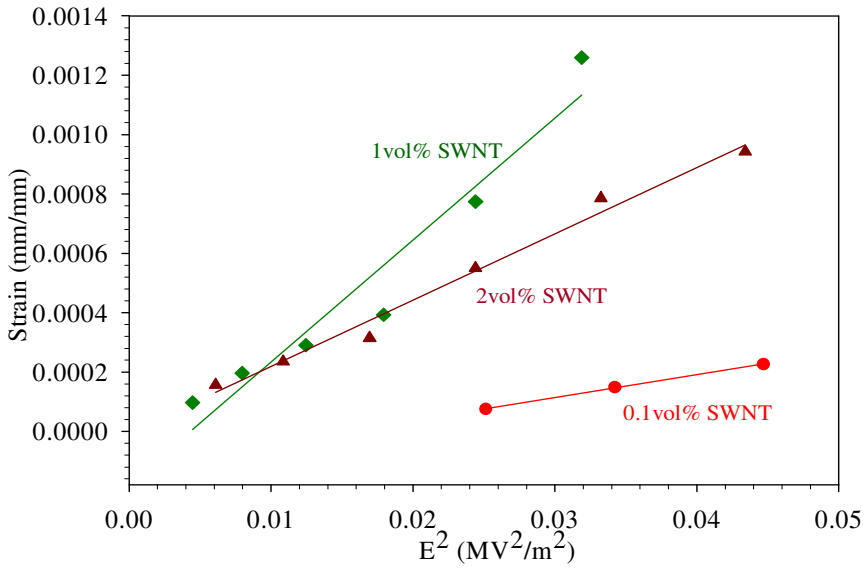

Figure 3.19 Strain vs squared electric field for SWNT + CP2 (AC, square wave, 0.5Hz)

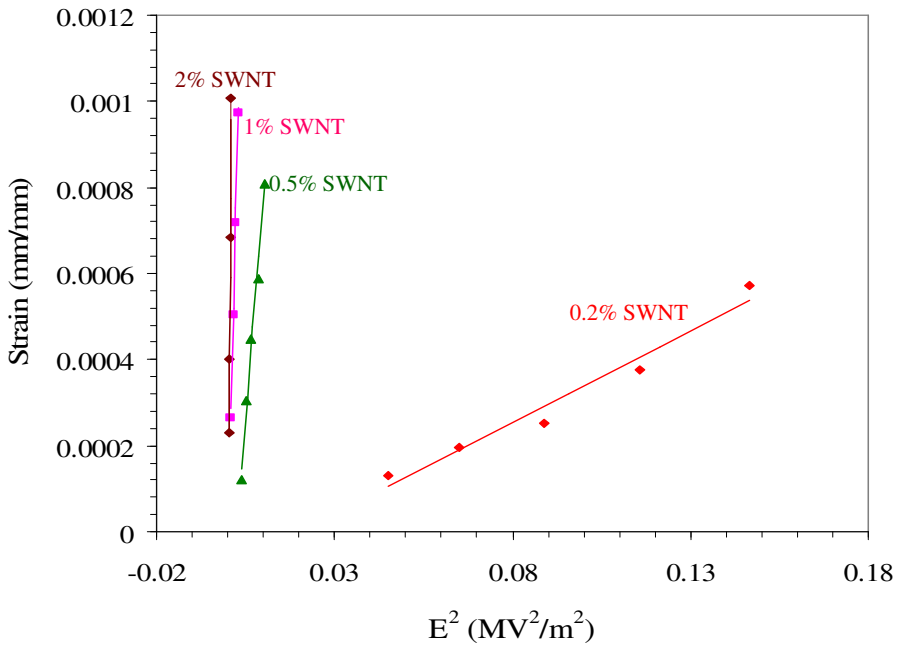

Figure 3.20 Strain vs squared electric field for SWNT + (β-CN) APB-ODPA (DC)

3.3.4 Coefficient of Electrostriction

The electrostriction coefficient (M_{1333}) is calculated at each SWNT loading for DC and AC fields. M_{1333} relates the applied field through the thickness to the measured strain through

$$S_{13}=M_{1333}E_3^2 \tag{3.3}$$

The M_{1333} value is the slope of the strain vs squared electric field plot. The effect of the loading on M_{1333} can be seen in Figure 3.21 for both CP2 and (β-CN) APB-ODPA. For the CP2 case, an increase in the coefficient up to 1vol% SWNT is seen above which the value plateaus off. (β-CN) APB-ODPA based nanocomposites show a steady increase in value to 2vol% SWNT content samples. At SWNT concentrations of 1-2 vol% (β-CN) APB-ODPA nanocomposites show an order higher value of M_{1333}.

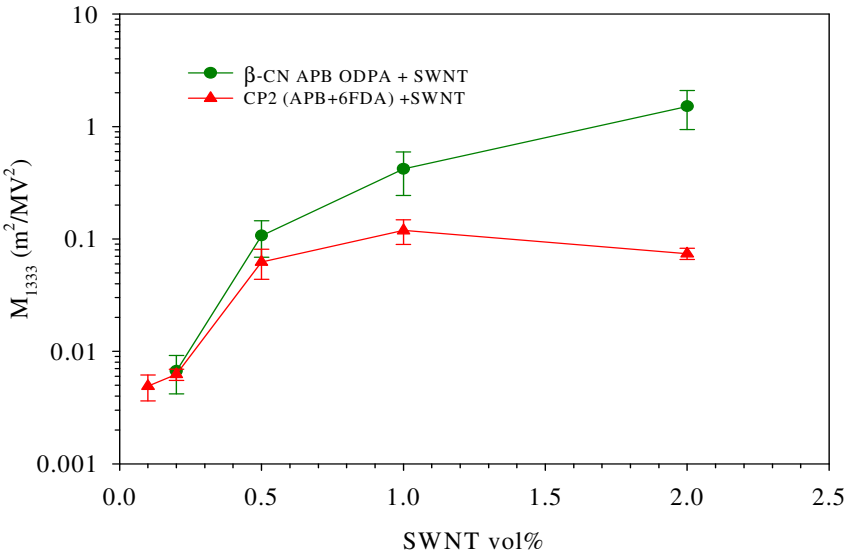

Figure 3.21 Comparison of coefficient of electrostriction (M_{1333}) as a function of SWNT loading for both polyimide matrices (DC)

It is also observed that, under AC conditions, there is a decrease in the electrostrictive response compared to the DC case, which is seen from the M_{1333} values in Figure 3.22. The figure shows M_{1333} as a function of SWNT content for DC and AC case of SWNT+CP2 nanocomposites. The value increases with the SWNT content for both cases, but the value for the coefficient is almost an order lower for the AC square wave signal than the DC values.

Figure 3.23 shows the effect of frequency on the coefficient of electrostriction for 0.5 vol% SWNT + (β-CN) APB-ODPA nanocomposite. The coefficient shows an initial drop in value as frequency increases from that of zero for DC; but the value does not show a big decrease further as frequency is increased. Also the square wave data has a higher value compared to the sine wave data. This decrease in M_{1333} with frequency could be a result of the dipoles present in the polyimide not able to keep up with the fluctuations of the electric field.

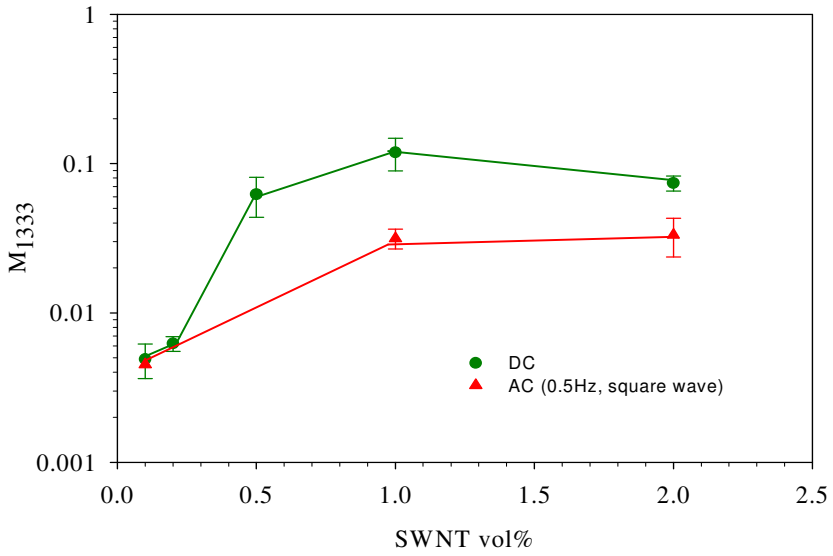

Figure 3.22 Comparison of coefficient of electrostriction (M_{1333}) as a function of SWNT loading at DC and AC (0.5Hz, square wave) signals for SWNT+CP2

The dependence of M_{1333} on the SWNT content and polyimide matrix demonstrated in Figure 3.21 further confirms the inference drawn earlier that the electrostrictive response is dependent on the nanotube content in the nanocomposites samples and polarity of the polyimide matrix. Frequency also shows an effect on the response and a decrease is seen in M_{1333} initially as frequency increases.

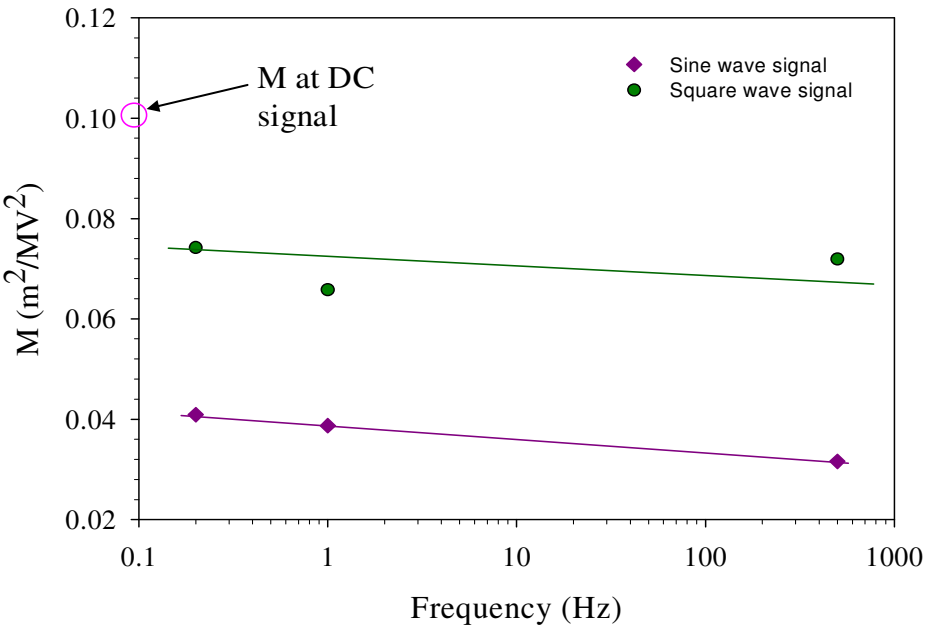

Figure 3.23 Effect of frequency on the coefficient of electrostriction (M_{1333}) for 0.5 % SWNT + (β-CN) APB-ODPA

3.4 Discussion on Actuation Response

An increase is thus seen in the electrical conductivity, dielectric constant and dielectric relaxation in SWNT-PI nanocomposites. The most interesting result of this study though is the effect of SWNT content on the actuation response of the nanocomposites. Both pristine CP2 and (β-CN) APB-ODPA do not show any actuation response under an applied electric field. However, addition of SWNTs at concentrations above percolation initiates an electromechanical response. The actuation response is identified as electrostriction with the strains proportional to the square of polarization experienced by the dielectric material (Equation 1.3). This response gets stronger with

increase in SWNT content. This is reflected in the increase in M_{1333} value with SWNT content.

The results of dielectric spectroscopy and TSC experiments discussed in Table 3.1 and Figures 3.10, 3.12 respectively offer an explanation to the initiation and enhancement of electrostrictive response as SWNT content increases. An enhancement is seen in the remnant polarization with increase in SWNT content and the polarity of the polyimide matrix. Electrostrictive strains are proportional to the square of the polarization experienced by the material and hence this enhancement in polarization results in an enhanced electrostrictive effect.

The enhanced polarization in the nanocomposites can be due to the inherent properties of the SWNTs themselves and/or due to SWNT – PI interaction. In Section 1, actuation of individual MWNTs and SWNTs was discussed. In case of MWNTs the actuation is due to the electrostatic attraction seen in the nanotube nanotweezers experiment[84], while that in SWNTs it results from injection of an electron or an electron hole and the resulting effect on the carbon-carbon bonds. Thus it is possible that the SWNTs themselves are the active component in the polyimide nanocomposites resulting in the observed actuation response. This hypothesis however does not account for the enhancement in remnant polarization as measured by dielectric relaxation (Table 3.1) and TSC studies (Figures 3.10, 3.12).

Based on the work of Dumitrică et al[74] a local dipole moment exists at the atomic sites of SWNTs. Due to the symmetry of the SWNTs however a net dipole moment does not exist. But when the nanotube is bent the symmetry is disturbed and a net dipole

moment can exist. The bend in nanotubes dispersed in the polyimides is seen in the SEM images of the fracture surface of 0.5vol% SWNT+(β-CN) APB-ODPA composite (Figure 3.3). Figure 3.24 shows a magnified part of the fracture surface which shows a bent nanotube or a bundle of nanotubes. It is also noted that the fracture surface of 2 vol% SWNT+CP2 does not show much bending in the SWNTs. This may be attributed to a better interaction between the SWNT and (β-CN) APB-ODPA due to a non-covalent relationship[93] between the polyimide and the SWNT. Thus a higher dipole moment and hence polarization will be seen with a higher nanotube content for (β-CN) APB-ODPA nanocomposites. The relaxation of the dipoles due to the nanotube bend will occur when the polymer chains relax around the glass transition of the system. This is supported by the dielectric relaxation and TSC data documented in Table 3.1 and Figures 3.10, 3.12 respectively. Thus polarization due to bent nanotubes could add to the polarization inherent to the polyimide structure and can be one of the contributions to the remnant polarization and hence the electrostrictive response.

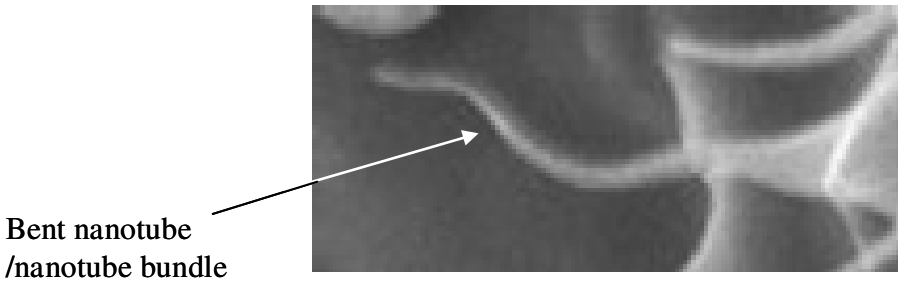

Figure 3.24 SEM showing bent SWNTs

Another possibility is that the increase in polarization could be due to higher mobility of dipoles present on the main chain due to the SWNTs acting as electrodes, essentially extending the electrodes into the polyimide. Ounaies et al[114] in the previous study on these materials have stated that the low percolation is thought to result from an electron hopping phenomenon called quantum tunneling, rather than from physical contact between the SWNTs. Thus, presence of nano and micro- capacitors in between the SWNTs is possible. This seems to be supported by the increase in the dielectric constant of the nanocomposites with the SWNT content (Figure 3.7). For example, in a percolated 0.05vol% SWNT structure an applied voltage of 10V to a sample of thickness 30μm (0.33MV/m field) can cause a field of around 3MV/m between the nanotubes; thus a field an order higher than the applied field could exist between nanotubes. The nano or micro-capacitors can be considered in series as shown in Figure 3.25 in one conducting path. To account for the random orientation of the nanotubes an angular averaging is carried out on α between 0 and π/2 degrees. The distance between two nanotubes is computed based on the volume fraction and then we can compute approximately the number of nanotubes in one conducting path through the thickness. This number is estimated at around 39 for 0.05vol% SWNT content resulting in a local field of 3 MV/m between two nanotubes, assuming that the nanotubes form capacitors in series. Same calculations result in a local field of 4MV/m for 0.1vol% SWNT content for the given thickness. Thus an increase in the SWNT content leads to higher local electric field. Also averaging the projection lengths L' instead of angle gives the number of nanotubes as 40 resulting in almost the same local electric field.

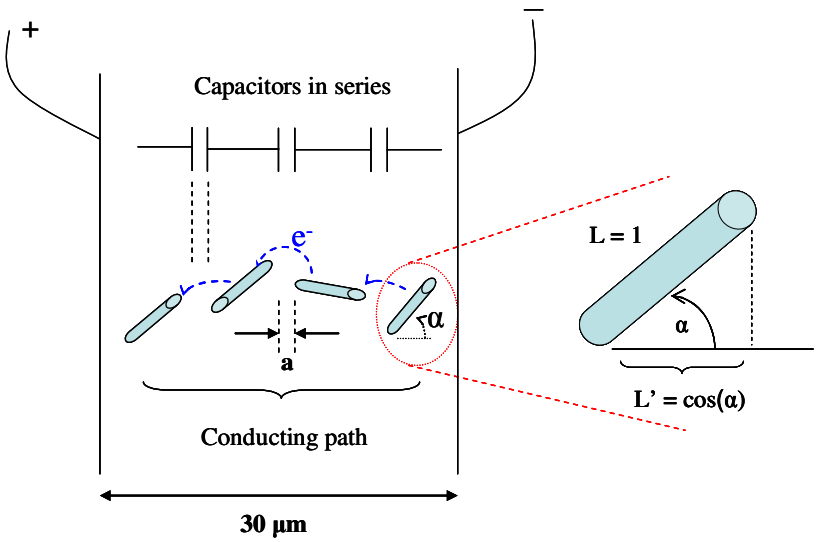

Figure 3.25 Computing local electric field by angular averaging and projection averaging.

The higher electric field could cause even the weak dipoles to rotate, contributing to the enhanced induced polarization. In CP2, the C-CF_3 bonds (Figure 2.1) result in a dipole moment of around 2.93 debye[146, 147]. This dipole which is usually not mobile due to the rigid dianhydride structure can move due to the enhanced local field causing higher polarization. Another study has calculated the dipole moment of (β-CN) APB-ODPA polyimide as 8.8 debye[12, 148]. Thus the higher strength of the dipole moment results in a higher polarization for SWNT+(β-CN) APB-ODPA composites and hence a higher electrostrictive response. Figure 3.26 is a schematic illustrating the higher mobility of polyimide dipoles due to local field enhancement. SWNTs are represented by cylinders, polymer by the continuum between the electrodes and the arrows represent the dipoles on the polymer chains.

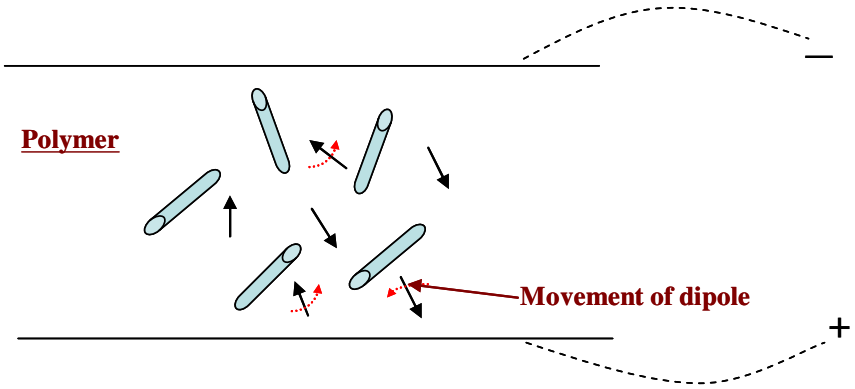

Figure 3.26 Schematic of SWNTs acting as local electrodes

When we discuss the interaction between the SWNTs and polyimide matrix as the cause of the enhanced polarization, the interface assumes a pivotal role. As discussed in the introduction, due to the nanometer scale of these inclusions, their high surface area and a distance between them which is comparable to the nano dimension, there is an increasing influence of the interface on the physical properties of composites. This offers an opportunity to create novel physical responses in nanocomposites by using nanoinclusions and by tailoring their relationship with matrix. It was mentioned in the introduction that a stronger interface results in an increase in the mechanical properties. Consider particle A embedded in phase B with different dielectric properties as shown in Figure 3.27. In A each atom/molecule equilibrates with its surrounding via short and long range forces. These forces however on an average remain constant with fluctuations over short distances. But as the interface with B is approached these forces become increasingly modified by the presence of B. The interface is then the region over which these forces are different from the bulk values. The volume of the interface can exceed 50% of the whole volume if the interface is 0.5nm thick and diameter < 5nm[149]. Thus the

properties of the interface can become a dominant influence on the dielectric properties of the nanocomposites.

In colloids a polarization is known to exist in the electric double layer interfaces due to applied electric field. The cloud of counterions surrounding a charged particle can be distorted by an electric field leading to an increase in the induced polarization under an applied field. This possible scenario is illustrated in Figure 3.28.

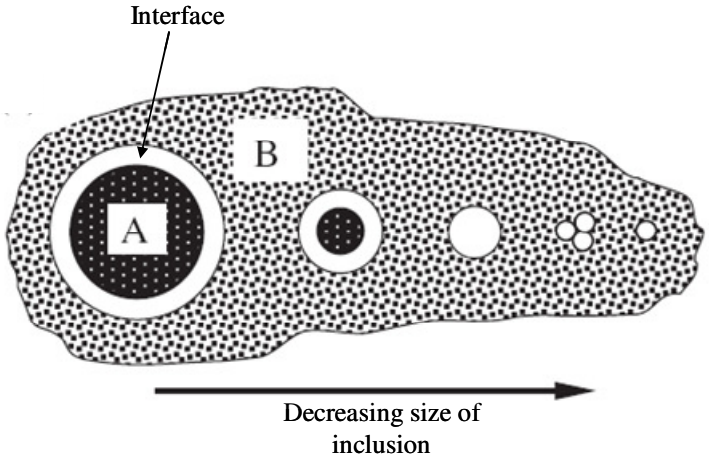

Figure 3.27 Interface between phases with different dielectric properties and its increasing importance with decrease in inclusion size [adapted from [150]]

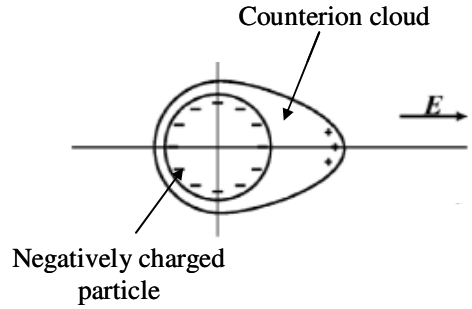

Figure 3.28 Distortion of counter ion cloud due to applied field adding to the induced dipole[151]

Double layers exist not only in polar liquids (liquids with ions) but also in weakly-polar liquids [152]. The difference in electronic properties in a heterogeneous system would still lead to surface charging of the particles and counterions could exist in low concentrations. Though in this case the double layer is not as strong as in the case of the polar liquids and thus the interface itself would be very thin. Thus under a high enough applied field the interface regions can add to the polarization experienced by the material.

In the SWNT + polyimide system however such interface if present would be due to ions introduced by the catalyst used during CNT synthesis and purification or due to the presence of polar solvents used during solution processing. Thus interfaces like those described, possessing an active nature under an applied field, would be weak in nature due to small amount of ions present in the system. Thus the active nature of the nanocomposites is most likely due to other causes. As stated earlier, the dielectric constant of metallic nanotubes can theoretically be infinite. The nanotubes used are usually a mixture of semi-conducting and metallic tubes. The dielectric constant of both polyimides ranges between 3 and 4. Thus a drastic difference can exist between the dielectric properties of SWNTs and those of the polyimide matrices. This disparity in dielectric properties can lead to interfacial polarization described in the experimental section. Interfacial polarization leads to increase in the dielectric constant seen in Figure 3.8. The region containing the interfacial polarization is the interface and would add to the polarization experienced by the composites. Thus this increasing role of the interface

due to interfacial polarization could be one of the factors contributing to increase in the remnant polarization and the dielectric constant with increasing SWNT content.

An interaction could also exist between the SWNT and the polyimide due to the non-covalent interaction between the polymer and the SWNTs. This interaction may be due to a charge donor-acceptor relationship between the polyimide and the SWNTs. Existence of different types of non-covalent relationship has been discussed briefly in the introduction. In (β-CN) APB-ODPA the electronegative group CN could accept an electron donated by the SWNT to form secondary electron donor-acceptor relationship[113]. CP2 also has an electronegative group CF_3 which could possibly lead to a similar but weaker relationship than that observed for (β-CN) APB-ODPA. This non-covalent interaction zone constitutes the interface region. Enhancement in polarization can result from the non-covalent relationship, due to the donor acceptor interaction resulting from the transfer of electron and also due to deformation of this secondary bond subjected to an applied electric field. This idea is schematically represented by Figure 3.29. The CN electronegative group accepts an electron from the SWNT resulting in an interaction between the SWNT and the polyimide. This interaction region when subjected to an electric field results in an induced dipole represented in the figure. The relaxation of the system in this case too is closely related to the relaxation of the polymer system itself. As the polyimide goes through the glass transition temperature of the polymer, the induced dipole, which exists due to the relationship between the SWNT and polymer and its subjection to an applied field, would relax too. This induced dipole

results in an enhancement in the remnant polarization reflected in the dielectric relaxation (Table 3.1) and the TSC data (Figures 3.10, 3.12).

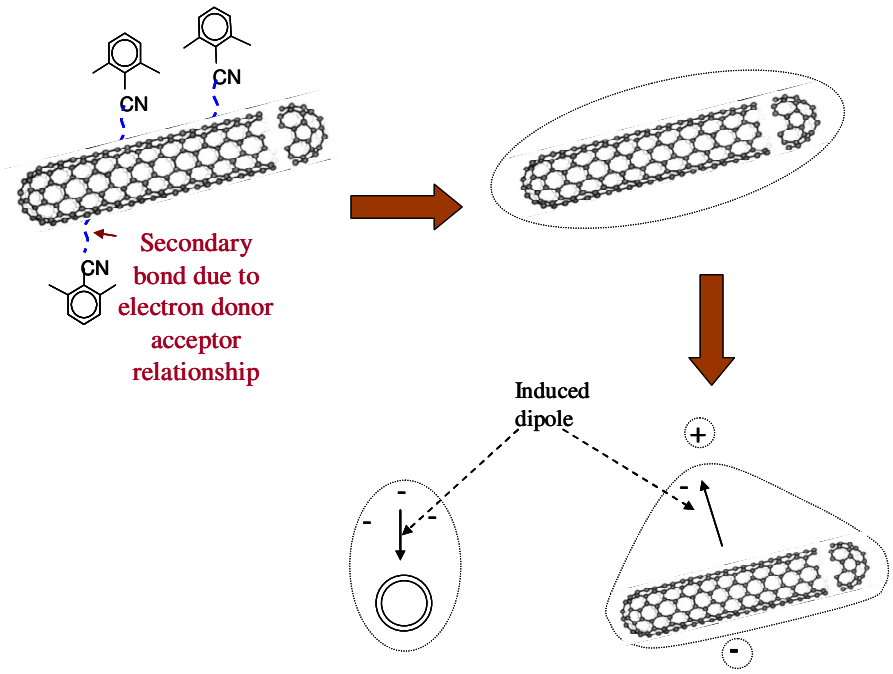

Figure 3.29 Enhanced polarization due to formation of an active interface due to secondary non covalent interaction between SWNT and polymer due to electron donor acceptor relationship

4. SUMMARY AND CONCLUSIONS

This study investigates the electric and dielectric properties, and the actuation response of single walled carbon nanotube (SWNT) – polyimide (PI) nanocomposites. Two different polyimides are used as the matrix materials. The first is a non-polar polyimide, CP2, while the second is a polar, weakly piezoelectric polyimide, (β-CN) APB-ODPA. The nanocomposites are based on SWNTs dispersed in the two polyimides using an *in-situ* polymerization under ultrasonication technique, which was developed at NASA Langley Research Center[93].

Electrical and dielectric characterization of the nanocomposite films is accomplished at varying SWNT content, temperature and frequency. This analysis quantifies the electric and dielectric properties of the nanocomposites and it also provides an insight into the quality of dispersion of the SWNTs in the polyimide matrices. Electrical conductivity shows an increase with frequency up to a particular SWNT concentration, the material is a dielectric below this concentration. Above this concentration the electrical conductivity remains constant with frequency, indicating a transition from a dielectric to a conducting material. This concentration, called the percolation threshold, can also be estimated by plotting the DC electrical conductivity as a function of SWNT concentration. The percolation threshold is determined as 0.04vol% in the case of SWNT+CP2 nanocomposites and 0.06vol% for SWNT+(β-CN) APB-ODPA [130]. For both nanocomposites, the electrical conductivity shows an increase with the SWNT content. The (β-CN) APB-ODPA composites show a couple of orders of higher conductivity values than CP2 composites for the 0.5-2 vol% SWNT content samples.

Dielectric constant values remain constant below percolation while above it, the values show a decrease due to the inability of interfacial polarization to respond to high frequency fields. The dielectric constant values of both composites increase with SWNT content, as in the case of electrical conductivity. The (β-CN) APB-ODPA composites exhibit higher dielectric constant values compared to CP2 composites, with around three orders of magnitude higher values above 0.5 vol% SWNT content as compared to the pristine case. Thus the electrical conductivity of the material and its ability to store electrical energy increases with the SWNT content and is higher for the (β-CN) APB-ODPA composites compared to CP2 composites.

Dielectric constant is measured as a function of temperature to assess the dielectric relaxation in these composites. The dielectric relaxation strength is estimated as the difference between the dielectric constant at high and low temperature ($\Delta\varepsilon$). It quantifies the relaxation of the dipoles in the system and it is a measure of the remnant polarization experienced by a material under an applied electric field. This value increases with SWNT content for both CP2 and (β-CN) APB-ODPA. The dielectric relaxation strength $\Delta\varepsilon$ is higher for composites with (β-CN) APB-ODPA matrix compared to CP2 for the same SWNT content. Thus the remnant polarization P_R that the composites experience is a function of the SWNT content and also depends on the polarity of the matrix material. These results are further supported by the TSC experiments which show an increase in the remnant polarization P_R with SWNT content. Also 0.05vol% SWNT+(β-CN) APB-ODPA composites show a higher polarization than 0.1 vol% SWNT+CP2 composites, indicating that the polar polyimide-based nanocomposites show a higher induced

polarization for the same SWNT content than the non-polar one. Thus the TSC results confirm the findings of the dielectric relaxation studies.

Actuation tests are carried out on the nanocomposite samples with varying SWNT content. A cantilever type arrangement is used resulting in a bending response of the samples under an applied electric field. The strains are measured under applied DC and AC fields. The relationship between the strains and applied fields is non-linear for both polyimide-based nanocomposites. The strains are found to be proportional to the square of the electric field, indicating an electrostrictive response. This is also observed physically with the samples bending in the same direction even after the polarity of the field is reversed. Strain rates are measured for the nanocomposite samples which show an increase in the rate of response with SWNT content. A higher strain rate is measured for the (β-CN) APB-ODPA nanocomposites compared to the CP2 nanocomposites. Coefficient of electrostriction (M_{1333}) is measured from the strain versus electric field squared plots for both types of nanocomposites. The value shows an increase with the SWNT content for (β-CN) APB-ODPA nanocomposites till 2vol% SWNT content. For CP2 nanocomposites, an increase is seen up to 1vol% SWNT content above which a plateau is reached. For the DC case, (β-CN) APB-ODPA composites show an order of magnitude higher value of M_{1333} over CP2 above 0.5vol% SWNT content. Below 0.5 vol% SWNT content the M_{1333} values for polyimide nancocomposites are comparable. With an AC square wave at 0.5 Hz also an increase in M_{1333} value up to 1 vol% SWNT content above which a slight decrease is observed. A significant drop in M_{1333} value is seen as the driving frequency is changed from DC to 0.5 Hz AC signal but as the

frequency is further increased the decrease in value is less pronounced. Also square wave signal gives a higher strains and M_{1333} values than sine wave signal for the same frequency.

Electrostriction is a polarization dependent phenomenon. Electrostrictive strains can also be expressed as proportional to the square of polarization; hence the dielectric relaxation and TSC measurements can be correlated to the observed electrostrictive effect. The enhancement in the polarization experienced by both types of composites under an electric field increases with the SWNT content. This is reflected in the enhancement of the electrostrictive effect with the SWNT content. Also the remnant polarization is higher for the (β-CN) APB-ODPA nanocomposites than for the CP2 nanocomposites for the same SWNT content. The electrostrictive effect mirrors this trend with a higher response for the (β-CN) APB-ODPA nanocomposites compared to the CP2 based composites.

The increase in the remnant polarization and electrostriction could be due to the inherent properties of the SWNTs, namely their high electrical conductivity and their inherent polarization, where both will affect the local field in their vicinity. Some researchers have shown that SWNTs have a local dipole moment at each atomic site but that, due to symmetry of the nanotube, a net dipole moment does not exist. A bent nanotube, which aptly represents the state of SWNTs when embedded in a composite, would then possess a net nonzero dipole moment. This polarizability will modify the local field around the nanotubes, possibly leading to induced polarization. It is noted that bent and wavy SWNTs in a polymer is a qualitative indication of a strong interaction

between the nanotubes and the polymer. In our results, SEM images of (β-CN) APB-ODPA composites shows more pronounced wavy nature of SWNTs than in the CP2 composites. Also due to their high electrical conductivity, the SWNTs can act as local electrodes, effectively extending the electrode into the polymer and enhancing the local field. which would then cause even weak dipoles to move as is the case of CP2. The higher the nanotube content the higher the local field enhancement leading to an enhancement in polarization. Equation 2.17 relates the applied field to the remnant polarization experienced by the dielectric materials through the dielectric relaxation strength $\Delta\varepsilon$. The higher the electric field in the system, the higher the remnant polarization observed. The starting polarization of (β-CN) APB-ODPA is higher than that of CP2, therefore, it follows that the electrostriction response of (β-CN) APB-ODPA is higher. Dielectric relaxation and TSC experiments show that the dielectric relaxation occurs around the glass transition temperature of the polymer in both nanocomposites, further indicating that the higher remnant polarization is due to higher dipolar mobility.

An alternate explanation for the enhanced polarization and actuation is the nature of the SWNT-polymer interaction in the interface region. Due to the nanometer scales of the nanotubes and the comparable distance between them along with the correlation with the length scale of important parameters like radius of gyration of the polymer, the interface becomes a dominant factor on the physical properties of the nanocomposites. The resulting interfacial polarization, which can arise due to a number of reasons as described below, will modify the overall polarization.

Electric double layers are known to exist in colloids due to charged particles and counterions present in the system. This electric double layer forms the interface between the particles and the medium. The double layers which are usually passive can now possess active properties due to their response to an applied electric field. In the polyimide nanocomposite system, the quantity of ions present is expected to be low, mostly resulting from the SWNT purification process and the solvent solutions used during processing. Therefore, the role of an electric double layer due to ions is most likely negligible in our case. However, interfacial polarization can exist due to the difference in the dielectric properties between the SWNTs and the polymers. The interface with active properties predicted by Lewis [150] can exist in a composite system where dielectric nonhomogeneity gives rise to charge separation leading to interfacial polarization. This increase in the interfacial polarization, which would increase with the SWNT content, could lead to the enhancement in polarization of the composites. Additionally, in the case of SWNT-(β-CN) APB-ODPA composites, a previous study by Park et al. [113] showed that a non-covalent, donor-acceptor bond exist between the electron withdrawing CN group and the SWNT. This non-covalent interaction would result in induced dipole and enhanced polarization. It is foreseeable that such an interaction could also exist between the electronegative CF_3 group and the SWNTs in the SWNT-CP2 composite but such an interaction is anticipated to be weaker compared to the (β-CN) APB-ODPA composites. The polarization resulting from the interaction between the SWNTs and polymer would contribute to the remnant polarization and it would undergo relaxation around the glass transition temperature T_g of the polymer

matrix. This is corroborated by the dielectric spectroscopy and TSC test results. Thus it is more likely that an interface resulting from a SWNT-polymer interaction contributes to the enhancement in remnant polarization. This polarization would be stronger with higher nanotube content and for the case of (β-CN) APB-ODPA nanocomposites.

It can thus be concluded from this study that the addition of nanoscale inclusions like SWNTs results in enhanced electrical conductivity and dielectric constant of the composites. Along with this enhancement, a creation of an actuation response is seen in non actuating polyimides. The actuation response can be tailored by changing the SWNT content and the polyimide matrix to get the desired combination of electrical, dielectric and actuating properties in the nanocomposites.good.

It is suggested that future work should focus on the following: 1) To complete the actuation characterization by measuring the actuation stress exhibited by the nanocomposites. 2) To experimentally investigate the nanoinclusion – polymer interaction using experimental techniques like Raman and FTIR spectroscopy. 3) To analytically qualify the role of SWNTs and the SWNT- polymer interaction in the actuation response of the polymer nanocomposite. 4) To optimize the actuation response in polymer composites by judiciously choosing and engineering a stronger non-covalent interaction between the polymer matrix and the inclusions 5) To investigate actuation in polymers with other nanoinclusions such as carbon nanofibers or piezoelectric boron nitride nanotubes.

REFERENCES

1. Sherrit, S. In *Proc. SPIE Smart Structures and Materials* **2005**, 1-12 Bar-Cohen, Y., Ed.

2. Smela, E. *Advanced Materials* **2003,** 15, (6), 481-494.

3. Stutzmann, N.; Friend, R. H.; Sirringhaus, H. *Science* **2003,** 299, 1881-1884.

4. Madden, J. D. W.; Vandesteeg, N. A.; Anquetil, P. A.; Madden, P. G. A.; Takshi, A.; Pytel, R. Z.; Lafontaine, S. R.; Wieringa, P. A.; Hunter, I. W. *IEEE Journal of Oceanic Engineering* **2004,** 29, (3), 706-728.

5. Curie, J.; Curie, P. *Comp. Rend.* **1880,** 91, 294-297.

6. Cady, W. G., *Piezoelectricity*. McGraw-Hill: Dover, New York, 1964.

7. Ballato, A. *IEEE Ultrasonics Symposium* **1996**, 575-583.

8. Uchino, K., *Ferroelectric Devices*. Marcel Dekker, Inc: New York, 2000.

9. Mason, W. P., *Piezoelectric Crystals and Their Application to Ultrasonics*. D. Van Nosrand Company Inc.: New York, 1949.

10. Decarpigny, J.-N.; Hamonic, B.; Wilson, O. B. J. *IEEE Journal of Oceanic Engineering* **1991,** 16, (1), 107-122.

11. Broadhurst, M. G.; Davis, G. T., *Electrets*. Springer-Verlag: New York, 1980; Vol. 33.

12. Harrison, J. S.; Ounaies, Z. 2001-43; NASA Langley Research Center: Hampton, VA, 2001; pp 1-26.

13. Kawai, H. *Japanese Journal of Applied Physics* **1969,** 8, 975.

14. Berlepsch, v. H.; Kunstler, W.; Wedel, A.; Danz, R.; Geib, D. *IEEE Transaction on Electrical Insulation* **1989,** 24, 357-362.

15. Comstock, R. J.; Stupp, S. I.; Carr, S. H. *Journal of Macromolecular Science-Physics* **1977,** B13, (1), 101-115.

16. Broadhurst, M. G.; Malmberg, C. G.; Mopsik, F. I.; W.P., H., Piezo-and pyroelectricity in polymer electrts. In *Electrets: Charge Storage and Transport in Dielectrics*, Perlman, M. M., Ed. The Electrochemical Society Inc. Princeton, NJ,

1973; pp 492-504.

17. Furukawa, T. In *Piezoelectricity in Polymers*, IEEE Trans. Electrical Insulation, **1989**; pp 375-393.

18. Mopsick, F. I.; Broadhurst, M. G. *Journal of Applied Physics* **1975,** 46, 4204-4208.

19. Bharti, V.; Nath, R. *Journal of Applied Physics* **1997,** 82, 3488-3492.

20. Ounaies, Z.; Young, J. A.; Harrison, J. S., *Overview of the Piezoelectric Phenomenon in Amorphous Polymers*. American Chemical Society: Washington DC, 1999.

21. Sundar, V.; Newnham, R. E. *Ferroelectrics* **1992,** 135, 431-446.

22. http://www.tf.uni-kiel.de/matwis/amat/elmat_en/kap_3/backbone/r3_2_3.html. Search: Ionic Polarization, Access date: June, 2006

23. Newnham, R. E.; Sundar, V.; Yimnirun, R.; Su, J.; Zhang, Q. M. *Journal of Physical Chemistry B* **1997,** 101, 10141-10150.

24. Yang, W.; Suo, Z. *Journal of Mechanics and Physics of Solids* **1994,** 42, (4), 649-663.

25. Uchino, K. *American Ceramic Society Bulletin* **1986,** 65, (4), 647-652.

26. Nakajima, Y.; Hayashi, T.; Hayashi, I.; Uchino, K. *Japanese Journal of Applied Physics* **1985,** 24, (2), 235-238.

27. Gomi, M.; Miyazawa, Y.; Uchino, K.; Abe, M.; Nomura, S. *Applied Optics* **1982,** 21, (14), 2616-2619.

28. Sato, T.; Ishikawa, H.; Ikeda, O. *Applied Optics* **1982,** 21, (20), 3669-3672.

29. Heydt, R.; Kornbluh, R.; Pelrine, R.; Mason, V. *Journal of Sound and Vibration* **1998,** 215, (2), 297-311.

30. Su, J.; Harrison, J. S.; St Claire, T. L.; Bar-Cohen, Y.; S, L. In *Materials Research Society Symposium Proceeding* **2000**, 600,131-136

31. Su, J.; Ounaies, Z.; Harrison, J. S. In *Materials Research Society Symposium Proceeding* **2000**, 95-98.

32. Cheng, Z. Y.; Bharti, V.; Xu, T. B.; Xu, H.; Mai, T.; Zhang, Q. M. *Sensors and Actuators A* **2001,** 90, 138-147.

33. Li, J. Y. *Physical Review Letters* **2003,** 90, (21), 217601-1:217601-4.

34. Watanabe, M.; Wakimoto, N.; Shirai, H.; Hirai, T. *Journal of Applied Physics* **2003,** 94, (4), 2494-2497.

35. Watanabe, M.; Yokoyama, M.; Ueda, T.; Kasazaki, T.; Hirai, M.; Hirai, T. *The Chemical Society of Japan, Chemistry Letters* **1997,** CL-970171, 773-774.

36. Watanabe, M.; Kato, T.; Suzuki, M.; Hirako, Y.; Shirai, H.; Hirai, T. *Journal of Polymer Science Part B. Polymer Physics* **2001,** 39, 1061-1069.

37. Kornbluh, R.; Pelrine, R.; Eckerle, J.; Joseph, J. *IEEE International Conference in Robotics and Automation* **1998,** 3, 2147-2154.

38. Burcsu, E.; Ravichandran, G.; Bhattacharya, K. *Applied Physics Letters* **2000,** 77, (11), 1698-1700.

39. Uchino, K. *IEEE International Symposium on Application of Ferroelectrics* **1986**, 610-618.

40. Kornbluh, R.; Pelrine, R.; Pei, Q.; Oh, S.; Joseph, J. In *Proc. SPIE Smart Structures and Materials 2003: Electroactive Polymer Actuators and Devices (EAPAD)* **2003**, Bar-Cohen, Y., Ed. SPIE Press: Bellingham, WA, 2003; pp 281-290.

41. Kornbluh, R.; Pelrine, R., Applications of dielectric EAP actuators. In *Electro active Polymers (EAP) as Artificial Muscles: Reality Potential and Challenges*, Bar-Cohen, Y., Ed. SPIE Press: SPIE Press: Bellingham, WA, 2001; Vol. 67-83, pp 457-495.

42. Pei, Q.; Rosenthal, M. A.; Pelrine, R.; Stanford, S.; Kornbluh, R. In *Proc. SPIE Smart Structures and Materials 2003: Electroactive Polymer Actuators and Devices (EAPAD),* Bar-Cohen, Y., Ed. SPIE Press: Bellingham, WA, 2003; pp 281-290.

43. Sommer-Larsen, P.; Kofod, G.; MH, S.; Benslimane, M.; Gravesen, P. In *Proc. SPIE Smart Structures and Materials 2002: Electroactive Polymer Actuators and Devices (EAPAD),* Bar-Cohen, Y., Ed. SPIE Press: Bellingham, WA, 2002; pp 126-137.

44. Wingert, A.; Lichter, M. D.; Dubowsky, S.; Hafez, M. In *Proc. SPIE Smart*

Structures and Materials 2002: Electroactive Polymer Actuators and Devices (EAPAD), Bar-Cohen, Y., Ed. SPIE Press: Bellingham, WA, 2002; pp 415-495.

45. Madden, J. D. W. Conducting Polymer Actuators, PhD Dissertation, Massachusetts Institute of Technology, Cambridge, 2000.

46. Lehmann, W.; Skupin, H.; Tolksdorf, C.; Gebhard, E.; Zentel, R.; Kruger, P.; Losche, M.; Kremer, F. *Nature* **2001,** 410, (6827), 447-450.

47. Shahinpoor, M. *Journal of Intelligent Material Systems and Structures* **1995,** 6, 307-314.

48. Hamlen, R. P.; Kent, C. E.; Shafer, S. N. *Nature* **1965,** 206, 1149-1150.

49. Shiga, T. *Advances in Polymer Science* **1997,** 134, 131-163.

50. Nemat-Nasser, S.; Thomas, C. W., In *Electroactive Polymer(EAP) Actuators as Artificial Muscles*,
Bar-Cohen, Y., Ed. SPIE Press: Bellingham, WA, 2001; pp 171-230.

51. Gierke, T. D.; Munn, C. E.; Walmsley, P. N. *Journal of Polymer Science, Polymer Physics* **1981,** 19, 1687-1704.

52. Shahinpoor, M.; Kim, K. J. *Smart Materials and Structures* **2001,** 10, 819-833.

53. Shahinpoor, M.; Bar-Cohen, Y.; Xue, T.; Simpson, J. O.; Smith, J. In *Proceedings of SPIE's 5th Annual International Symposium on Smart Structures and Materials,* 1998, Bar-Cohen, Y., Ed. SPIE Press: Bellingham, WA, 1998; pp 1-6

54. Ferrara, L.; Shahinpoor, M.; Kim, K. J.; Schreyer, H. B.; Keshavarzi, E. B.; Lantz, J. W. In *Proceedings of SPIE Smart Structures and Materials 1999: Electroactive Polymers and Devices (EAPAD),* Bar-Cohen, Y., Ed. SPIE Press: Bellingham, WA, 1999; pp 394-401.

55. Pei, Q.; Inganas, O. *Journal of Physical Chemistry* **1992,** 96, 10507-10514.

56. Mastragostino, M.; Arbizzani, C.; Soavi, F. *Journal of Power Sources* **2001,** 97-98, 812-815.

57. Shimidzu, T.; Ohtanu, A.; Iyoda, T.; Honda, K. *Journal of the Chemical Society - Chemical Communications* **1986,** 18, 1415-1417.

58. Schuhmann, W.; Lammert, R.; Uhe, B.; Schmidt, H. L. *Sensors and Actuators B*

-*Chemical 1* **1990,** 1-6, 537-541.

59. Oberlin, A.; Endo, M.; Koyama, T. *Journal of Crystal Growth* **1976,** 32, (3), 335-349.

60. Iijima, S. *Nature* **1991,** 354, 56-58.

61. http://en.wikipedia.org/wiki/Image:Types_of_Carbon_Nanotubes.png, Search: Carbon Nanotubes Wikipedia, Access date: June, 2006

62. http://students.chem.tue.nl/ifp03/images/mwnt.gif. Search: Multi Walled Carbon Nanotubes, Access date: August, 2006

63. www.nec.com/global/corp/images/H0602.jpg, Search: Double Walled Carbon Nanotubes, Access date: June, 2006

64. http://www.tmcnanotech.com/tmcnanotech/dwnt.html, Search: Properties of Double Walled Carbon Nanotubes, Acess date: August, 2006

65. Zheng, L. X.; O Connell, M. J.; Doorn, S. K.; Liao, X. Z.; Zhao, Y. H.; Akhadov, E. A.; Hoffbauer, M. A.; Roop, B. J.; Jia, Q. X.; Dye, R. C. *Science* **2004,** 3, 673-676.

66. Endo, M. Iijima, S. Dresselhaus, M.S., In *Carbon Nanotubes*, Elsevier Science Limited: NY, 1996; pp 1-180.

67. Li, F.; Cheng, M.; Bai, S.; Su, G.; Dresselhaus, M. S. *Applied Physics Letters* **2000,** 77, (20), 3161-3163.

68. Lu, J. P. *Journal of Physics and Chemistry of Solids* **1997,** 58, 1649-1652.

69. Zhou, G.; Duan, W. H.; Gu, B. L. *Chemical Physics Letters* **2001,** 333, (5), 344-349.

70. Tans, S. J.; Devoret, M. H.; Dai, H.; Thess, A.; Smalley, R. E.; Geerligs, L. J.; Dekker, C. *Nature* **1997,** 386, 474-477.

71. Hone, J.; Whitney, M.; Piskoti, C.; Zettl, A. *Physical Review B* **1999,** 59, (4), R2514-R2516.

72. Spinks, G. M.; Wallace, G. G.; Baughman, R. H.; Dai, L., Carbon Nanotube Actuators: Synthesis, Properties, and Performance. In *Electroactive Polymer (EAP) Actuator as Artificial Muscles*, Bar-Cohen, Y., Ed. Bar-Cohen, Y., Ed. SPIE Press: Bellingham, WA, 2001; p 261.

73. Ouyang, M.; Huang, J. L.; Lieber, C. M. *Accounts of Chemical Research* **2002,** 35, (12), 1018-1025.

74. Dumitrică, T.; Landis, C. M.; Yakobson, B. I. *Chemical Physics Letters* **2002,** 360, 182-188.

75. Chen, P.; Wu, X.; Sun, X.; Lin, J.; Ji, W.; Tan, K. L. *Physical Review Letters* **1999,** 82, (12), 2548-2551.

76. Kleiner, A.; Eggert, S. *Physical Review B* **2001,** 64, (113402), 1-4.

77. Chen, P.; Lin, J.; Tan, K. L. *Life* **1999,** 49, 105-108.

78. Bonard, J.-M.; Salvetat, J.-P.; Stöckli, T.; Forró, L.; Châtelain, A. *Applied Physics Letters* **1998,** 73, (7), 918-920.

79. Wang, Q. H.; Setlur, A. A.; Lauerhaas, J. M.; Dai, J. Y.; Seelig, E. W.; Chang, R. P. H. *Applied Physics Letters* **1998,** 72, (22), 2912-2913.

80. Saito, Y.; Uemura, S.; Hamaguchi, K. *Japanese Journal of Applied Physics* **1998**, (37), L346.

81. Baughman, R. H.; Zakhidov, A. A.; de Heer, W. A. *Science* **2002,** 297, 787-792.

82. Dillon, A. C.; Jones, K. M.; Bekkedahl, T. A.; Kiang, C. H.; Bethune, D. S.; Heben, M. J. *Nature* **1997,** 386, 377-379.

83. Collins, P. G.; Bradley, K.; Ishigami, M.; Zettl, A. *Science* **2000,** 287, 1801.

84. Kim, P.; Lieber, C. M. *Science* **1999,** 286, 2148-2150.

85. Liu, J.; Rinzler, G.; Dai, H.; Hafner, J. H.; Bradley, R. K.; Boul, P. J.; Lu, A.; Iverson, T.; Shelimov, K.; Huffman, C. B.; Rodriguez-Macias, F.; Shon, Y.-S.; Lee, T. R.; Colbert, D. T.; Smalley, R. E. *Science* **1998,** 280, 1253-1256.

86. Baughman, R. H.; Cui, C.; Zakhidov, A. A.; Iqbal, Z.; Barisci, J. N.; Spinks, G. M.; Wallace, G. G.; Mazzoldi, A.; De Rossi, D.; Rinzler, A. G.; Jaschinski, O.; Roth, S.; Kertesz, M. **1999,** Science, (284), 1340-1344.

87. Roth, S.; Baughman, R. H. *Current Applied Physics* **2002,** 2, 311-314.

88. Barisci, J. N.; Spinks, G. M.; Wallace, G. G.; Madden, J. D. W.; Baughman, R. H. *Smart Materials and Structures* **2003,** 12, 549-555.

89. Andrews, R.; Jacques, D.; Minot, M.; Rantell, T. *Macromolecular Materials Engineering* **2002,** 287, 395.

90. Breuer, O.; Sundararaj, U. *Polymer composites* **2004,** 25, (6), 630-645.

91. Ajayan, P. M.; Ebbesen, T. W. *Reports of Progress in Physics* **1997,** 60, (10), 1025-1062.

92. Moon, J. M.; An, K. H.; Lee, Y. H.; Park, Y. S.; Bae, D. J.; Park, G. S. *Journal of Applied Chemistry B* **2001,** 105, (24), 5677-5681.

93. Park, C.; Ounaies, Z.; Watson, K. A.; Crooks, R. E.; Smith, J. J.; Lowther, S. E.; Connell, J. W.; Siochi, E. J.; Harrison, J. S. *Chemical Physics Letters* **2002,** 364, 303-308.

94. Kim, Y. K.; Lewis, A. F.; Patra, P. K.; Warner, S. B.; Calvert, P. *National Textile Center Research Briefs-Materials Competency* **2001**, 24.

95. Mitchell, C. A.; Bahr, J. L.; Sivaram, A.; Tour, J. M.; Krishnamoorti, R. *Macromolecules* **2002,** 35, (23), 8825-8830.

96. Hirsch, A. *Angew. Chem. Int. Ed.* **2002,** 41, (11), 1853-1859.

97. Andrews, R.; Jacques, D.; Qian, D.; Rantell, T. *Accounts of Chemical Research* **2002,** 35, 1008-1017.

98. Biercuk, M. J.; Llaguno, M. C.; Radosavljevic, M.; Hyun, J. K.; Johnson, A. T.; Fischer, J. E. *Applied Physics Letters* **2002,** 80, 2767.

99. Qian, D.; Dickey, E. C.; Andrews, R.; Rantell, T. *Applied Physics Letters* **2000,** 76, (20), 2868-2870.

100. Vaia, R. A.; Wagner, H. D. *Materials Today* **2004,** 7, (11), 32-37.

101. Shaffer, M. S. P.; Windle, A. H. *Advanced Materials* **1999,** 11, (11), 937-941.

102. Barber, A. H.; Cohen, S. R.; Wagner, H. D. *Applied Physics Letters* **2003,** 82, (23), 4140-4142.

103. Ramanathan, T.; Fisher, F. T.; Ruoff, R. S.; Brinson, L. C. *Chemistry of Materials* **2005,** 17, 1290-1295.

104. Ramanathan, T.; Liu, H.; Brinson, L. C. *Journal of Polymer Science Part B.*

Polymer Physics **2005,** 43, 2269-2279.

105. Miyagawa, H.; Drzal, L. T. *Polymer* **2004,** 45, 5163-5170.

106. Gojny, F. H.; Nastalczyk, J.; Roslaniec, Z.; Schulte, K. *Chemical Physics Letters* **2003,** 370, 820-824.

107. Garg, A.; Sinnott, S. B. *Chemical Physics Letters* **1998,** 295, 273-278.

108. Santos, C. V.; Martinez-Hernandez, A. L.; Fisher, F. T.; Ruoff, R. S.; Castano, V. M. *Chemical Materials* **2003,** 15, 4470-4475.

109. Zhao, J.; Park, H.; Han, J.; Lu, J. P. *Journal of Physical Chemistry B* **2004,** 108, 4227-4230.

110. Ramesh, S.; Ericson, L. M.; Davis, V. A.; Saini, R. K.; Kittrell, C.; Pasquali, M.; Billups, W. E.; Adams, W. W.; Hauge, R. H.; Smalley, R. E. *Journal of Physical Chemistry B* **2004,** 108, 8794-8798.

111. O'Connell, M. J.; Boul, P.; Ericson, L. M.; Huffman, C.; Wang, Y.; Haroz, E.; Kuper, C.; Tour, J. M.; Ausman, K. D.; Smalley, R. E. *Chemical Physics Letters* **2001,** 342, 265-271.

112. Chen, J.; Ramasubramaniam, R.; Xue, C.; Liu, H. *Advanced Functional Materials* **2006,** 16, 114-119.

113. Wise, K. E.; Park, C.; Siochi, E. J.; Harrison, J. S. *Chemical Physics Letters* **2004,** 391, 207-211.

114. Ounaies, Z.; Park, C.; Wise, K. E.; Siochi, E. J.; Harrison, J. S. *Composite Science and Technology* **2003,** 63, 1637-1646.

115. Blanchet, G. B.; Fincher, C. R.; Gao, F. *Applied Physics Letters* **2003,** 82, 1290-1292.

116. Blanchet, G. B.; Fincher, C. R.; Gao, F. *Applied Physics Letters* **2003,** 82, 1290.

117. Kilbride, B. E.; Coleman, J. N.; Fraysse, J.; Fournet, P.; Cadek, M.; Drury, A.; Hutzler, S.; Roth, S.; Blau, W. J. *Journal of Applied Physics* **2002,** 92, (4024).

118. Harris, P. J. F. *International Materials Reviews* **2004,** 49, (1), 31-43.

119. Ounaies, Z.; Young, J. A.; Simpson, J. O.; Farmer, B. L. *Materials Research Society Proceedings: Materials for Smart Structures II* **1997,** 459, 59.

120. Simpson, J. O.; Ounaies, Z.; Fay, C. *Materials Research Society Proceedings: Materials for Smart Structures II* **1997,** 459, 53.

121. Ounaies, Z.; Park, C.; Harrison, J. S.; Smith, J. G.; Hinkley, J. *SPIE Proceedings, Electroactive Polymer Actuators and Devices* **1999,** 3369, 171.

122. Thess, A.; Lee, R.; Nikolaev, P.; Dai, H.; Petit, P.; Robert, J.; Xu, C.; Lee, Y. H.; Kim, S. G.; Rinzler, A. G.; Colbert, D. T.; Scuseria, G. E.; Tomanek, D.; Fischer, J. E.; Smalley, R. E. *Science* **1996,** 273, 483-487.

123. Guo, T.; Nikolaev, P.; Thess, A.; Colbert, D. T.; Smalley, R. E. *Chemical Physics Letters* **1995,** 243, 49-54.

124. Nikolaev, P.; Bronikowski, M. J.; Bradley, R. K.; Rohmund, F.; Colbert, D. T.; Smith, K. A.; Smalley, R. E. *Chemical Physics Letters* **1999,** 313, 91-97.

125. St Claire, A. K.; St Claire, T. L.; Slemp, W. S. In *2nd International Conference on Polyimides, 1987;* Weber, W.; Gupta, M., Eds. Society of Plastics Engineers, CT, 1987; p 16.

126. Simpson, J. O.; Ounaies, Z.; Fay, C. In, *Materials Research Society Symposium 1997*; pp 53-55.

127. Kirkpatrick, S. *Review of Modern Physics* **1973,** 45, (4), 574-588.

128. McLachlan, D. S. *Physical Review B* **1999,** 60, (18), 12 747-12 751.

129. Pötschke, P.; Dudkin, S. M.; Alig, I. *Polymer* **2003,** 44, 5023-5030.

130. Banda, S. Characterization of aligned carbon nanotube/polymer composites, M.S. Thesis, Virginia Commonwealth University,VA, 2004.

131. http://en.wikipedia.org/wiki/Dielectric_spectroscopy, Search: Dielectric Spectroscopy Wikipedia, Access date: August, 2006

132. Frohlick, H., Dipolar molecules in gases. In *Theory of Dielectrics*, Oxford University Press: Oxford, U.K., 1958; p 15.

133. Ounaies, Z.; Young, J. A.; Harrison, J. S. *NASA/TM-1999-209359* **1999**.

134. Bucci, C.; Fieschi, R.; Guidi, G. *Physical Review* **1966,** 148, (2), 816-823.

135. Teyssedre, G.; Mezghani, S.; Bernes, A.; Lacabanne, C., Thermally stimulated current of polymers. In *Dielectric Spectroscopy of Polymeric Materials*, Runt, J.

P.; Fitzgerald, J. J., Eds. American Chemical Society: Washington, DC, 1997.

136. Belana, J.; Mudarra, M.; Calaf, J.; Canadas, J. C.; Menendez, E. *IEEE Transaction on Electrical Insulation* **1993,** 28, (287-293).

137. Lacabanne, C.; Chatain, D. *The Journal of Physical Chemistry* **1975,** 79, (3), 283-287.

138. http://thermal-analysis.setaram.com/thermal-analysis/fiche_produit.aspx?id=114, Search: TSC Setaram, Access date: June, 2006

139. Runt, J. P.; Fitzgerald, J. J., *Dielectric Spectroscopy of Polymeric Materials*. American Chemical Society: Washington DC, 1997; p 230.

140. Sauer, B. B.; Avakian, P.; Starkweather, H. W. J.; Hsiao, B. S. *Macromolecules* **1990,** 23, 5119-5126.

141. Ramamrutham, S.; Narayan, R., *Strength of Materials*. Dhanpat Rai and Sons: New Delhi, 1993.

142. Banda, S.; Ounaies, Z.; Park, C.; Harrison, J. S., Dynamic mechanical analysis of single wall carbon nanotube polyimide composite. Submitted to *Composite Science and Technology*, 2006

143. Kao, K. C., Electrical conduction and photoconduction. In *Dielectric Phenomenon in Solids*, Elsevier Academic Press, UK; 2004; p 381.

144. Ebbesen, T. W.; Lezec, H. J.; Hiura, H.; Bennett, J. W.; Ghaemi, H. F.; Thio, T. *Nature* **1996,** 382, 54-56.

145. Fischer, J. E.; Dai, H.; Thess, A.; Lee, R.; Hanjani, N. M.; Dehaas, D. L.; Smalley, R. E. *Physical Review B* **1997,** 55, (8), R4921-R4924.

146. Dean, J. A., *Lange's Handbook of Chemistry*. 15th ed.; McGraw-Hill INC, NY;1999.

147. Hinkley, J. A.; Dezern, J. F. CASI (301) 621-0390. NASA Langley Research Center: Hampton, VA, 2000.

148. Young, J. A.; Farmer, B. L.; Hinkley, J. *Polymer* **1999,** 40, 2787-2795.

149. Lewis, T. J. *2004 International Conference on Solid Dielectrics* **2004**.

150. Lewis, T. J. *Journal of Physics D: Applied Physics* **2005,** 38, 202-212.

151. Zhou, H.; Preston, M. A.; Tilton, R. D.; White, L. R. *Journal of Colloid and Interface Science* **2005,** 285, 845-856.

152. Briscoe, W. H.; Horn, R. G. *Langmuir* **2002,** 18, 3945-3956.

VITA

Sujay Deshmukh received his Bachelor of Engineering in Mechanical from the University of Pune, India in 2003. He entered the Aerospace Engineering program at Texas A&M University in Fall 2004 and received his M.S. in December 2006. His research concentration is Smart Materials.

Mr. Deshmukh can be reached at Texas A&M Aerospace Engineering Department, H.R.Bright building, TAMU-3141. His e-mail is sujay_jd@tamu.edu.